STRUCTURE AND MECHANICAL PROPERTIES OF FAT CRYSTAL NETWORKS

SURESH S. NARINE

Department of Agricultural, Food and Nutritional Science
University of Alberta
Edmonton, Alberta T6G 2P5, Canada

ALEJANDRO G. MARANGONI

Department of Food Science
University of Guelph, Guelph
Ontario N1G 2W1, Canada

I. Introduction
II. Literature Review
  A. Microstructure
  B. Fractals
  C. Scaling Theory as Applied to Colloidal Gels
  D. Application of Scaling Theory Developed for Colloidal Gels to Fat Crystal Networks
  E. Network Models
III. Where Lies the Fractality in Fat Crystal Networks?
  A. Characterizing Microstructure
  B. Structural Model of the Fat Crystal Network
  C. Fractality
  D. Traditional Methods of Fractal Dimension Determination
  E. Particle Counting Method
  F. The Fractal Nature of Fat Crystal Networks
  G. The Weak Link Revisited
  H. Relating the Particle Volume Fraction to the Solid Fat Content
  I. Rheology
  J. Physical Significance of Fractal Dimension
  K. Elastic Constant and Fractal Dimension
  L. Order, Density, and Fractal Dimension
  M. Order and Heat Limitations
  N. Conclusions
IV. Mechanical Model at Low Deformations: Investigating γ
  A. Theory
  B. Structural Model

ADVANCES IN FOOD AND NUTRITION RESEARCH VOL 44
ISBN: 0-12-016444-2

C. Fractal Network Model
D. Forces Acting within the Network
E. Storage Modulus
F. Dimensional Analysis
G. Discussion
H. Conclusions
References

I. INTRODUCTION

This publication is based on the doctoral thesis of Suresh S. Narine (2000). Most of the ideas presented here have already appeared in the scientific literature (Narine and Marangoni, 1999a; 1999b; 1999c; 1999d; 1999e; 1999f; 2000a; 2000b), but this is the first time that these ideas have been presented as a comprehensive whole.

Lipids form a group of compounds that are generally soluble in organic solvents and slightly soluble or insoluble in water. This definition of lipids includes a group of compounds that is very diverse and composed of a vast collection of organic substances. However, as is usually the case with natural materials, there is an underlying order to the structure of these compounds, which makes this definition easier to work with in reality. This underlying order or underlying logic to the structural organization of complex natural materials will be a repetitive theme in this publication. For example, 99% of the lipids of plant and animal origin are made up of glycerol esters of fatty acids. These materials have traditionally been called fats and/or oils, fats being used to describe solid oils. However, the two terms are used interchangeably.

Lipids used as food are either in the form of constituents in foods such as milk, cheese, spreads, etc. or in the form of "visible" fats such as butter, lard, ghee, etc. Dietary lipids assume an important role in human nutrition. They can supply a number of essential functions, such as providing calories and essential fatty acids and acting as vitamin carriers. Additionally, fats increase the palatability of foods. It is important to note that fats have also been implicated in the controversy over a number of adverse food-related health issues, such as obesity, cancer and cardiovascular disease. Lipids in foods also provide essential characteristics of texture and functionality, due to their unique physical and chemical properties, which include their composition, crystalline structure, melting and solidification behavior, association with water and non-lipid molecules, and rheological behavior.

The macroscopic rheological properties of networks formed by lipids are of extreme importance in food products that contain significant amounts of fats. Such products include butter, margarine, chocolate, peanut butter,

many spreads such as cream cheese, and ice cream. Many of the sensory attributes such as spreadability, mouthfeel, snap and texture are dependent on the mechanical strength of the underlying fat crystal network. However, it must not be inferred from this that knowledge of the mechanical properties of the fat network provides complete knowledge of the food product within which it is formed. In addition to this obvious industrial importance, fat crystal networks form a particular class of soft materials, which demonstrate a yield stress and viscoelastic properties, rendering these materials plastic. From a materials sciences point of view, the rheological behavior of these materials is also extremely important.

This work provides a review of the development of techniques and models which attempt to relate the microstructural structural organization of fat crystal networks to their mechanical properties. In addition, the work provides a chronicle of the authors' own attempts at the problem, focusing mainly on the effects of the microstructural level of structure on the macroscopic elastic moduli of fat crystal networks, and the quantification of this level of structure utilizing fractal geometrical analysis techniques.

Fat crystal networks, like many other materials, demonstrate distinct hierarchies of structural organization, the identification and quantification of which provide insight into the relationship of composition, processing, structure, and mechanical properties of the networks formed by these materials. As such, the macroscopic properties of the network are influenced by the different levels of structure as well as the processing conditions under which the network is formed. Figure 1 depicts the structural hierarchy defined during the crystallization of a typical fat crystal network.

Efforts to model the mechanical strength (Kamphuis and Jongschaap, 1985; Kamphuis *et al.*, 1984; Nederveen, 1963; Papenhuijzen, 1971; Papenhuijzen, 1972; Payne, 1964; Van den Tempel, 1961; Van den Tempel, 1979) of these networks have met with more failure than success over the past 50 years, mainly due to the lack of a comprehensive model to relate *all* structural network characteristics and solid/liquid ratios of lipid networks to their mechanical strength. This lack stemmed partly from the fact that many scientists in this area concentrated only on the lipid composition and the polymorphism of the networks, in large part ignoring the *in situ* microstructure of the network. Lately, much work has been done in analysis of the microstructural level of the network, leading to encouraging results, which suggests that consideration of this level of structure (together with the other levels previously studied) is absolutely essential in assessing the mechanical strength of the fat network.

This publication details work by the authors and coworkers which has resulted in the ability to quantify microstructure with the application of fractal mathematics to the geometry of the microstructure. Over a period

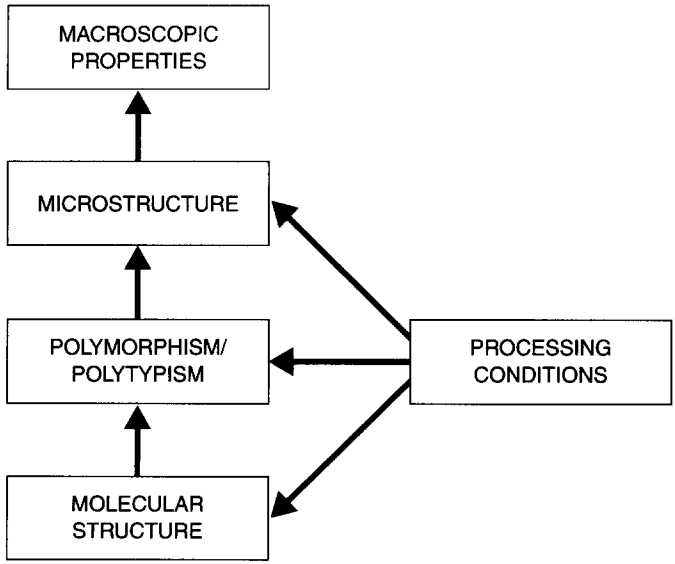

FIG. 1. Schematic showing the structural hierarchy defined during the formation of a fat crystal network.

of seven years, this area of microstructural quantification using fractal geometry has seen an explosive burst of success, reviewed in Section II. In addition, microstructural analysis via fractal methods is also applicable to other food areas, for example in characterizing structures of whey protein gels (Hagiwara *et al.*, 1997; Marangoni *et al.*, 2000; Stading *et al.*, 1993; Vreeker *et al.*, 1992a).

In order to place the work to be detailed in this publication in the context of the larger effort to predict the sensory impressions of a fat-containing food product, the reader is referred to Figures 2 and 3. Referring to Figure 2, the sensory impressions of a fat-containing product such as chocolate will be determined by the physical and chemical properties of the fat crystal network, in conjunction with the properties of any composite network that is formed with fat and other ingredients. Additionally, the properties of any other non-fat networks (and non-fat ingredients present in a random fashion) will also affect the sensory impressions of the product. One of the many factors determining the physical properties of the fat network is the hardness of the network. Referring to Figure 3, the shear storage modulus is only one of the rheological properties of the network that determines the hardness. This work is concerned primarily with the relationship between microstructure and the storage modulus of the network.

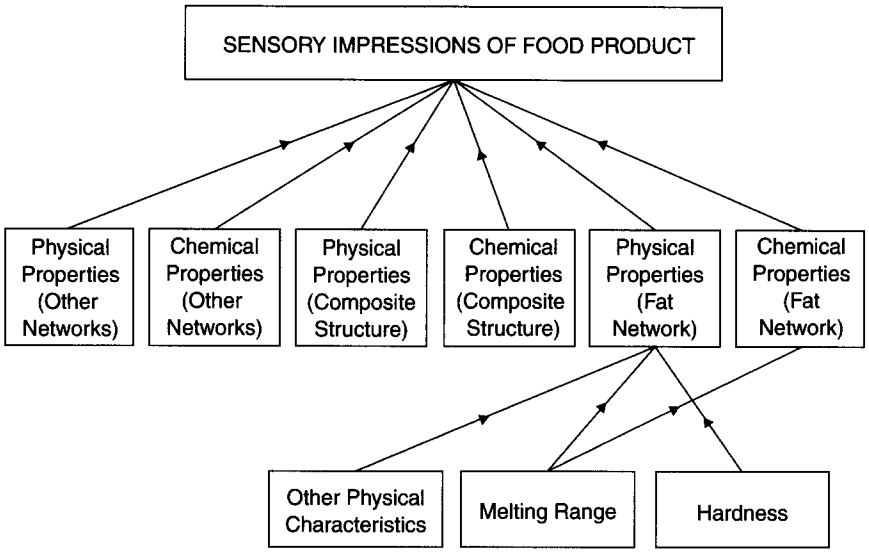

FIG. 2. Schematic showing origins of sensory impressions of a fat-containing food product.

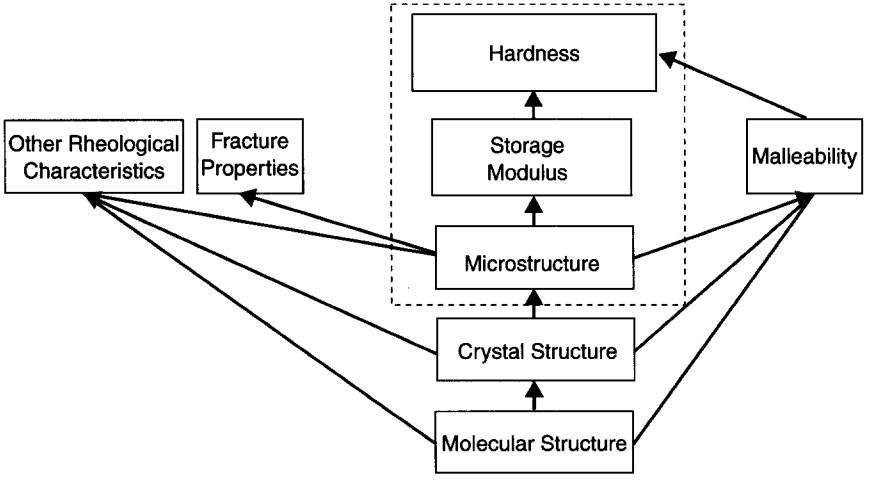

FIG. 3. Schematic of the relationship between the structural hierarchy, rheological properties, and hardness of fat crystal networks.

II. LITERATURE REVIEW

A. MICROSTRUCTURE

The microstructural level of the fat crystal network may be defined as those structures in the length range between 1 μm and 200 μm. This level of structure has an enormous influence on the macroscopic rheological properties of the network, noted as early as 1987 by deMan and Beers (1987). Other researchers have also noted the importance of the microstructural level on the rheological properties of the network, and the fact that the microstructure is easily changed with processing conditions of crystallization (Heertje *et al.*, 1987a; Heertje *et al.*, 1988; Shukla and Rizvi, 1996), as well as with interesterification (Marangoni and Rousseau, 1996).

With the advent of confocal laser scanning fluorescence microscopy (CLSFM) (Heertje *et al.*, 1987b) and multiple photon microscopy (MPM) (Marangoni and Hartel, 1998; Xu *et al.*, 1996), two new tools have been added to the standard tools of light microscopy (LM) (Flint, 1984; Flint, 1991; Inoe, 1987; Yiu, 1985) and electron microscopy (EM) (Brooker, 1990; Buchheim, 1982; de Man, 1982; Heertje *et al.*, 1987a; Kalab, 1983; Sargeant, 1988) that was most widely used in the past to study the microstructure of fats and foods in general. Heertje's work (1993; 1987a; 1987b; 1988) on the visualization of the microstructure in fats remains one of the most important contributions to the field. In his method, a cold solvent mixture (butanol-methanol) was used to remove the liquid oil from the solid fat in a sample mounted on a special holder. After removal of the liquid oil, the structure of the solid fat network could be visualized.

Interest in the microstructure of fat crystal networks in our laboratory arose during studies of factors affecting the hardness and spreadability of chemically interesterified (CIE) and enzymatically interesterified (EIE) milkfat, and chemically interesterified (CIE) palm oil and lard (Rousseau *et al.* 1996a; 1996b; 1996c; Marangoni and Rousseau, 1996; Rousseau and Marangoni, 1998a; Rousseau and Marangoni, 1998b; Rousseau *et al.*, 1998; Marangoni and Rousseau, 1998a; Marangoni and Rousseau, 1998b). The hardness index and elastic moduli of CIE milkfat at equivalent solid fat contents was lower than their noninteresterified (NIE) counterparts. The traditional indicators of macroscopic hardness such as dropping points, solid fat content and polymorphism of the chemically interesterified and non-interesterified milkfat samples were investigated, in an attempt to explain the observed changes in G' and hardness index. Figure 4 (adapted from Rousseau *et al.*, 1996c) shows the dropping points of CIE and NIE milkfat-canola oil blends (here, the canola is used strictly as a diluent to vary the solid fat content), Figure 5 (created from data published by Rousseau *et al.*, 1996a) shows the solid fat contents of CIE and NIE

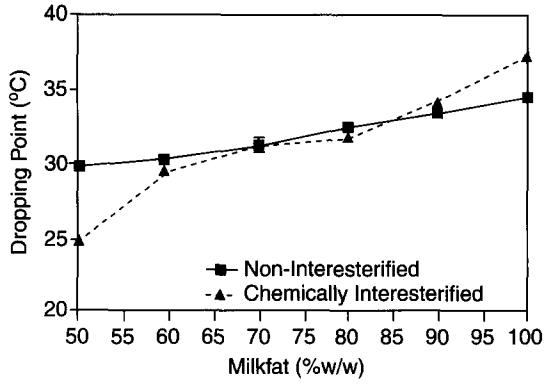

FIG. 4. Dropping points of chemically and non-interesterified milkfat–canola oil blends.

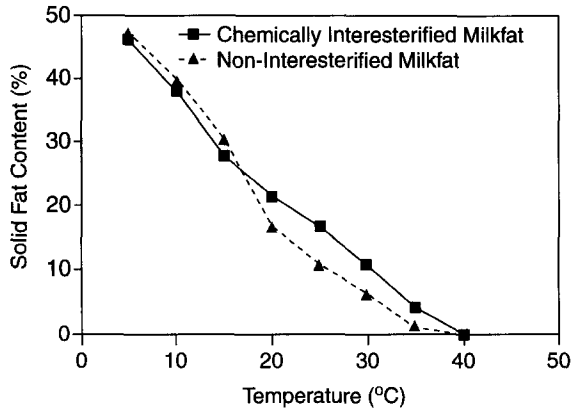

FIG. 5. Solid fat content of chemically and non-interesterified milkfat at different temperatures.

milkfat at different temperatures, and Figure 6 (data collected by Rousseau) shows the film from X-ray diffraction studies of CIE and NIE milkfat. As is evidenced by these figures, there was little or negligible change in dropping points of NIE and CIE milkfat at w/w percentages of milkfat between 60% and 90%. There was little or negligible change in solid fat content of NIE and CIE milkfat between 25% and 50% solid fat contents, and crystalline packing due to chemical interesterification was similar to that observed for non-interesterified milkfat (the polymorphism, as was defined earlier are the same). Figure 7(A) and (B) (adapted from Rousseau *et al.*, 1996c) shows the hardness, as measured by the hardness index, of CIE and NIE milkfat-canola oil blends at different solid fat contents and

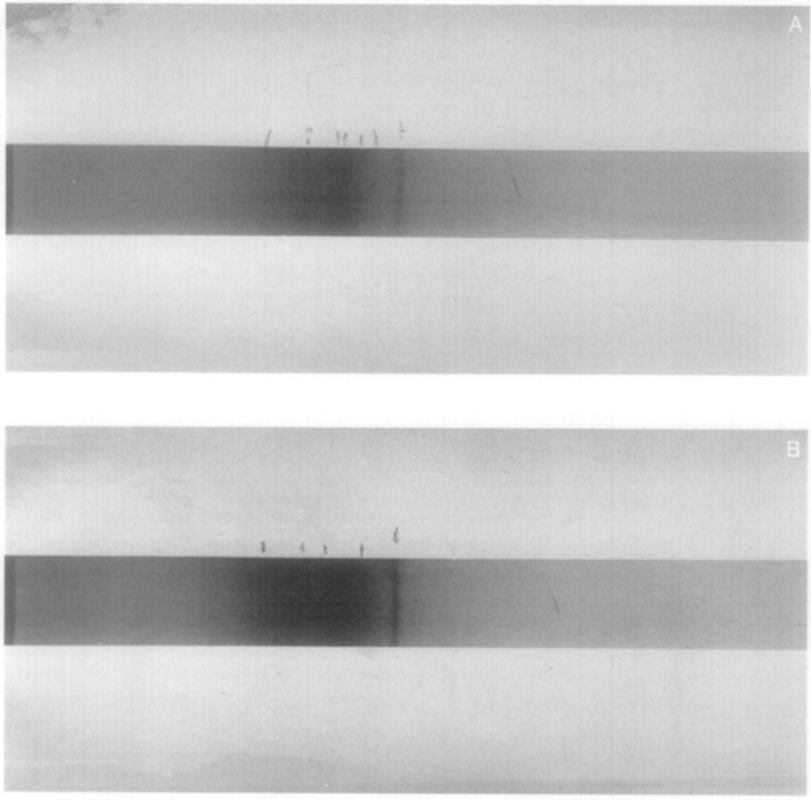

FIG. 6. X-ray diffraction film of (A) non-interesterified milkfat and (B) chemically interesterified milkfat.

w/w percentages respectively. As is evident, the NIE milkfat is consistently harder than the CIE milkfat at solid fat contents above 38%, and w/w percentages of milkfat-canola oil above 70%. Figure 8(A) and (B) (created from data published by Rousseau *et al.*, 1996c) shows the shear elastic moduli of CIE and NIE milkfat-canola oil blends at different solid fat contents and w/w percentages respectively. The elastic moduli of the NIE milkfat-canola oil blends at solid fat contents above 40% are consistently higher than the shear elastic moduli of the CIE milkfat-canola oil blends. This trend is also true for w/w percentages of milkfat-canola oil above 70%. Therefore, it was obvious that the traditional indicators of macroscopic hardness were insensitive to the changes in the structure of the milkfat on chemical interesterification, which caused the resulting changes in elastic moduli and hardness index. It must be mentioned here, in order to avoid misinterpretation, that the above phenomena was observed

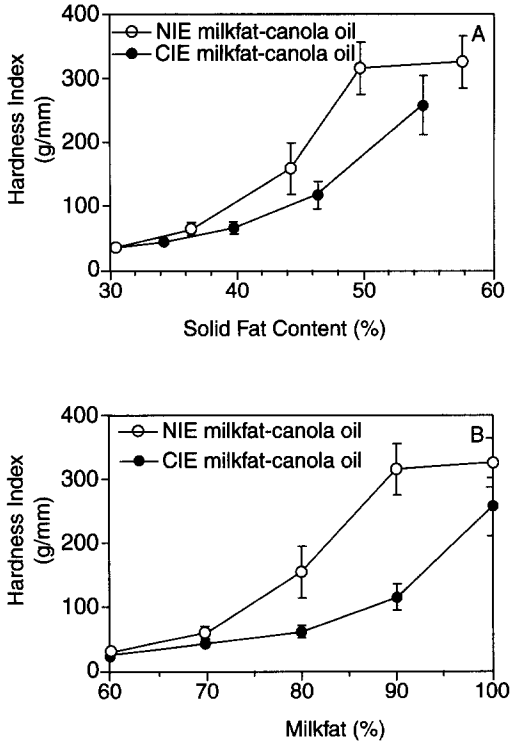

FIG. 7 (A) Hardness index vs. solid fat content, and (B) hardness index vs. weight percent of milkfat/canola oil, of chemically and non-interesterified milkfat.

for chemically interesterified and non-interesterified milkfat, but that this does not imply that traditional indicators such as dropping points, polymorphism, and solid fat content are *always* insensitive to changes in macroscopic mechanical properties. What this case study proved was that it was possible for these indicators to prove insensitive in some cases, therefore suggesting that perhaps there existed other structural indicators that must also be taken into consideration. It was interesting, however, that polarized light microscopy and confocal laser scanning microscopy demonstrated that the structure of the fat network at the microstructural level (i.e. at the level of structure that is visible by light microscopy) upon chemical interesterification was significantly altered (Rousseau *et al.*, 1996b). This provided motivation to search for new "structural indicators" of the mechanical strength of fat crystal networks, that were somehow related to the next logical structural level; the microstructural level of structure of the network. A rheological approach was adopted by Rousseau and Marangoni (Marangoni and Rousseau, 1996; 1998b; Rousseau and

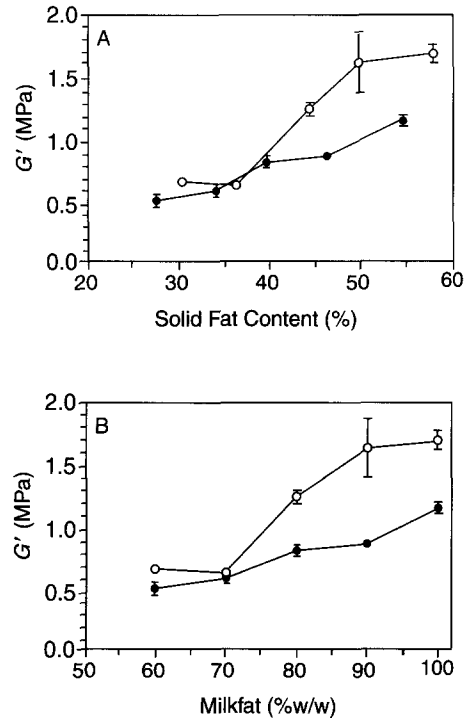

FIG. 8 Shear elastic modulus of chemically and non-interesterified milkfat vs. (A) solid fat content and (B) weight percentage of milkfat-canola oil.

Marangoni, 1998b), the motivation for which stemmed from work done on the fractal nature of colloidal gels and adapted to fat crystal networks (Vreeker *et al.*, 1992b). In order to introduce the reader to the developments made in the rheological analysis of fat crystal networks utilizing the progress in the colloidal field, we provide an introduction first to fractal theory, and then to the application of fractal theory to colloidal gels.

B. FRACTALS

Classical or Euclidean geometry is based upon the use of regular shapes to describe objects. The reader will be familiar with the use of straight lines, circles, conic sections, polygons, spheres, quadratic surfaces, etc. and combinations of these elements to describe objects around us. However, many patterns in nature defy description by these regular shapes. The geometry of coastlines, mountains, trees and vegetables, for instance, cannot always be defined adequately by spheres, cubes, or cones. Fractal geometry

was born out of this lack of geometrical tools. Benoit Mandelbrot is credited with having developed the field of fractal geometry to describe many of these natural shapes (Mandelbrot, 1982). According to Mandelbrot (1982), "... I conceived and developed a new geometry of nature and implemented its use in a number of diverse fields. It describes many of the irregular and fragmented patterns around us, and leads to full-fledged theories, by identifying a family of shapes I call fractals."

The unifying concept underlying fractals is the concept of self-similarity. Self-similarity essentially means invariance against changes in scale or size, and is demonstrated in many of the laws of nature. Self-similarity is one of a vast number of symmetries that exist in nature. Symmetry is usually taken to mean invariance against some change – i.e. some aspect of an object stays the same regardless of changes in the state of the observer. For example, there is symmetry in regular bodies such that they may be operated upon by a number of operations, and yet after the operation is carried out, every point of the body in its original state is coincident with an equivalent point in its altered state. We have been able to take advantage of underlying symmetries in nature – notably in the previous example in the application of group theory to the symmetry operations which render groups of molecules invariant against sets of operations consisting of reflections, rotations, translations, inversions, and combinations of these operations (Cotton, 1971). Equally useful and more popular symmetries in nature include the exploitation of invariance against uniform motion, which has spawned the theory of special relativity, and the equivalence of acceleration and gravity which is the basis of Einstein's general theory of relativity. Even classical physics is built along the lines of symmetry in nature – the electrostatic or gravitational attraction or repulsion between two bodies demonstrates mirror symmetry – there is no partiality shown to left or right. Suffice it to say, therefore, that symmetry in nature has aided us tremendously in understanding and quantifying our world. As will be demonstrated, the symmetry of self-similarity at different length scales is equally as useful as those mentioned above. To quote Schroeder (1991), "Yet, among all these symmetries flowering in the Garden of Invariance, there sprouts one that, until recently, has not been sufficiently cherished: the ubiquitous invariance against changes in size, called self-similarity."

The word fractal stems from the fact that fractal objects demonstrate fractional dimensions, rather than the integer dimensions for objects encountered in Euclidean geometry. The connection between fractional and self-similarity is that the easiest way to construct a set that has fractional dimension is through self-similarity (Crownover, 1995). In classical Euclidean geometry, objects have integer dimensions: the reader would be familiar with the reasoning that a line is a one-dimensional

object, a plane a two-dimensional object and a volume a three-dimensional object. In this way, Euclidean geometry is suited for quantifying objects that are ideal, man-made, or regular.

One may imagine that if enough kinks are placed in a line or a plane, the result is to have an object that may be classified as being an intermediate between a line and a plane or a plane and a cube. The dimension of such an object is fractional (i.e. between 1 and 2 or between 2 and 3) and the object may be classified as a fractal object; from the fact that instead of having an Euclidean dimension (integer) it has a fractional dimension. One of the most important features of fractal objects is that they are self-similar; i.e. there is a repetition of patterns in the object at many different scales. For natural objects such as trees, clouds, coastlines, etc., Euclidean geometry fails to provide an adequate quantification, but many of these natural objects are self-similar at different scales. For example a tree has branches, these branches have smaller branches and so on, and if one changes the scale of observation of the tree, the same pattern is observed, at least in a statistical sense if not in a deterministic sense. Therefore, fractal geometry provides a good measure of such objects with non-integral dimensions.

The concept of fractional dimension was introduced by Hausdorf (1919). As early as 300 years ago, Leibniz (1721) used the scaling invariance of the infinitely long straight line for its definition. However, as self-similar entities with fractional dimensions started appearing in the mathematical literature, they were met with distaste. Charles Hermite, the famous mathematician, for example, labeled such entities monsters. However, largely due to the efforts of Benoit Mandelbrot (1982), fractal geometry is now an accepted and extremely useful method of describing and quantifying entities that demonstrate scale invariance and fractional dimensions.

The reviews by Jullien and Botet (1987), Meakin (1988) and Lin *et al.* (1989) on the subject of fractal aggregation are recommended.

For a disordered distribution of mass, such as in a clustering of stars in the Milky Way or the clustering of particles in a colloid, fractal geometry is also useful. A short example is useful. For a solid two-dimensional disk, the relationship of mass to the radius of the disk is given by:

$$M(r) \sim R^2 \tag{1}$$

so that is this case, the dimension is an integer and the object is an Euclidean object. However, for a disordered distribution of mass, if at different scales of observation the patterns are statistically self-similar, then the relationship of radius to mass may be given by (Mandelbrot, 1982; Jullien and Botet, 1987; Uriev and Ladyzhinsky, 1996; Vreeker *et al.*, 1992b):

$$M(r) \sim R^D \tag{2}$$

where D is a fractional or *fractal dimension*, know as the mass fractal dimension. Here, the symbol ~ is taken to mean "approximately proportional to."

C. SCALING THEORY AS APPLIED TO COLLOIDAL GELS

The irreversible aggregation of small particles to form clusters is a common natural phenomenon; for example this is seen in colloids (Medalia, 1971), coagulated aerosols (Friedlander, 1977), chemical species precipitating from a supersaturated matrix and crystals growing from a supercooled melt (Mullins and Sekerka, 1963). The final structure of such aggregates is important not only because it potentially can yield information about the mechanical strength of the resulting structures, but can also suggest methods to alter the structure kinetically. In many cases, the rate limiting step of the formation of these aggregates is the diffusion of species towards a growing surface (mass-limited transfer), or the transfer of heat away from the growing surface, or a combination of these factors, depending on the stage of growth.

As early as 1979, Forrest and Witten (1979) demonstrated a class of aggregates that were shown to have density correlations of a power-law form. These aggregates were formed when a metal vapor produced by heating a plated filament was quench condensed, causing metal particles of the order of 40 Å radius to drift down onto a microscope slide. The particles were found to arrange in aggregates of the order of 10^5 particles per aggregate. In 1981, Witten and Sander (1981) constructed a computer simulation model for random aggregation which is diffusion limited, and demonstrated that the density correlations within the model aggregates fall off with distance with a fractional power-law, like those of the metal aggregates. Following their earlier work, Witten and Sander (1983) showed that by constructing diffusion limited aggregation models, the objects so formed are scale-invariant whose fractional dimensionality (Hausdorf dimension) is independent of short-range details. Additionally, they showed that diffusion-limited aggregation has no upper critical dimension. This study made the point that the properties associated with scale invariance are long-range and universal, and that such long-range properties do not arise from long-range forces – rather, these long-range correlations are built up by short-range forces. In 1983, cluster-cluster aggregation models which are diffusion-limited were introduced by Meakin (1983) and Kolb *et al.* (1983), serving to fuel the flurry of interest in analyzing the structural

properties of aggregated colloids using fractal theories generated by the work of Witten and Sanders. Meakin's and Kolb *et al.*'s simulation studies suggested that the colloidal aggregates behave as stochastic mass-fractals on a scale that is large compared to the primary particle size. Subsequent experimental studies by Weitz *et al.* (1984, 1985) on aqueous gold colloids and Schaefer *et al.* (1984) on colloidal aggregates of small silica particles, confirmed the behavior suggested by the simulations. Following this, in 1985, Brown and Ball produced a computer model, which simulated chemically limited aggregation, and suggested that the structures so formed should also behave as mass fractals. Much experimental work in this area ensued in the following years, with Aubert and Cannell (1986) performing further work on colloidal silica aggregates, Schaefer and Keefer (1986), Courtens *et al.* (1987) and Vacher *et al.* (1988) on silica aerogels, Rojanski *et al.* (1986) on mesoporous silica gels, Dimon *et al.* (1986) on gold colloids, Bolle *et al.* (1987) on polystyrene lattices, and in a *Nature* paper, Lin *et al.* (1989) investigated three different colloids – colloidal gold, colloidal silica, and polystyrene latex. In all the experimental work detailed above, the fractal nature of the colloidal aggregates was well demonstrated. Additionaly, colloidal-like gels such as casein gels (e.g. Bremer *et al.*, 1989) have been shown to be composed of homogenous clusters of particles, with the structure within the clusters being fractal in nature.

For a particulate system that is composed of a number of aggregate clusters which are fractal, the number of particles, assumed identical, making up the fractal aggregate may then be given by (following Eqn (2)):

$$N_p(\xi) \sim \left(\frac{\xi}{\sigma}\right)^D \tag{3}$$

where $N_p(\xi)$ is the number of particles in a fractal aggregate of size ξ containing particles of size σ, and the system is assumed to be fractal within the range bounded by the size of one primary particle and the size of the entire structure. The particle volume fraction of the object may be expressed in terms of the size of the aggregate and the fractal dimensionality, if one assumes a model such as is described below, originally developed by de Gennes (1979) for polymer gels, independently by Brown (1987) for a network of fractal clusters, and shown experimentally to be applicable to colloidal gels by Dietler *et al.* (1986). The treatment below is loosely adapted from Bremer *et al.* (1989), since these researchers provide an elegant development of the model originally developed by de Gennes and Brown.

One may imagine that a regular square lattice is laid over the fractal object, where each lattice site is occupied by a primary particle, or by a volume element of solution. If the particles are arranged in a fractal manner, the number of lattice sites occupied by particles in an aggregate is given by Eqn (3). It is important to note that each particle does not completely fill each lattice site; we do not often encounter square particles in nature. The total number of lattice sites taken up by an aggregate, either with solution, or as particles, is given by:

$$N_a = \left(\frac{\xi}{\sigma}\right)^3 \tag{4a}$$

Again, this assumes a completely square aggregate, which is not usually the case, so that Eqn (4a) is more correctly written as:

$$N_a \sim \left(\frac{\xi}{\sigma}\right)^3 \tag{4b}$$

Therefore, the volume fraction of particles within an aggregate is given by:

$$\Phi_a = \frac{N_p}{N_a} \sim \frac{(\xi/\sigma)^D}{(\xi/\sigma)^3} = \left(\frac{\xi}{\sigma}\right)^{D-3} \tag{5}$$

According to the models for cluster-cluster diffusion-limited aggregation which were verified experimentally as discussed above, the aggregates grow until they become space filling, thus forming a gel. Therefore, the fractal dimensionality within each gel is maintained, whilst at length scales above the characteristic length of one aggregate, the colloid scales in a Euclidean manner. The sum of all the lattice sites occupied by all the aggregates is equal to the number of lattice sites occupied by the gel, N_t (both by solution and particles):

$$N_t = \sum_{i=1}^{n} N_{a,i} \sim \sum_{i=1}^{n} \left(\frac{\xi}{\sigma}\right)_i^3 \tag{6}$$

where n is the total number of aggregates. Therefore, the overall volume fraction of particles, Φ_t, is given by the total number of sites filled by particles, divided by the total number of sites in the gel:

$$\Phi_t = \frac{\sum_{i=1}^{n} \Phi_{a,i} N_{a,i}}{N_t} \sim \frac{N_t \sum \left(\frac{\xi}{\sigma}\right)^{D-3}}{N_t} = \left(\frac{\xi}{\sigma}\right)^{D-3} \tag{7}$$

From Eqn (7):

$$\xi \sim (\Phi_t)^{\frac{1}{D-3}} \tag{8}$$

Therefore, the characteristic diameter of an aggregate is related to the overall volume fraction of particles via the mass fractal dimension of the aggregates. This relationship suggests that the two factors influencing this relationship is the degree of occupancy of the regular lattice by particles, and the degree of order of the packing of the lattice sites by particles.

1. Elastic Properties of Colloidal Gels: exploiting the fractal nature of the aggregates

Colloidal gels respond to small amplitude deformations as elastic solids. In 1986, Sonntag and Russel (1986) showed that the storage modulus of a volume-filling network formed by Brownian flocculation of aqueous polystyrene lattices scaled with the volume fraction of particles in a power-law manner, given by:

$$G' \sim \Phi^u \tag{9}$$

Sonntag and Russel were not the first to experimentally demonstrate this behavior for aggregated systems, for example, other researchers such as Nederveen (1963) and Van den Tempel (1979) showed that storage modulus of dispersed systems of microcrystals formed from oils vary with the particle concentration in a power law manner, and Payne (1964) showed that the storage modulus of systems formed from aggregates of carbon-black particles in mineral oil demonstrated a power law relationship with particle concentration. Buscall *et al.* (1988) demonstrated a similar relationship with systems of polystyrene lattices in water. However, Sonntag and Russel were among the first researchers to suggest that scaling arguments put forward by other researchers such as Kantor and Webman (1984), on the elastic properties of random percolating systems, and computer simulations of random lattices by Feng *et al.* (1984(a), 1984(b)) may support the relationship that they observed experimentally. At this point, however, the scaling theory had not been developed sufficiently to totally explain the experimental behavior observed by Sonntag and Russel.

Brown (1987) soon after addressed the elasticity of a network of clusters. His method consisted of calculating the elasticity of an individual fractal cluster, and then supposing that in an overcrowded system, fractal behavior survived on a scale related to the overall volume fraction by:

$$\xi \sim \Phi^{\frac{1}{D-3}} \tag{10}$$

which is the same relationship arrived at in the treatment above (Eqn (8)). Brown predicted that the storage modulus should scale in the following manner:

$$G \sim \Phi^{u} \tag{11}$$

which is consistent with that seen by Sonntag and Russel and a number of other researchers, cited above. Additionally, Brown suggested that the exponent u is given by:

$$u = \frac{3 + d_{chem}}{3 - D} \tag{12}$$

where d_{chem} is the so-called chemical length exponent, introduced earlier in simulation studies by Brown and Ball (1985). Soon after the model of Brown, Buscal *et al.* (1988) published experimental evidence supporting this model, for a system of silica particles. Later work by Ball (1989) on the elasticity of aggregates explains higher fractal dimensions (than was originally suggested by Kolb *et al.* (1983) and Meakin (1983)) that had been reported by Courtens *et al.* (1987) and Vacher *et al.* (1988), by considering that there may be consolidation beyond a critical size of the clusters. Soon after, Edwards and Oakeshott (1989) outlined broad guidelines for the treatment of the transmissions of stress in an aggregate, without really achieving more than stating the complexity involved. However, this work is worth mentioning here, since it does point out that the model by Brown (1987) assumes that stress is transmitted in one-dimensional paths, which are branched and are characterized by a fractal dimension, whilst in some cases the situation is more complicated, since the stress has to be spread amongst several neighbours in order to maintain stability of the aggregate.

Following Brown and Ball, Bremer *et al.* (1989, 1990, 1993) suggested elastic models for colloidal protein networks. These researchers envisioned the networks to be composed of strands of elastic material, where deformation causes a stretching of the strands of the network. The storage modulus is then a function of the number of stress-carrying strands per unit area, the geometry of the network, and the character of the bonds within the strands. Bremer *et al.* formulated two different scaling relationships for the storage modulus to the particle volume fraction, depending on the geometry of the strands. For straight stress-carrying strands, the relationship is:

$$G' \sim \Phi^{\frac{2}{3-D}} \tag{13}$$

and for curved stress-carrying strands the relationship is:

$$G' \sim \Phi^{\frac{3}{3-D}} \tag{14}$$

In 1990, Shih *et al.* (1990) developed a scaling theory to explain the elastic properties of colloidal gels well above the gelation threshold. The model of a colloidal gel visualized by Shin *et al.* corresponds well with the model of a colloidal gel described above: i.e. they define a colloidal gel above the gelation threshold to be a collection of flocs or clusters, which are fractal in nature. These researchers defined two regimes based on the relative value of the elastic constant of the inter-floc links to that of the flocs themselves, and claim that the scaling in these types of gels is affected mainly by the structure of the individual flocs as opposed to percolation-type scaling.

An in-depth development of the model created by Shih *et al.* (1990) is provided below, since this model is used extensively in other parts of this review. In large part ignoring the progress made in describing the scaling relationship of the characteristic length of the cluster/floc size with particle volume fraction for colloidal gels described earlier, Shih *et al.* uses this identical relationship (given by Eqns (8) and (10)), but justifies its use because of the fact that it was found to be true for polymeric gels by de Gennes (1979). They defend the use of this relationship for colloidal gels because colloidal gels are similar to polymeric gels by the fact that both are viscoelastic materials, and that both are formed by aggregation processes; polymeric gels by polymerization and/or crosslinking, and colloidal gels by particle aggregation. However, Shih *et al.* does quote the experimental evidence of Dietler *et al.* (1986) for the validity of this relationship for colloidal gels. It is important to mention that there is indeed sound theoretical reason why this relationship may be used for colloidal gels as well, as was developed above (after Brown (1987), and Bremer *et al.* (1989)).

According to Shih *et al.*, the elastic properties of a floc/cluster is dominated by its effective backbone (connected path of particles responsible for transmission of stress), the size of which is ξ, same as the size of the floc/cluster. This backbone may be assumed to be a linear chain of springs, with each spring representing the bond between particles forming the backbone; a justifiable assumption, since the formation of aggregates via cluster-cluster aggregation which is either reaction limited or diffusion limited have very few loops. The point made by Edwards and Oakeshott

(1989), as discussed above, concerning the limitations of an effective backbone argument must also be reiterated at this point – it is not entirely clear to the author whether this is a valid assumption, for the reasons given by Edwards and Oakeshott. An earlier publication by Kantor and Webman (1984) formulated the elastic constant of a linear chain of springs as:

$$K_s = \frac{G}{N_{bb}S^2} \tag{15}$$

where G is the bending elastic energy, N_{bb} is the number of springs in the chain and S is the radius of gyration of the projection of the nodes of the chain in the $\mathbf{F} \times \mathbf{Z}$ direction, $\mathbf{F}$ being the applied force and $\mathbf{Z}$ being the normal of the plane within which the chain lies. Eqn (15) ignores the stretching elastic energy of the chain, since it has been shown by Kantor and Webman (1984) to be negligible for long chains, and is only important for comparatively straight chains stretched along their long dimension. Therefore, when the chain in question is the effective backbone of a floc/cluster, the elastic constant of the floc is given by:

$$K_\xi = \frac{G}{N_{bb}\xi^2} \tag{16}$$

where the radius of gyration has now been replaced by the size of the effective backbone (or the size for the floc), since these two quantities would be the same. Now, the backbone of the flocs themselves are fractal objects, for which a fractal dimension between 1 and 2 can be defined, since instead of a straight chain, the backbone would have a certain tortuosity. In keeping with the fractal concept, where a line is kinked enough so that its dimension is raised to a fractional index between 1 and 2, the number of particles, and therefore the number of springs, in the backbone is given by:

$$N_{bb} \sim \xi^x \tag{17}$$

where x is the fractal dimension of the effective backbone, or the tortuosity of the effective backbone, and $x \geq 1$ in order to provide a connected path through the floc/cluster. Now, combining Eqns (16) and (17), one may represent the elastic constant of the floc by:

$$K_\xi \sim \frac{G}{\xi^x \xi^2} = \frac{G}{\xi^{2+x}} \tag{18}$$

Now, if the elastic energy G is not a function of concentration, then the elastic constant of the flocs should decrease rapidly with increasing floc size. This point strikes the author as being suspect, since it is inconceivable that the elastic energy of a bent chain is not dependent on the density of the springs which comprises the chain. It is conceivable that the density of the particles (density of springs) never really changes with concentration, since the length of the effective backbone (length of the chain) also changes with concentration (via Eqn (8)). If the change in particle volume concentration of the entire system is compensated for in terms of an increased effective backbone length, resulting in no change of the density of particles in the effective backbone, then the bending elastic energy, G, may be considered independent of particle volume concentration. Therefore, if the flocs are allowed to grow larger, they behave as weaker springs. Now, the macroscopic elastic constant of the system of flocs may be expressed either as a function of the elastic constant of the flocs, K_ξ, or the elastic constant of the links between flocs, K_l, depending on the relative strength of K_ξ and K_l. Since from Eqns (8) and (10) the characteristic length of the flocs/clusters, ξ, is related to the particle volume concentration, and since the elastic constant of the flocs will decrease with increasing ξ to a power of $2 + x$ (> 3), then the relative strengths of K_ξ and K_l will be affected by the particle concentration of the system. To illustrate this, one may express the elastic constant of the flocs in terms of the particle volume concentration, by substituting for ξ in Eqn (18):

$$K_\xi \sim \frac{G}{\xi^{2+x}} \sim \frac{G}{\left(\Phi^{\frac{1}{D-3}}\right)^{2+x}} = \frac{G}{\Phi^{\frac{2+x}{D-3}}} = G\Phi^{\frac{2+x}{3-D}} \tag{19}$$

Therefore, the elastic constant of the flocs will get larger with increasing particle volume concentration. Obviously, as the particle volume concentration increases, there will be a cross-over point at which the elastic constant of the flocs is greater than the elastic links between the flocs, resulting in the elastic constant of the entire system being determined by the nature of the links between clusters (this is called the weak link regime). The converse, where the particle volume fraction decreases beyond the cross-over point, is also true, and in this case the elastic constant of the flocs grow weaker than the elastic constant of the links between flocs, leading to the elastic constant of the system being determined by the nature of the elastic constant of the flocs (this is called the strong link regime).

Therefore, for the strong link regime, the macroscopic elastic constant of the system is given by:

$$K \sim \left[\frac{L}{\xi}\right] K_{\xi} \tag{20}$$

where L is the macroscopic size of the system. Therefore, for a constant macroscopic size of the system, combining Eqn (20) with Eqn (19), and again substituting for ξ from Eqn (8):

$$K \sim \xi^{-1} G \Phi^{\frac{2+x}{3-D}} \sim \Phi^{\frac{1}{3-D}} \Phi^{\frac{2+x}{3-D}} = \Phi^{\frac{3+x}{3-D}} \tag{21}$$

assuming that the elastic energy of the effective backbone does not change with concentration. Therefore, the macroscopic elastic constant of a colloidal gel at comparatively low concentrations is given by (the strong link relationship):

$$K \sim \Phi^{\frac{3+x}{3-D}} \tag{22}$$

As is evident from Eqns (22) and (12), the strong-link formulation of Shih *et al.* is consistent with that developed by Brown (1987), if one assumes that the tortuosity, x, is the same as the chemical length exponent, a concept which is does not deviate from the explanation offered by Brown. Shih *et al.* (1990) also studied two types of boehmite alumina gels, Catapal and Dispal powders, rheologically. The elastic behavior of both gel confirmed the strong link relationship given by Eqn (22). Fractal dimensions calculated from the rheological measurements agreed well with those calculated from static light-scattering measurements.

For the weak link regime, the macroscopic elastic constant of the system is given by:

$$K \sim \left[\frac{L}{\xi}\right] K_{l} \tag{23}$$

Substituting for ξ from Eqn (8):

$$K \sim \Phi^{\frac{1}{3-D}} \sim G' \tag{24}$$

where G' is the shear storage modulus of the system. Here, Eqn (24) assumes that the links between flocs/clusters are of constant strength. It is important to note that the elastic constant of the links between flocs is not expressed in terms of the geometry of the network. However, Eqn (24) does provide a scaling relationship of the elastic constant of colloidal gels at high concentrations, with the particle volume fraction.

After the development by Shih *et al.* (1990), Chen and Russel (1991) studied the elastic behavior of a synthesized model system consisting of submicrometer silica spheres coated with octadecyl chains suspended in hexadecane. This study demonstrated that the storage modulus of the colloidal system increased with particle volume concentration in a power law manner, and that the power law exponent increased with increasing temperature, indicating a structural change in the network. It was obvious that the power law exponent was sensitive to the packing of the particles (disturbed when the temperature is increased) – suggesting that the power was dependent on the fractal dimension. This work further served to lend credibility to the scaling models outlined by Brown (1987), Bremer *et al.* (1989, 1990) and Shih *et al.* (1990).

Vreeker *et al.* (1992a) showed that colloidal-like aggregates of whey protein gels are fractal in nature, utilizing dynamic light scattering measurements. Additionally, they analyzed the protein gels rheologically, showing that the elastic moduli and yield stresses varied with protein concentration according to a power law. They related the power law exponent to the equivalent models by Brown (1987) and (strong link model) by Shih *et al.* (1990), and to the models by Bremer *et al.* (1989, 1990). By the value of the exponent measured experimentally, they were able to calculate fractal dimensions according to the various models. The fractal dimensions so calculated were all in reasonable agreement with those measured by the dynamic light scattering experiments. Therefore, these researchers concluded that there was no basis for the validity of one model versus another, based on their experiments. This partly stemmed from their inability to measure the chemical length exponent or tortuosity. In this work, they assumed x had a value which varied between 1.0 and 1.3 (suggested by Shih *et al.* (1990) based on conductivity measurements).

Hagiwara *et al.* (1997, 1998) have analyzed a number of different types of protein gels using both rheological measurements to study the elasticity of the gels, and analysis of confocal laser scanning microscopy images of the gels, to study the structure of the gels. These researchers found that for the gels they studied, the weak link regime of Shih *et al.* (1990) was valid. The gels demonstrated a power-law dependence on particle volume concentration, and the fractal dimensions calculated from the power law exponent, using the weak link formulation, agreed very well with fractal dimensions calculated from image-analysis of the confocal laser scanning micrographs of the gels. Therefore, both the strong link formulation and the weak link formulation of Shih *et al.* (1990) have been demonstrated experimentally. The weak link has been demonstrated more convincingly, since with the strong link regime, experimentalists have had to assume a value for the tortuosity of the backbone, and therefore the theory could not be tested well against those of Bremer *et al.* (1989, 1990).

D. APPLICATION OF SCALING THEORY DEVELOPED FOR COLLOIDAL GELS TO FAT CRYSTAL NETWORKS

In 1992, Vreeker *et al.* (1992b) presented an interpretation of rheological data for aggregate fat networks in the framework of scaling theories developed for colloidal gels. These authors showed that the storage modulus of the network (G') varied with solid fat content (Φ_{SFC}), according to a power law, similar to that predicted by models for the elasticity of colloidal gels. We have used the symbol Φ_{SFC} for the solid fat content of the fat network to distinguish it from the particle volume concentration Φ, since these two parameters are not equivalent, but in the Vreeker *et al.* (1992b) paper and in many such publications following, these two parameters have been used as being equivalent. As will be demonstrated in Section III of this publications, Φ_{SFC} and Φ are directly proportional to each other, however. The article by Vreeker *et al.* provides an interpretation of rheological data for low Φ_{SFC} fats in terms of the strong link model of Shih *et al.* (1990), developed, as is detailed above, for colloidal gels at low particle concentrations. From this rheological investigation of the fat network, a fractal dimension could be calculated, using the strong link formulation given by Eqn (22), and assuming that the tortuosity of the system, x, had a value between 1 and 1.3. This article also details the measurement of a fractal dimension of the network via light scattering methods, which agreed well with that calculated from the strong link formulation. However, no attempt was made in this article to show that the structure of a fat crystal network at such low solid fat contents (low Φ_{SFC}) is organized in a similar manner to the way a colloidal gel is organized, in order to warrant the use of the strong link formulation. It was unclear as well, in this article, what the primary particles of the gel constituted, and at what length scales the network was fractal (although the fact that light scattering methods were used to calculate the fractal dimension suggests that perhaps the length scales of importance lay in the microstructure region, i.e., at a length scale greater than the crystalline level of structure). Therefore, this article served to demonstrate solely that the elastic constant of the network varied in a power law manner, reminiscent of that demonstrated by colloidal gels. No justification for using the strong link model was made from a structural perspective, mainly because these authors did not adequately define the structure of the network. However, this article remains one of the most important developments in the field, for it demonstrated conclusively that the storage modulus of low Φ_{SFC} fat crystal networks scale in a power law fashion with the solid fat content. The physical and structural implications of the calculated fractal dimension using the strong link formulation of Shih *et al.* (1990) was at this point unclear.

The analysis of Vreeker *et al.* was interesting enough for Marangoni and Rousseau (1996) to apply the model developed by Shih *et al.* (1990) for high concentration colloidal gels (weak-link theory described above) to fat crystal networks of high solid fat concentration. As is explained above, the weak link model offers the ability to relate small deformation rheological measurement (shear storage modulus) to the fractal dimension of the network. As was the case with the work by Vreeker *et al.* (1992b), Marangoni and Rousseau had no structural basis upon which to justify the application of the weak link theory, developed for a particular geometry of colloidal aggregates, to fat crystal networks. The main reason for applying this type of analysis was the fact that the analysis by Vreeker *et al.* (1992b) produced a power-law relationship for low solid fat content fats. Additionally, as described before, the only variation of structure that accompanied the decrease in hardness index and elastic moduli of milkfat upon chemical interesterification, was a change in the microscopically observed microstructure. Marangoni and Rousseau (1996) attributed the weak link model with a quantification of the microstructure of the network, but offered no explanation as to why the fractal dimension calculated from the application of the weak link theory was a quantification of microstructure. However, the rheological application of the weak link theory of Shih *et al.* (1990) to NIE and CIE milkfat blends demonstrated a power law relationship between the shear elastic moduli of the networks and the solid fat content of the networks, given by $G' \sim \Phi^u$. Fractal dimensions calculated using the weak link theory produced fractal dimensions of 2.46 and 2.15 for the NIE milkfat and CIE milkfat, respectively. Given that there was a qualitative change in microstructure upon chemical interesterification, and that there was a large change in the fractal dimension of these gels upon application of the weak link theory, it did indeed seem possible that the fractal dimension was a measure of microstructure, in some undefined manner. At any rate, Marangoni and Rousseau (1996) attributed the change in structure indicated by a change in fractal dimension to the change in hardness of the milkfat upon chemical interesterification, a reasonable conclusion. In defense of the claim by Marangoni and Rousseau (1996) that the fractal dimension was in some manner a quantification of microstructure, it must be recalled that Vreeker *et al.* (1996) utilized dynamic light scattering measurements to calculate a fractal dimension that agreed well with their rheological analysis, therefore suggesting that the structures that were indeed fractal are in the microstructural range.

Following their 1996 work, Rousseau and Marangoni (1998b) utilized the weak link model to analyze the rheological behavior of non-interesterified (NIE) milkfat and enzymatically interesterified milkfat (EIE). The fractal dimension of milkfat changed from 2.59 to 2.50 upon

interesterification. However, there was also a large decrease in solid fat content upon enzymatic interesterification, so that the drop in hardness index and shear elastic moduli observed by these authors was not entirely due to the decrease in fractal dimension. However, here again, the rheological scaling behavior was observed, and fractal dimensions could be calculated from the weak link formulation. One is reminded by the results of this study that indicators of macroscopic mechanical properties such as solid fat content are indeed valid and necessary for a comprehensive description of the mechanical properties of the network, although as in the case of the CIE and NIE milkfat samples detailed earlier, such variables are not always direct indicators of changes in mechanical properties.

Marangoni and Rousseau (1998b) also studied the rheological scaling behavior of non-interesterified (NIE) and chemically interesterified (CIE) lard-canola oil blends and palm oil-soyabean oil blends. The power law relationship of storage modulus to solid fat content was again observed, and fractal dimensions could be calculated for all the systems, by using the weak link formulation. No change was observed in hardness index or storage modulus of the palm oil-soyabean oil blends upon chemical interesterification, and neither were there any changes in the fractal dimension upon chemical interesterification. Solid fat content did not change upon chemical interesterification either. Therefore, it seems that indeed the fractal dimension was an indicator of macroscopic hardness: whether this was true because it was an indicator of the microstructure could not reasonably be extrapolated from the evidence presented by Marangoni and Rousseau (1998b). The hardness index and elastic moduli of lard increased upon chemical interesterification, but the fractal dimension did not change, neither did the solid fat content. It therefore seems at first glance that not only is the solid fat content an insensitive indicator of macroscopic hardness, but so is the fractal dimension. Here again, one is reminded that there are many structural indicators of macroscopic mechanical properties, and one must consider them all in concert. However, are there other indicators of hardness that can be accessed through the rheological analysis? At this point, it is perhaps important to briefly examine the method of rheological analysis used by these authors. The weak link theory of Shih *et al.* was tested by plotting $\ln(G')$ as a function of $\ln(\Phi_{SFC})$ for various fat systems. According to the weak link theory of Shih *et al.* (Eqn (24)) the slope of such a plot should yield (1/3–D). What about the intercept of the graph? Marangoni and Rousseau (1998b) wrote Eqn (24) as:

$$G' \sim \gamma \Phi^{\frac{1}{3-D}} \tag{25}$$

and defined γ as a constant which is related to the particles which make up the network. In this, Marangoni and Rousseau were influenced by Bremer *et al.* (1990), who in their publication, formulated a similar law, where the pre-exponential factor was a constant depending on the nature of the particles and the links between them. Equation (25) bears further scrutiny at this point – it should be evident that Eqn (24) may be written as:

$$G' \sim \Phi^{\frac{1}{3-D}} K_l \tag{26}$$

where, as the reader would recall, K_l is the elastic constant of the links between aggregates. Certainly, therefore, K_l would depend on the nature of the particles and the links between them, and would contribute to the value of γ. Although Marangoni and Rousseau (1998b) did not offer this justification for their description of the constant γ, it however seems to be appropriate. At any rate, the intercept of the $\ln(G')$ vs. $\ln(\Phi_{SFC})$ graph should yield $\ln(\gamma)$ as the intercept, allowing a value of γ to be calculated. Therefore, if the fractal dimension offered a quantification of the spatial distribution of the microstructure (as yet undefined how), then the constant γ contained information on the influence of the particles and the links between them on the elastic constant of the network. Now, on chemical interesterification, there was a four-fold increase in the value of the constant γ for the lard-canola oil system which, according to Eqn (25), should have been accompanied by an increase in the storage modulus, as was observed experimentally by Marangoni and Rousseau. As for the palm oil-soyabean oil system, there was comparatively no change in the value of γ. Therefore, the scaling behaviour of the fat crystal network, if the weak link is utilized, seems to suggest that there are three important indicators of macroscopic hardness: solid fat content, the fractal dimension, and the constant γ. It must be stated at this point that this does not mean that other indicators such as the crystalline nature of the network and the molecular ensemble of the network is being ignored by identifying D, Φ, and γ as the three important indicators. Since γ has been suggested to depend on the nature of the particles and the links between them, it almost certainly is dependent on the polymorphism of the network, which in turn is dependent on the molecular composition of the network.

E. NETWORK MODELS

As presented above, phenomenological investigations have been made on the rheology of fat crystal networks, the results of which have been interpreted by models developed for colloidal gels. Not only has this not

been structurally justified, but this analysis excluded any structural and mechanical model of the fat network. In large part, the authors working in the field (mainly Marangoni and Rousseau *et al.* and Vreeker *et al.*, detailed above) could not include a structural and mechanical model of the network, since there existed at the time no mechanical and structural model that predicted that the structure of the fat crystal network at any length-scale was fractal in nature. It must also be mentioned that the scaling behavior demonstrated experimentally by these authors was not adequately explained by the existing network models. Presented below is a brief introduction to the network models that existed in the literature before the work to be detailed in this publication.

Early work on a network model was performed by van den Tempel (1961). In his 1961 publication, he suggested modeling the network as a collection of particles held together by van der Waals-London forces. The structural model that was assumed by van den Tempel was that the network is made up of straight chains oriented in three mutually perpendicular directions, each chain consisting of a linear array of particles. The bonds between particles were formed from van der Waals-London forces. The relationship of the storage modulus to the solid fat content of the network arrived at by van den Tempel is:

$$G' = \frac{5AD^{0.5}\Phi_{SFC}}{24\pi H_o^{3.5}} \tag{27}$$

where A is the Hamaker's constant, D is the diameter of the particles, H_o is the equilibrium distance between particles, and Φ_{SFC} is the solid fat content.

The relationship of G' to Φ_{SFC} is a non-linear, power-law type of relationship, as was experimentally verified by the researchers detailed in subsection D above. The work by van den Tempel failed to predict correctly this experimentally observed power law relationship of G' to Φ_{SFC} because, according to Vreeker *et al.* (1992b), it did not take into consideration the fractal arrangement of the network at certain length scales. Furthermore, van den Tempel only considered the attractive forces in his treatment, choosing to ignore whatever repulsive forces were present.

In 1963 Nederveen (1963) used the same structural model as van den Tempel, but incorporated the repulsive forces acting between particles (he considered the Lennard-Jones potential between two particles). Nederveen found the following formula for the modulus of elasticity:

$$E = \left(\frac{A\Phi_{SFC}}{2\pi d_o}\right)\left(1 - \frac{11R\varepsilon}{d_o^2}\right) \tag{28}$$

where R is the particle radius, ε is the strain of the deformation, d_o is the equilibrium distance between two particles, and A and Φ_{SFC} are as defined earlier. Again, Nederveen's formulation failed to show the non-linear dependence on Φ_{SFC}, due perhaps to an unrealistic structural model of the network which did not involve the fractal geometry claimed by the authors detailed in subsection D above.

In 1964, Payne (1964) tried to apply the linear chain concept of van den Tempel to carbon black network in oil, but found that the shear modulus was inversely proportional to some power of the particle diameter, not in agreement with van den Tempel's or Nederveen's equation. This study may however be inconclusive about the validity of these equations, since the discrepancy may have been due to the non-homogenous distribution of the carbon black spheres.

In 1968, Sherman (1968) proposed a different model for flocculated o/w emulsions involving chain-like configurations which form coils with cross-linkages, resulting in interlinked spherical structures. In this model, localized regions of densely packed particles are joined to less densely packed regions, consequently the degree of interlinking is not the same throughout the entire flocculate. The formulation of G' for this model is:

$$G' = \Phi_{SFC}(1 + 1.828v)\frac{A}{36\pi D^3 H_o^3} \tag{29}$$

where v is the total volume of the continuous phase held in voids between the particles, D is the diameter of the particles, H_o is the minimum equilibrium distance between particle surface and A is called the interaction constant (Hamaker's constant) and Φ_{SFC} is as defined above. Whilst Sherman's equation agreed with Payne's observations in terms of particle diameter, it also shows a linear relationship with Φ_{SFC}, contrary to what has been demonstrated experimentally.

In 1979, van den Tempel (1979) revised his structural model of fat crystal networks; he suggested that clusters (microstructures) of particles make up the chains, rather than particles. Additionally, he suggested that the forces holding the clusters together were due to common "chains" of particles between clusters. He used this argument to modify his original equation, but again did not take into consideration any fractal arrangement of the network. Various other researchers have tried to modify van den Tempel's work, in varying degrees of complexity (Kamphuis and Jongschaap, 1985; Kamphuis *et al.* 1984; Papenhuijzen, 1971; Papenhuijzen, 1972). However, none of these models took into consideration a fractal arrangement of the network, and none demonstrated a power-law dependence of G' on Φ_{SFC} as is observed experimentally.

III. WHERE LIES THE FRACTALITY IN FAT CRYSTAL NETWORKS?

In this chapter, the structure of fat crystal networks at the microstructural level will be investigated and discussed. It has been detailed in Section II that other authors have attributed some amount of importance to the microstructure of fats. Particularly, the microstructure will be investigated so as to determine whether there is a structural organization present which warrants the application of the weak link theory developed for colloidal gels to fat crystal networks. Furthermore, since the microstructure of fat networks have been rather loosely characterized before this work, effort will be made to utilize a number of different imaging techniques to attempt to provide a description of the network at the microstructural level that is supported by various types of microscopical evidence.

A. CHARACTERIZING MICROSTRUCTURE

Figure 9(A) and (B) show SEM micrographs of anhydrous milkfat with the liquid oil not removed. The entire network, however, has been frozen and then sputter-coated. As is evidenced by the figures, it is difficult to tell which part of the structure is due to liquid oil and which to solid crystals. However, there does seem to be evidence of some type of repeating structure at the 30 μm range. Figure 10 shows a sample of chemically interesterified milkfat from which the liquid oil was not removed. Two structures are shown in this figure, which seem to be in the range of 50–60 μm, and since this surface image is a fracture surface, these structures seem to belong to spherical structural entities in the fat. It however cannot be ascertained whether the area around the two entities is frozen oil or also are of crystalline nature. The fracture plane being imaged here also does not necessarily pass through the equator of these entities. Therefore, these entities may actually be larger than represented. Figure 11 shows a micrograph from a sample of chemically interesterified milkfat, from which the liquid oil has not been removed. This micrograph shows a structural entity that is approximately 6 μm across, and which may be spherical-like. Not much else can be determined from this micrograph. Micrographs of SEM images of fat are very typical of the images shown here. In other words, nothing definitive can be said about the structure of the fat network from such images in most cases, due to the destructive sample preparation methods necessary for SEM imaging.

Figure 12(A) shows polarized light micrographs of anhydrous milkfat, where the network has been broken and dispersed in paraffin oil (Narine, 2000). The figure demonstrate dense "particles" (which seems to be composed of smaller crystallites) and clusters of three or more of these

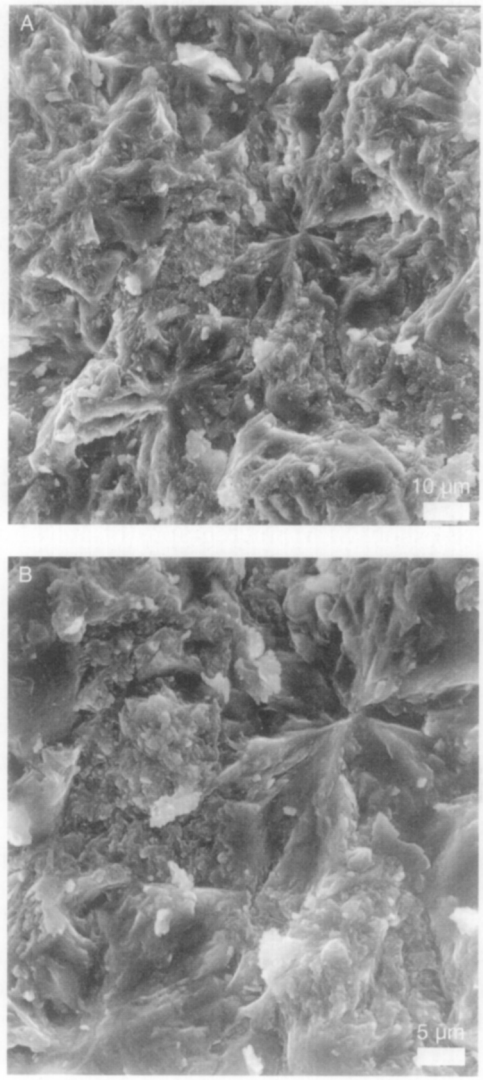

FIG. 9 Scanning electron microscopy images of anhydrous milkfat, with the liquid oil in the samples not removed.

particles which have been unbroken. The "particles" seem to be of the order of 3 µm to 4 µm. It seems likely that these particles once belonged to larger clusters, but the dispersing process allowed them to be separated. Figure 12(B) shows a similar image, of palm oil. The "particles" in the palm

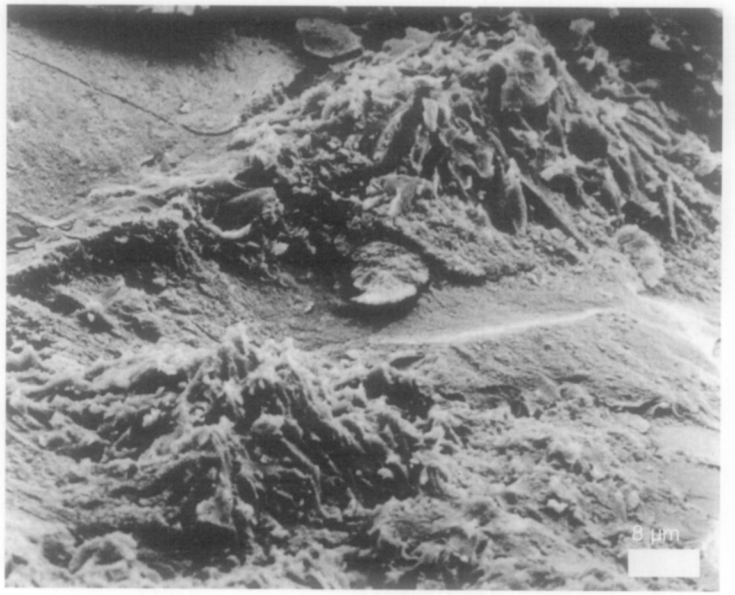

FIG. 10 Scanning electron microscopy image of chemically interesterified milkfat with the liquid oil not removed.

oil are approximately 2.5–3.0 µm, and there is also evidence of clustering. Therefore, although the network has been broken in an uncontrolled manner, there seems to be some amount of similarity in the structure demonstrated by the different fats imaged by this method. At this stage, there seems to be clusters of smaller entities which we have referred to up till now as "particles" and these clusters themselves seems to belong to even larger clusters. Given the evidence provided by Heertje and co-workers (Heertje *et al.*, 1987; Juriaanse and Heertje, 1988; Heertje, 1993) which demonstrated that clusters as large as 100 µm are possible, this emerging picture of the network is at least plausible.

Figures 13 and 14 show confocal laser scanning micrographs of the crystal network of milkfat at 18°C. The samples were negatively stained with Nile Blue, causing the solid crystals to appear as darker entities in the micrographs. It must be mentioned here that it is uncertain how the presence of Nile Blue affects the formation of the network itself. Additionally the solid crystalline material may appear to have tendrils that are actually as a result of solid particles being covered by liquid oil stained by the Nile Blue. Figure 13 suggests that there are clusters present of the order of 30 µm. One must bear in mind that the individual "particles" are not present in this

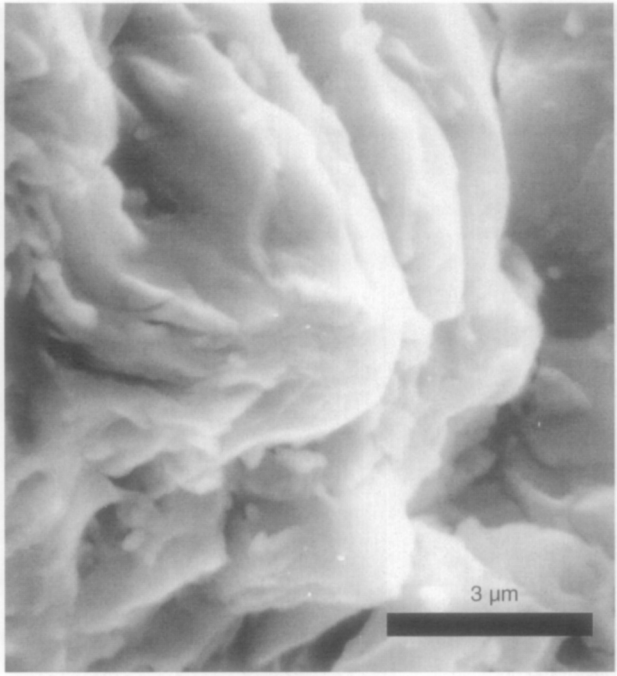

FIG. 11 Scanning electron microscopy image of chemically interesterified milkfat, with the liquid oil in the sample not removed.

figure, since here the network is being observed at a lower magnification. Furthermore, it is seen that these clusters are part of an even larger cluster, of the order of 70 μm. Interestingly, the intermediate clusters seem to pack in the same manner as the "particles" did in the clusters shown in the PLM images of Figure 12. Therefore, the network seems self-similar at these different length scales represented in Figures 12 and 13. This is important, and will be developed later in this Section. The evidence proposed by Figure 13 also is in agreement with the observations of Heertje and co-workers, since they have reported cluster sizes of 100 μm in milkfat. Although the size of the large cluster in this micrograph is approximately 70 μm, this disparity in size compared to the work of Heertje and co-workers could be dependent on the focus depth of the confocal microscope. It must be remembered that a confocal image is a two-dimensional slice of the network. Figure 14(A) and (B) serve to reinforce the arguments made above. Interestingly, the observations made above are also supported by the SEM images shown in Figures 9, 10 and 11. The structural entities

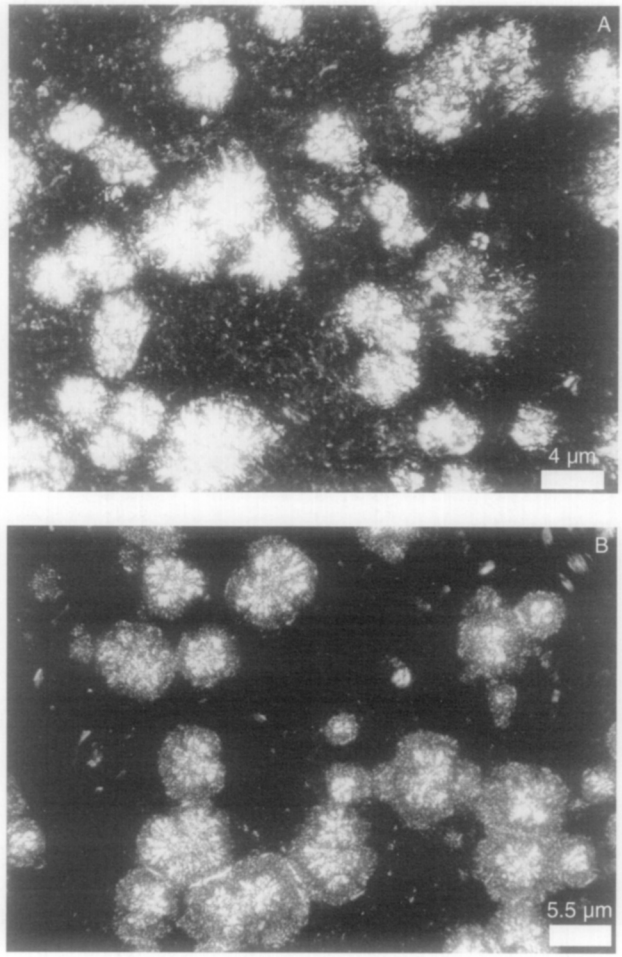

FIG. 12 Polarized light microscopy images of (A) anhydrous milkfat, and (B) palm oil. The network has been broken and dispersed in paraffin oil.

shown in Figure 9 are almost certainly clusters of intermediate size (recall they were of the order of 30–40 microns in size) and the larger structures shown in Figure 10 are almost certainly the large clusters – i.e. clusters of clusters. The "particle" shown in Figure 11 is also of a similar size to the particles seen in both the polarized light micrographs shown in Figure 12. Therefore, the emerging picture of the structural arrangement of the fat crystal network at the microstructural scale has been consistent in the three different methods of imaging so far discussed.

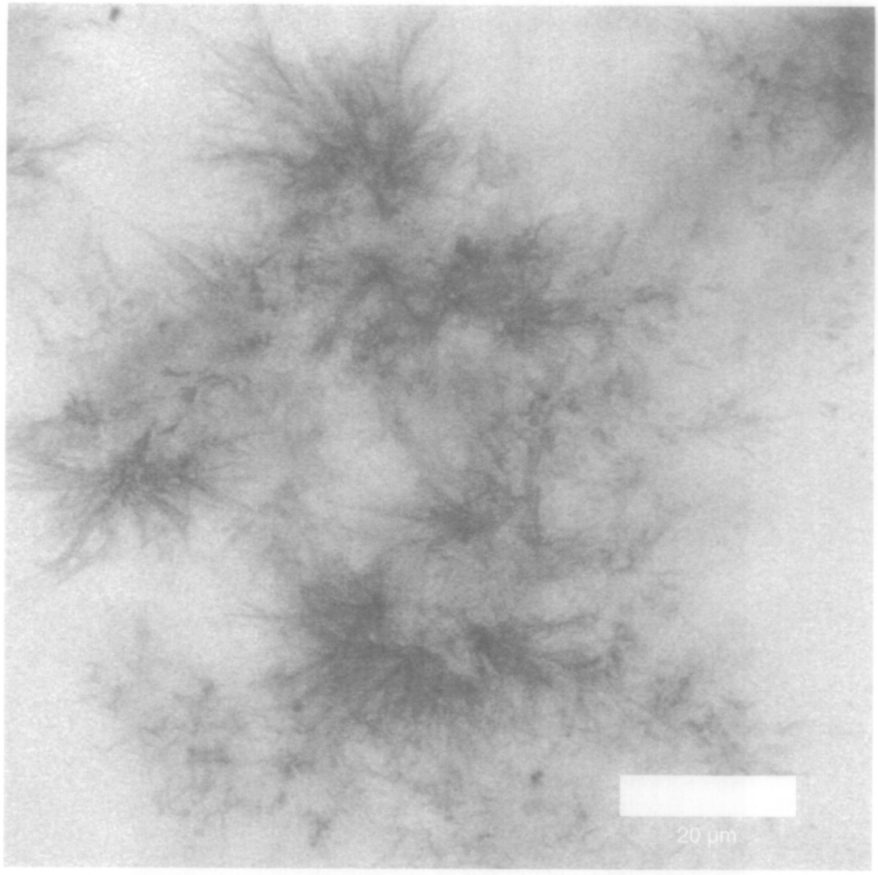

FIG. 13 Confocal laser scanning microscopy images of milkfat stained with Nile Blue.

Figure 15 shows a composite of atomic force microscopy images of a sample of the high melting fraction of milkfat that was spin coated onto a silicon substrate. Figure 15(A) shows what appears to be a "particle" of the order of 4–5 µm. The edges of this particle are not well defined, probably due to the nature of the atomic force microscope's method of imaging. It is difficult to effectively define the boundaries between closely spaced particles, since the vertical range of the atomic force microscope is limited – therefore, rather than define a definite boundary, the tip of the microscope will instead indicate a low point in the image, which may appear as an intermediate depth. Total darkness in these images represent the limit of the tip's vertical displacement, whilst the whitest colour in the

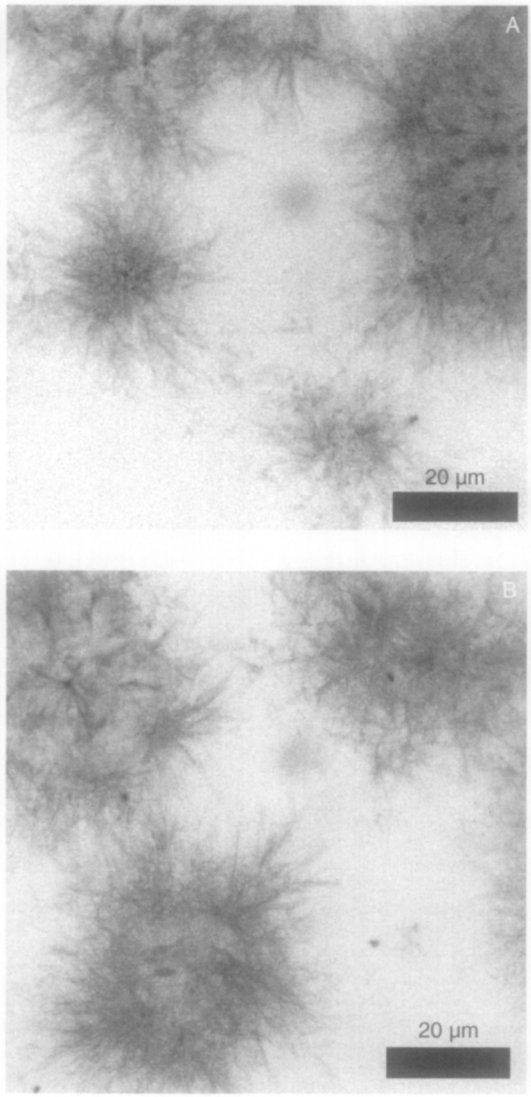

FIG. 14 Confocal laser scanning microscopy images of milkfat stained with Nile Blue.

image represents the highest point in the image. Figure 15(B) identifies at least three neighbouring "particles" of the same average size. Figure 15(C) and (D) show intermediately-sized clusters of particles, whilst Figure 15(E) shows what appears to be a section of a large cluster of the order of

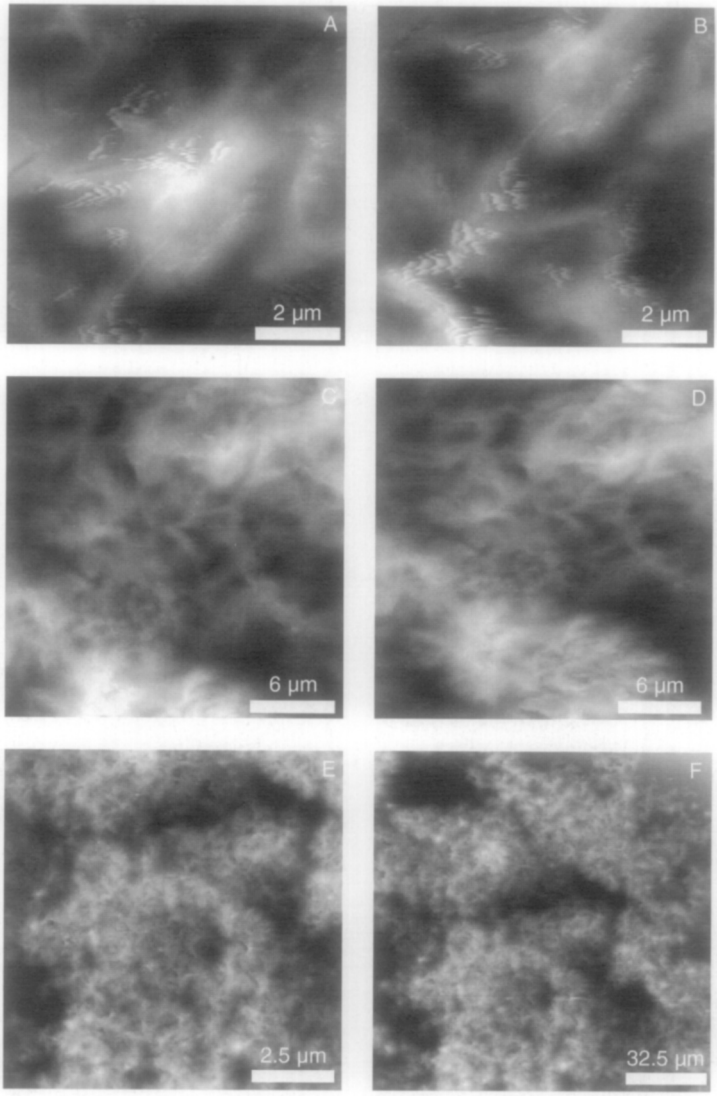

FIG. 15 Atomic force microscopy images of the high melting fraction of milkfat. Sample was spin-coated onto a silicon substrate.

90–100 μm. Figure 15(F) shows what appears to be the boundary between two or three large clusters. All of these images were imaged on the same sample, with Figure 15(E) being taken over a spot immediately adjacent to the spot over which Figure 15(F) was taken. Figure 15(D), (C), (B), and

(A) are all within the area shown in Figure 15(E). Figure 16 shows a composite of images taken of the same sample as Figure 15, except that these images were taken over a different spot on the surface of the sample. As can be seen, similar types of structure as described above are observed. Figure 17 is of the high melting fraction of milkfat as well, only this sample was prepared in a rheological mould rather than spin-coated onto a silicon substrate, as were the samples shown in Figures 15 and 16. As can be seen, this image is in agreement with Figures 15 and 16, except that at the low magnifications (i.e. for Figure 17(D), (E) and (F)) there are a series of very high, round spots. It is believed that these spots are due to wax particles found on the samples that were prepared in the rheological moulds (part of the process requires the sandwiching of the fat samples by Parfilm, which may have been contaminated with dust or wax crystals), since these

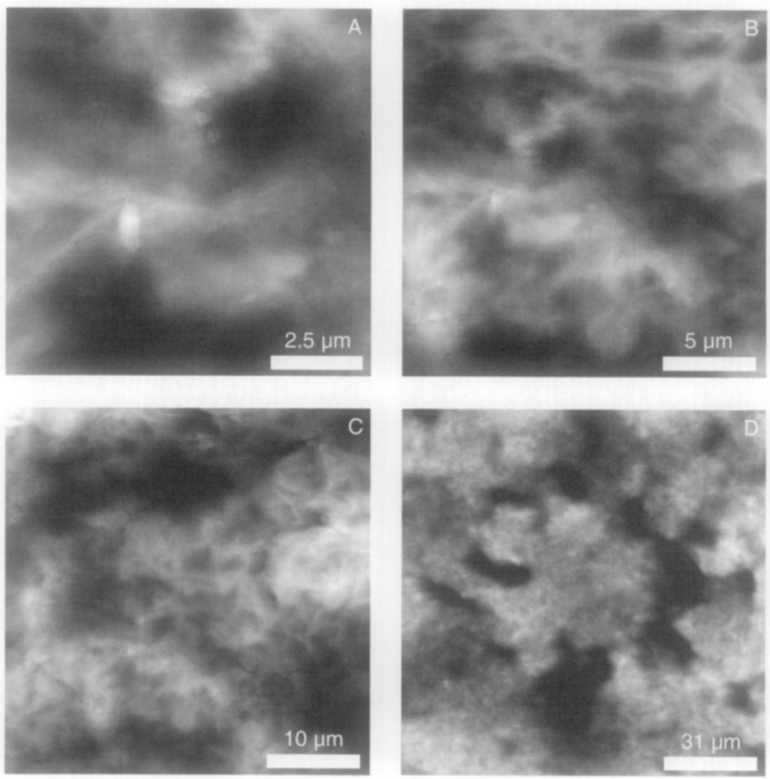

FIG. 16 Atomic force microscopy images of the high melting fraction of milkfat. Sample was spin-coated onto a silicon substrate.

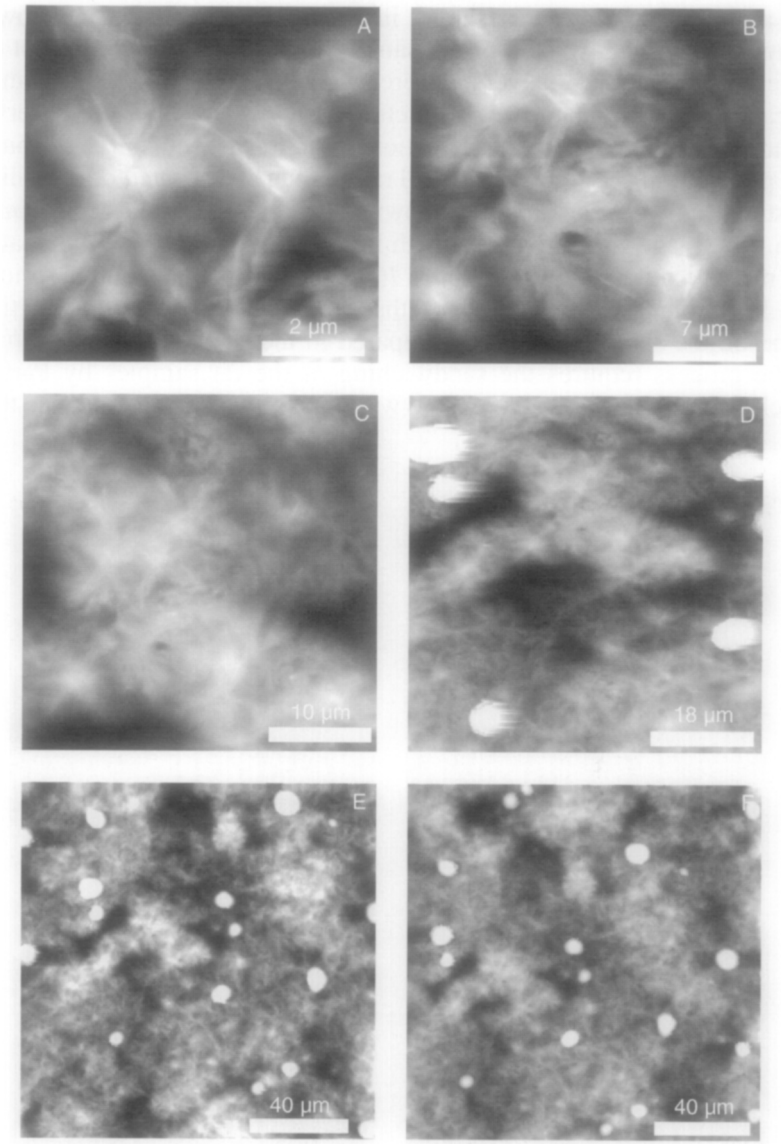

FIG. 17 Atomic force microscopy images of the high melting fraction of milkfat. Samp was prepared in a rheological mould.

types of spots were observed with all the samples prepared in the moulds. What is also important to note in Figures 15, 16 and 17, is that the structures at different magnifications, i.e. at different length scales, look quite similar. These structures seem to demonstrate some sort of statistical self-similarity at different length scales, bounded by the size of one "particle" and the size of one large cluster (since as we shall see from other images to be presented in this section and from Heertje's and co-workers publications, the large clusters pack in a regular space-filling manner to form the network). Identification of self-similarity in natural structures is usually a rather qualitative process (due to the inexact nature of the self-similarity) such as the realization that clouds and trees are self-similar. However, this process is usually the first physical clue that the object under scrutiny may be fractal in nature – for example, Figure 18 shows the qualitative self-similarity of a cauliflower, which is a typical natural fractal. Figure 19 show AFM images of a sample containing a 50:50 mixture of the high melting fraction of milkfat (HMF) and the medium melting fraction (MMF) of milkfat, spin coated onto a silicon

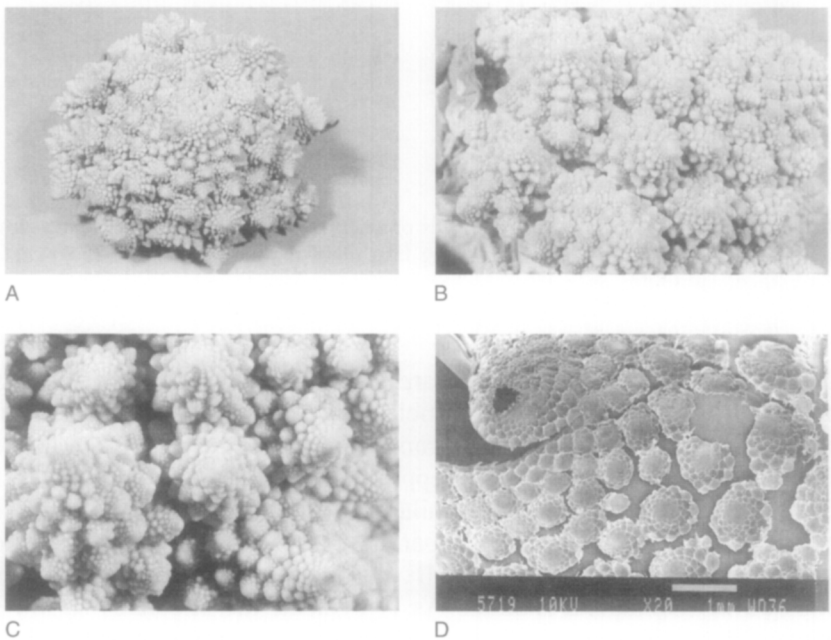

FIG. 18 (A–C) Photographs of a Minaret cauliflower showing self-similarity at different length scales. (D) Electron micrograph (SEM) of Alverda cauliflower on sub-millimeter scale (adapted from Grey and Kjems, 1989).

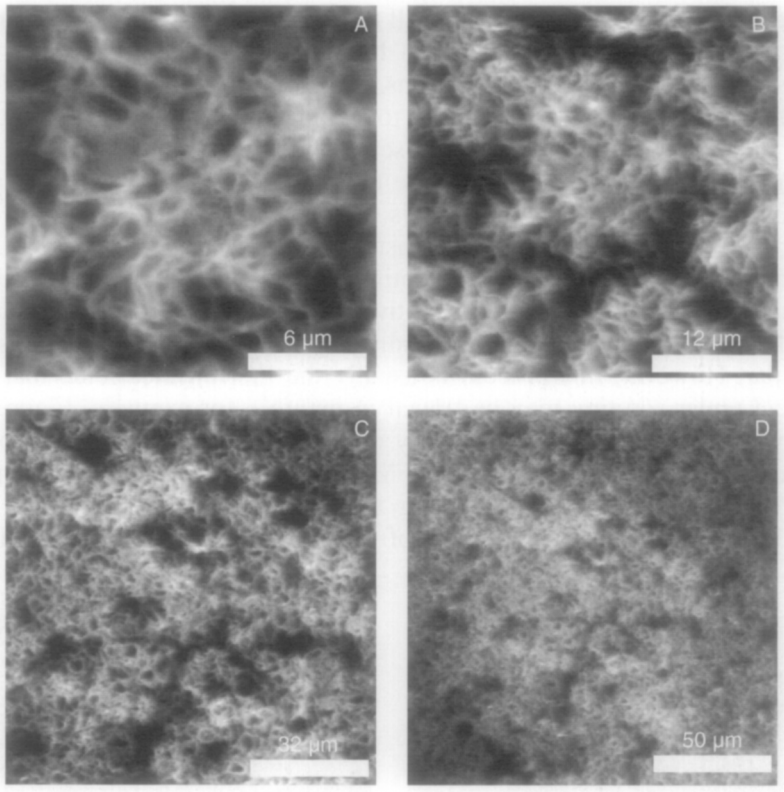

FIG. 19 Atomic force microscopy images of a 50:50 w/w mixture of the high melting fraction of milkfat and the medium melting fraction of milkfat. Sample was spin-coated into a silicon substrate.

substrate. Again, these structures are very similar to those of the high melting fraction – individual particles (not very defined, for reasons mentioned above) seem to be arranged in clusters, which are further arranged into one large cluster (of approximately 100–125 μm), shown in Figure 19(D). As well, the self-similarity of the structure at the different magnifications shown is readily apparent. Figure 20 shows composites of a 50:50 mixture of HMF and MMF, but in this case the samples were prepared in rheological moulds. As is evident, the structures shown in Figures 19 and 20 are quite similar, except for the appearance again of the suspected wax particles. As well, the self-similar nature of the structure at different magnifications is evident. Figure 21 show AFM images of a sample containing a 70:30 mixture of the high melting fraction of milkfat

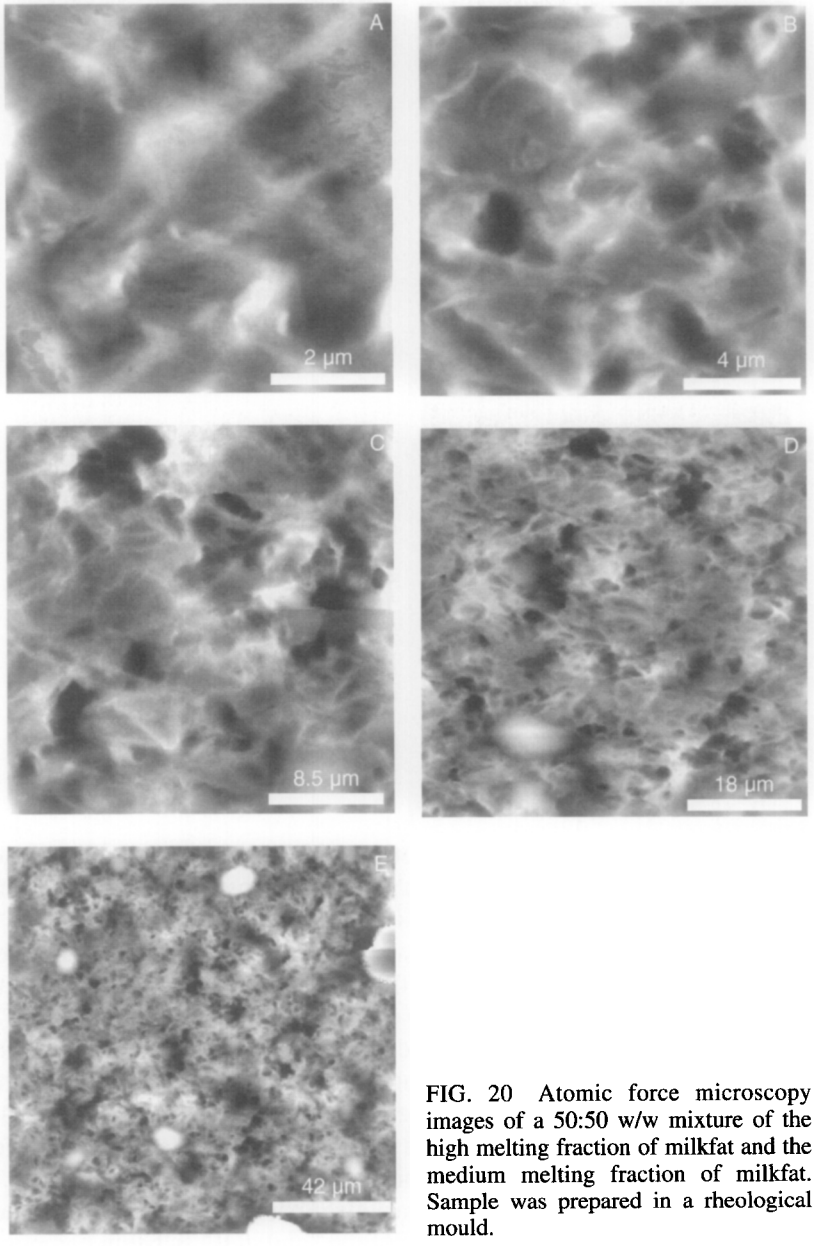

FIG. 20 Atomic force microscopy images of a 50:50 w/w mixture of the high melting fraction of milkfat and the medium melting fraction of milkfat. Sample was prepared in a rheological mould.

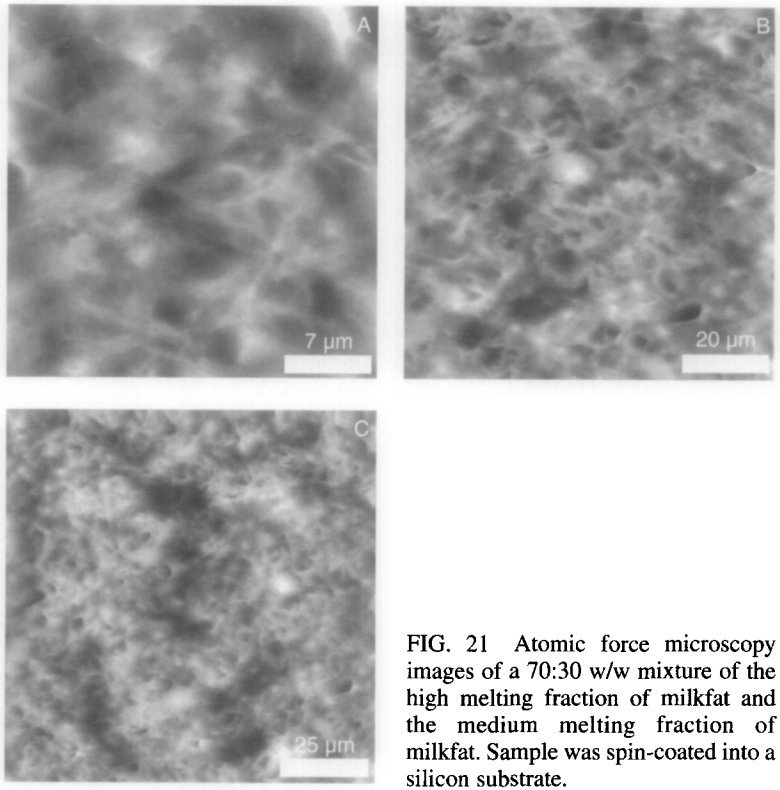

FIG. 21 Atomic force microscopy images of a 70:30 w/w mixture of the high melting fraction of milkfat and the medium melting fraction of milkfat. Sample was spin-coated into a silicon substrate.

(HMF) and the medium melting fraction (MMF) of milkfat, spin coated onto a silicon substrate. The structures shown demonstrate the same general organization as the other AFM images, and again the self-similar nature of the structures at all length scales within a large cluster (the smallest magnification, Figure 21(C) is still within an entire large cluster) is evident. Figure 22 shows AFM images of cocoa butter. Figure 22(A) is interesting in that it represents a level of magnification not shown previously in any of the AFM images. This level of magnification is showing structure that are within the "particles." The image suggests that the "particles" are composed of intertwined and sintered crystalline material, a picture which is reinforced by the polarized light micrographs shown in Figure 12.

Figure 22(B) shows the familiar "particles" packed fairly close together, and again in this image, the appearance of the "particles" as being composed of intertwined crystallites is reinforced. Figure 22(C) is a rather poor image at a lower magnification, which is however suggestive of the clustering of intermediately-sized clusters. It is unfortunate that current atomic force

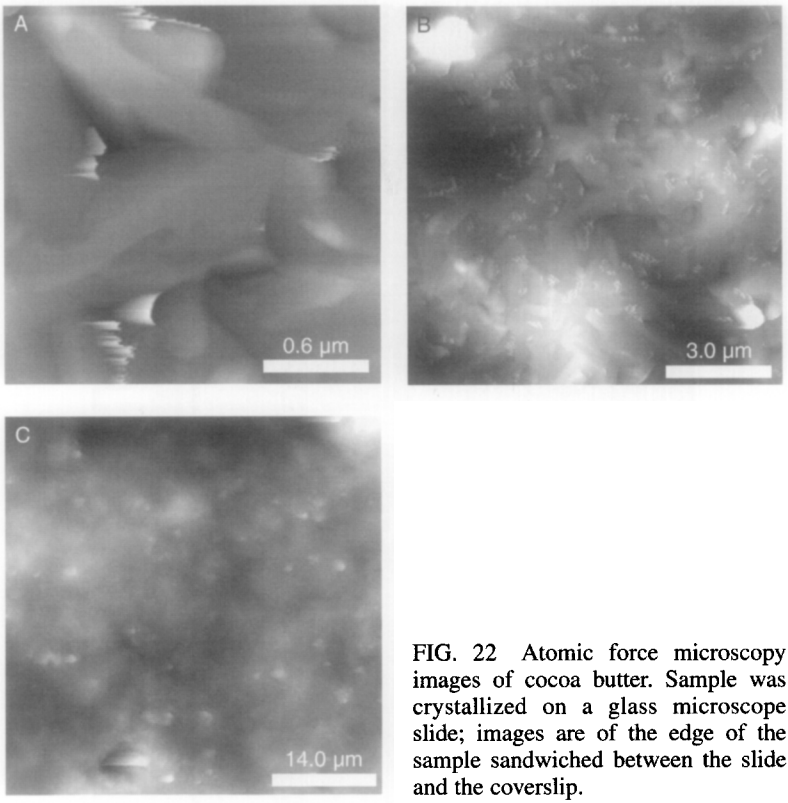

FIG. 22 Atomic force microscopy images of cocoa butter. Sample was crystallized on a glass microscope slide; images are of the edge of the sample sandwiched between the slide and the coverslip.

microscopes are not capable of a lateral range of scan much greater than 150 μm. As a result, using this method, it is very difficult to image two or more of the large clusters reported by Heertje and co-workers and seen in the confocal images. However, some of the images do indicate the presence of these large clusters, although it is obviously not possible to assign to these structures a finite size, shape and regularity of packing. It is conceivable that one may be able to perform adjacent scans of a surface and then reconstruct these images to represent the packing of a large area on the sample, but this procedure is not straightforward, due to the severe hysteresis found in the piezoelectric crystal drives of the atomic force microscope. However, the atomic force images presented here supports well the structural organization suggested by the other forms of microscopy outlined so far.

Figures 23 and 24 show *in-situ* polarized light micrographs of four different fat systems (microscopy method given in Narine, 2000). It is

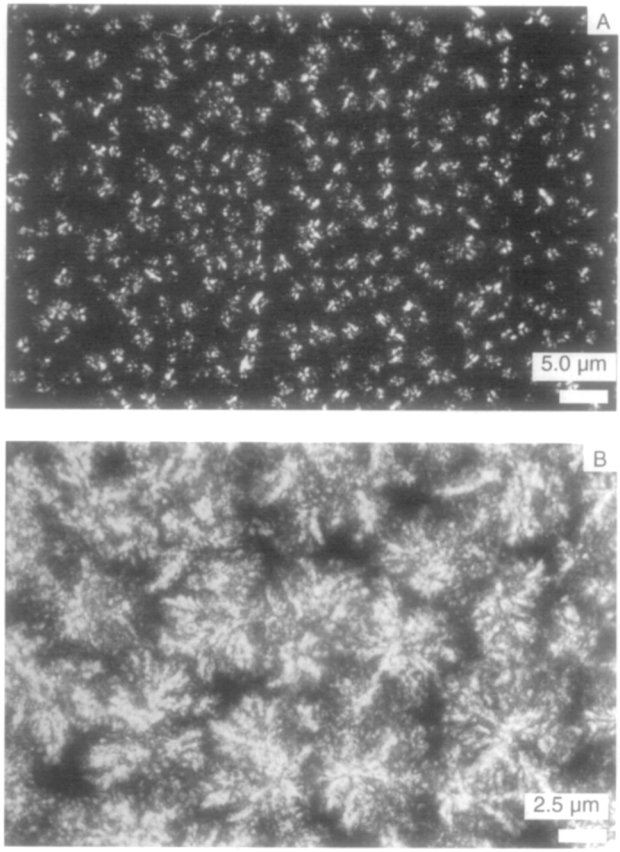

FIG. 23 *In-situ* polarized light microscopy images of (A) tallow at 5°C and (B) a 50/50 w/w mixture of the high melting fraction and the medium melting fraction of milkfat at 20°C.

important to discuss what these figures represent before we begin a discussion of the structures that are represented in them. Firstly, the maximum field of view represented in these images is approximately 65 μm – so therefore from all the evidence presented above, we are likely looking at an area which would be covered normally by two or three intermediate clusters. Secondly, these images are of the *in situ* network, and have a definite depth. Since the images have been deliberately made very thin, this depth is not significant enough to attenuate appreciable amounts of the light passing through, and therefore the image presented is not totally opaque, but gives a good representation of all the "particles"

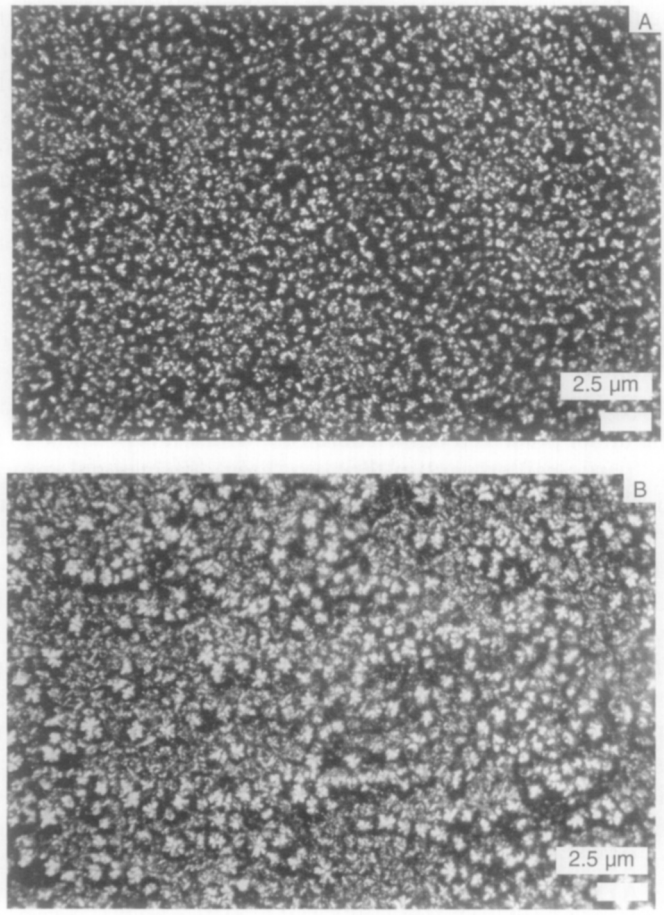

FIG. 24 *In-situ* polarized light microscopy images of (A) palm oil at 5°C and (B) lard at 5°C.

present – both in the depth of the sample as well as in the focal plane of the microscope. Care was taken to focus on those "particles" at the top of the sample, and those particles in the depth of the sample are therefore represented as out-of-focus entities that appear smaller than their actual size and as higher levels of grey than the in-focus particles which appear as higher levels of white. Since the depth of the samples are represented here, it is not possible to identify the boundaries of intermediate clusters that may be present – since if those were present, the boundaries would most likely be rendered indistinct due to the presence of particles

belonging to other clusters in the depth of the sample, which are not at the same x–y coordinates of the clusters in focus. Therefore, the field of view is representative of *all* "particles" in the thin three-dimensional sample, except for those in direct geometrical shadow of "particles" in focus. Now, since the images are due to the refraction of polarized light through the anisotropic crystalline nature of the "particles" only part of a typical particle will be visible – however, by rotating the polarizer by 45 degrees, it is possible to render those parts of the "particles" that were not visible, visible. This process of course renders the previously visible parts invisible. This process however serves to ensure that one can discern between neighbouring particles. The so-called Maltese Cross pattern is for instance due to a spherical-like "particle", but because of the orientation of the crystallites in the "particle" not all of them are visible when one looks at the particle under polarized light. Therefore, whilst it is possible to represent all of the "particles" present in the thin three-dimensional sample in the polarized light microscope image, each particle will be missing mass, some particles will appear larger than some, and some particles will appear more in-focus than some. However, the presence of all particles except those in direct geometrical shadow (negligible if the sample is sufficiently thin) may be noted, if the image is taken with some care. Figure 23 shows and *in-situ* image of tallow at 5°C. The approximate diameter one of the "particles" in focus is between 2–3 μm, and each particle appears as an image approximating a Maltese Cross pattern, suggesting that these "particles" may be spherical-like in shape. It should not be expected that the "particle" sizes agree exactly from the different methods of microscopy – for instance, the size of the "particles" (even the in-focus "particles") in the *in-situ* PLM images will be under-represented due to invisible mass. Figure 23(A) therefore, given the above discussion, is in agreement with the other forms of microscopy discussed so far, with the added fact that it is an *in-situ* image of the network. Figure 23(B) shows a similar micrograph of a 50/50 w/w mixture of the high melting fraction and the medium melting fraction of milkfat, taken at 20°C. One can identify "particles" of the order of 5–6 μm, in good agreement with the AFM images shown before of the same fat. Figure 24(A) shows "particles" in palm oil at 5°C and Figure 24(B) shows "particles" of lard at 5°C. These images are also quite similar to those of tallow and the 50/50 w/w sample of the high melting fraction and middle melting fraction of milkfat discussed before. One can easily identify that there are "particles" in the depth of the sample which are nevertheless represented in the image.

The evidence presented above by the different types of microscopy are all in agreement – the microstructure of fat crystal networks seems to be organized in hierarchical levels of structure: "particles" composed of

intertwined crystallites, of the order of 1–8 μm are organized in intermediately-sized clusters, which are packed in a similar manner to the way the "particles" pack, into large clusters of the order of 100–150 μm. Not much evidence has yet been presented of the large clusters themselves, although the work of Heertje and co-workers has been quoted, which demonstrates that the large clusters in a fat network pack in an orthodox space filling manner to form the network. Figure 25 shows the large clusters present in cocoa butter. These are of the order of 120 μm, and they were imaged by diluting the network with 50% canola oil, thereby allowing the large clusters to separate and become discernible under a polarized light

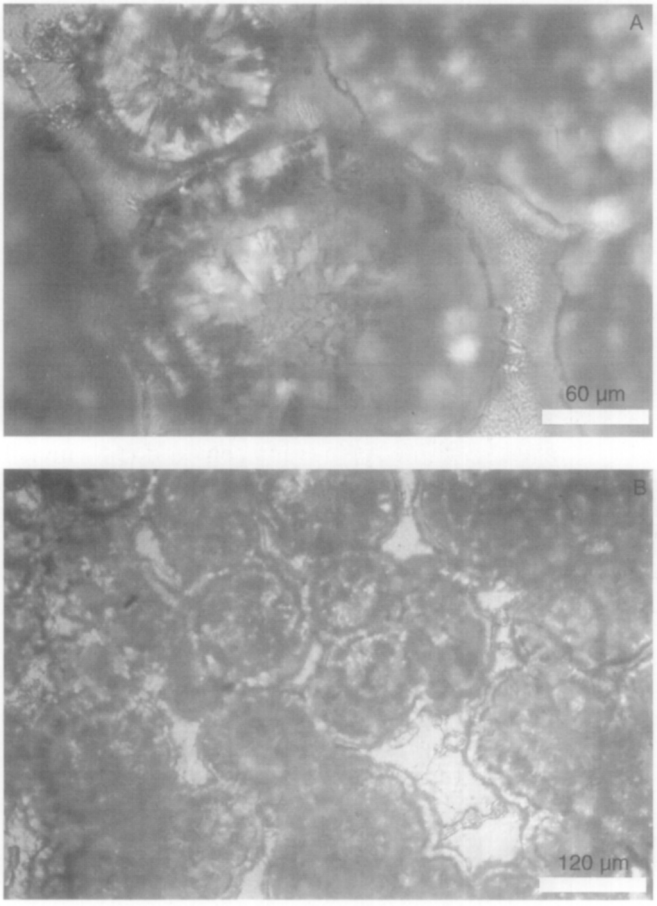

FIG. 25 Polarized light microscopy images showing large clusters of cocoa butter.

microscope. Figure 26 shows the formation of the large clusters in tallow, of the order of 100–150 μm.

In an effort to observe the formation of the fat crystal network from the melt, the kinetics of formation of the network was monitored by polarized light microscopy. Figure 27 show images of the network formed by pure milkfat triacylglycerols at 5.5 min (A), 7 min (B), 8.5 min (C), 10 min (D), 11.5 min (E), 13 min (F), 25 min (G), and 32.5 min (H) after appearance of the first visible signs of crystallization in the field of view. As is demonstrated by the figure, in the early stages of crystallization, growth is concentrated around a few centres of nucleation. However, as the growth process continues, there is an aggregation process that takes place, since there appears to be many more centres of growth (with advanced growth having already taken place, therefore suggesting that these "new" centres of growth were not new nucleation events) than there were nuclei in the field of view. The process of growth of the centres of crystallization continues until they reach a certain maximum size, whereupon the aggregation

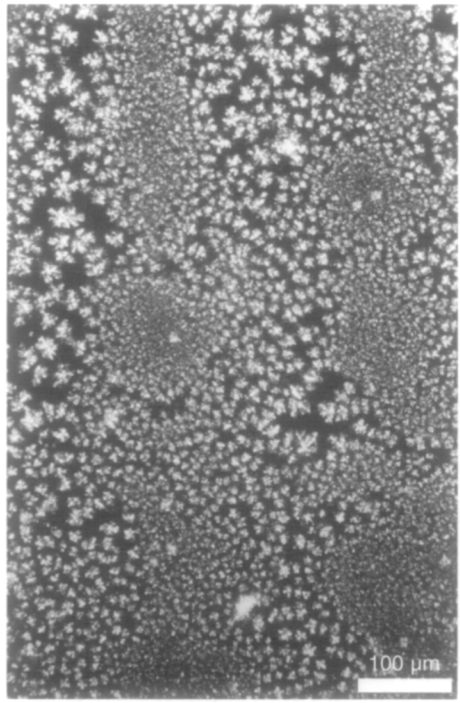

FIG. 26 Polarized light microscopy images showing large clusters of tallow.

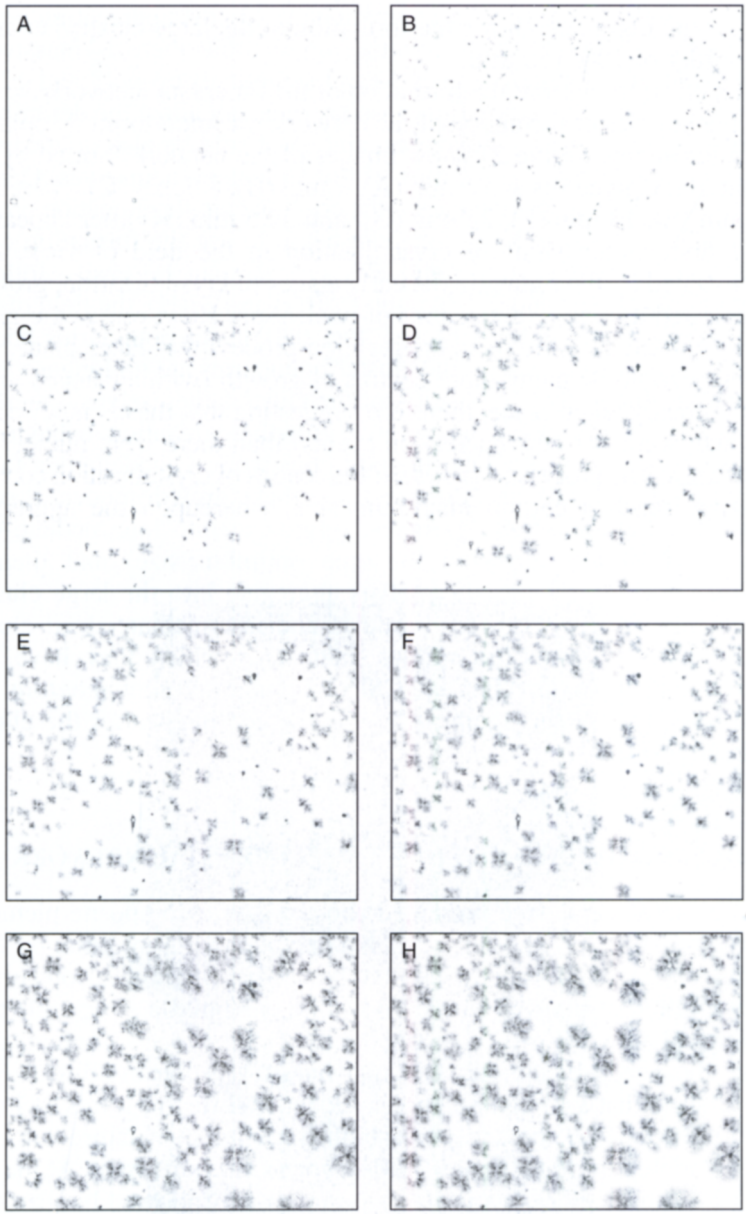

FIG. 27 Polarized light microscopy images of milkfat triacylglycerides at various times after appearance of first visible signs of crystallization: (A) 5.5 min, (B) 7 min, (C) 10 min, (D) 11.5 min, (E) 13 min, (F) 25 min, and (G) 32.5 min.

process continues slowly. After approximately $\frac{1}{2}$ h, the aggregation process is no longer visibly evident, although quite often there is massive rearrangement of the structure over 24 and sometimes even 48 and 72 h. It is unfortunate that this type of microscopy does not allow the definition of intermediate-size cluster boundaries, since it would be also interesting to observe the process of aggregation of these clusters themselves. One can begin to see cluster formation during the crystallization/aggregation process, for example, in Figure 27(C), one can begin to see the formation of the intermediately-sized clusters, and this process can be easily followed through Figure 27(E) and 27(F), but by 27(G) and 27(H), the field of view is sufficiently filled with "particles" that the cluster boundaries become indistinct. One of the reasons the cluster boundaries are no longer visible, of course, is due to the aggregation of the clusters themselves – therefore blurring the boundaries. This type of growth/aggregation behaviour is demonstrated by all of the fats studied in this work – cocoa butter, tallow, lard, palm oil and milkfat all demonstrate these growth modes. It seems reasonable to assume that "particles" aggregate into intermediate-sized clusters (whilst also growing to some optimum size) and then the intermediate-sized clusters themselves aggregate into the large clusters. The aggregation processes for particles and intermediate-sized clusters must be similar, given the similar manner in which they have been observed to pack, in the AFM and CSLCM images presented before. This is also true because the aggregation process continues after the clusters have been formed.

B. STRUCTURAL MODEL OF THE FAT CRYSTAL NETWORK

The microscopic evidence presented above forms a composite picture of the structure of fat crystal networks. No one method of microscopy on its own reflects the composite picture, but by considering the various images from the different types of microscopy, one can build a structural model of fat crystal networks which is supported by all the forms of microscopy. One of the needs in the fats and oils industry is the establishment of nomenclature that will unambiguously identify different levels of microstructure. Perhaps the best way to establish such nomenclature is to trace the development of the fat network as it forms from the melt. At the start of crystallization, there is a process of nucleation followed by growth of these nuclei into crystallites. Molecular thermodynamics and kinetics most probably control this process. As we have seen, these crystallites associate in dense packets, several intertwined crystallites tending to form "particles" of the order of 1–8 μm. It is proposed that these "particles" be

called *microstructural elements*, since they form the smallest repeating structure at a length scale visible under a light microscope. These microstructural elements then continue to grow larger through further crystallization, but there is an aggregation process that takes place as well, leading to the formation of intermediate-sized clusters, which further aggregate to form large clusters. This aggregation process is most probably controlled by mass and heat transfer limitations. The large clusters, which it is proposed be called *microstructures*, pack in an orthodox, space-filling manner to form the network, as has been shown by Heertje and co-workers. Additionally, evidence of the microstructures have been presented here, in CSLCM, AFM, and PLM images, and to a less certain extent, in SEM images. Figure 28 is a schematic two-dimensional representation of the structural hierarchy of the microstructure of fat crystal networks. The microstructural elements, the intermediate-sized clusters and the microstructures have all been represented by circles, indicating that they are spherical. There is evidence from all of the methods of microscopy that these structures are spherical-like (which may be taken to mean stretched and distorted spheres as well). However, whether they are smooth spheres is something that cannot be determined well, and this factor will most probably differ with the type of fat. Certainly, SEM and AFM micrographs of the microstructural elements suggest that these are not smooth spheres, and that the sphericity is not perfect. However, representing these structural entities as spheres is probably fairly representative, providing one keeps in mind that this is an imperfect approximation. The packing of the microstructural elements within the microstructures is quite disordered, as has been seen in the images presented before. However, it is important to recall that at length scales ranging from the diameter of the microstructural elements to the diameter of the microstructures, these structures appear to be statistically self-similar – i.e. the structure within this range of length scales, at different magnifications, appear to be similar. This of course is most strikingly obvious in the atomic force micrographs presented. Therefore, in an idealized attempt to demonstrate this self-similarity, Figure 28 shows that the packing of the microstructural elements within clusters are similar to the packing of the clusters themselves into the microstructures. In order to achieve this effect easily, the microstructural elements and the clusters are arranged in an ordered manner, but in reality, these arrangements are quite disordered, as is evidenced by the microscopy images shown before. The fact that there appears to be statistical self-similarity in the length ranges between the size of the microstructural elements and the microstructures is not surprising, since the method of growth/aggregation between these two length ranges is limited by the same physical constraints. This is

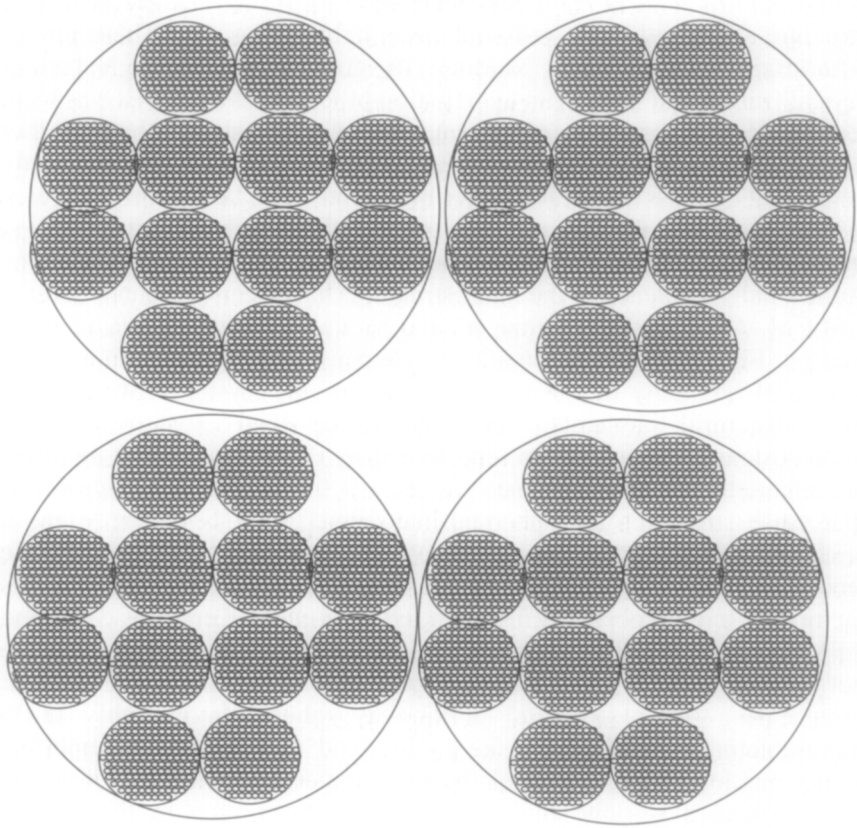

FIG. 28 Idealized two-dimensional schematic representation of the self-similar structural hierarchy of the microstructure of fat crystal networks.

supported by the kinetic picture of the growth of the network offered by Figure 27.

C. FRACTALITY

Now that the structural organization of the microstructural level of a typical fat crystal network has been established, the next logical step is an attempt to quantify this level of structure. Apart from monitoring microstructural element size, cluster size, and microstructure size (not an easy task, because of the nature of the methods of microscopy), it seems important as well to ask the question: what is the spatial arrangement of

the mass of the network at the microstructural level? Certainly, the size of the various hierarchical levels of structure will determine the way in which forces holding the network together will be affected, but equally as certain, the spatial arrangement of the various levels of structural entities will also affect the forces that hold the network together. Of course, additional factors such as the nature of the crystalline material (polymorphism) and the nature of the constituent molecules themselves are also important factors, but from a microstructural perspective, the parameters that can be determined are concerned with the size, shape, and spatial arrangement of the structural entities. Certainly, the density of this level of structure will yield some information about the spatial arrangement of the mass of the network, but does not give information about the actual packing – i.e. it is a rather macroscopic measurement, which does not yield structural information about the actual order of packing of the structural units of interest. Due to the extremely disordered nature of the packing of levels of structure below the size of the microstructures, it is difficult to assign lattice parameters to the positioning of the microstructural elements. Fractal analysis has in the past been used to characterize the spatial arrangement of such disordered structures that demonstrate self-similarity at different length scales. Additionally, based on the calculation of a fractal dimension from rheological measurements on fats which were fitted to a fractal model developed for colloidal gels (Section II), it seems fitting that one tries to apply fractal principles to the study of the microstructural level of structure in fats. Certainly, the self-similarity of the structure suggested by the AFM, CSLCM, SEM, and PLM images of the network encourages this endeavour. The issue then is to find a method of calculating fractal dimensions of images from one or more of the types of microscopy presented before. The challenge here is that each of the methods of microscopy that have been presented above demonstrate inherent artefacts, and none of them presents an unbiased, complete view of the network. What seems plausible is that the structure is self-similar at length ranges bounded by the size of the microstructural elements and the size of the microstructures.

D. TRADITIONAL METHODS OF FRACTAL DIMENSION DETERMINATION

To aid the reader unfamiliar with the topic, a brief description of the methods typically used to calculate fractal dimensions in the natural sciences is presented. This is not intended as an exhaustive review: for complete reviews, the work of Falconer (1990), Crownover (1995), and Mandelbrot (1982) are highly recommended. Additionally, a very concise

historical description of the many types of different fractal dimensions that have been defined, and their uses, is given in an eloquent publication by H. E. Stanley (Stanley, 1984).

There are several different concepts of the fractal dimension of a geometrical configuration. The most widespread method of calculating fractal dimensions in the natural sciences is the so-called box-counting dimension. Examples of other types of fractal dimension include the topological dimension and the Hausdorff dimension. It is worth mentioning here that the Hausdorf dimension was the dimension used by Mandelbrot to define a fractal in 1975, i.e. an object was defined to be fractal if it had a Hausdorf dimension strictly greater than its topological dimension – a line of reasoning that is in accordance with the brief description of fractals in Section II (if an object which is one- or two-dimensional is kinked and twisted sufficiently, its dimensionality is raised). The box-counting dimension is preferred for use in the natural sciences, since it is computationally easier to calculate, and is usually the same value as the more-difficult-to-compute Hausdorf dimension. This discussion is therefore limited to the calculation of box-counting fractal dimensions (variously called the Minkowski dimension, fractal dimension or similarity dimension).

Computer logarithms for the calculation of a box dimension are usually formulated by considering $N(r)$ as the least number of balls of radius r needed to cover the fractal object. Here, the fractal object is either a mathematically generated fractal object, or the representation of a fractal object which has maintained the spatial integrity of the object. The box counting dimension, D, is then given by:

$$N(r) \approx \frac{C}{r^D} \tag{30}$$

where $C > 0$. Taking logarithms on both sides of this equation yields:

$$\log N(r) \approx \log C - D \log r \tag{31}$$

since $\log r \to -\infty$ as $r \to 0_+$, D satisfies:

$$D = -\lim_{r \to 0} \frac{\log N(r)}{\log r} \tag{32}$$

The box dimension of the fractal object in question is therefore defined by Eqn (31), with the condition that the limit expressed by Eqn (32) exists. As have been mentioned before, various methods of calculating the box dimension exists, and for instance five of these are described succinctly by Falconer (1990).

In one method, square boxes are substituted for round balls in the actual computer algorithms used to calculate the box dimension. The value of $N(r)$ is taken as the least number of square boxes of side r needed to cover the fractal object. Then, values of $N(r)$ for several different values of r are recorded. A graph of log $N(r)$ vs. log(r) then yields $-D$ as its slope, from Eqn (31). It must be remembered that the values of $N(r)$ calculated are necessarily approximations, and therefore many values of r and corresponding values of $N(r)$ are usually used in this method. In the case of a planar fractal, one counts the number of squares, in the case of the fractal being a segment of a line, line intervals instead of squares are used, and in the case of the fractal object being a subset of three-dimensional space, the squares are replaced by constant-height volumes with a square base. In each of the cases, r corresponds to the side of the square, the line interval, or the side of the square base of the volume. For an exact object such as a Koch snowflake, shown in Figure 29, the method described above is well suited. This method, like all of the existing fractal methods, requires that the spatial integrity of the object be maintained in the image

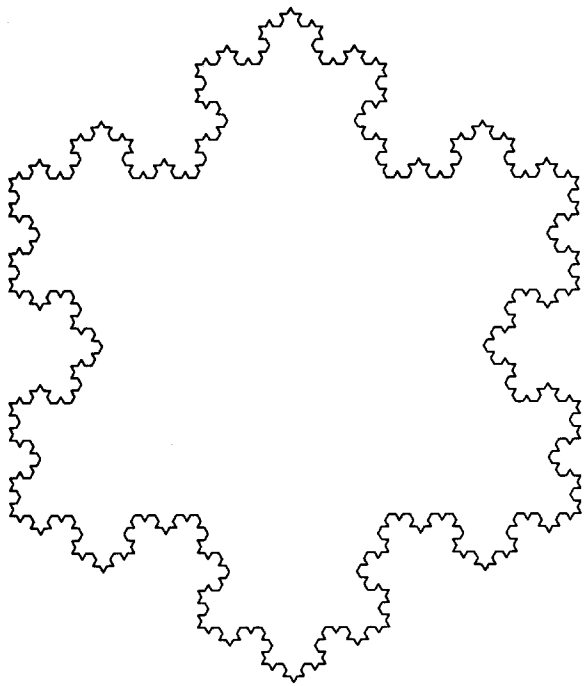

FIG. 29 The Koch snowflake (a mathematical fractal made by Helge von Koch in 1904).

that is being analyzed. Herein lies the problem with applying any of the existing traditional methods to calculate the fractal dimension of fat crystal networks at the microstructural level.

E. PARTICLE COUNTING METHOD

None of the methods of microscopy that have been discussed so far provides images which would be necessary for any of the traditional methods of calculating fractal dimension to be useful. The SEM images are very unreliable – the samples are frozen, and additionally they only provide images of the surface of the samples. The AFM images as well only provide information on the surface of the sample, and additionally, do not provide definition of the boundaries of the microstructural elements well enough. The CLSM images are two-dimensional slices of the network – it is conceivable that if a series of slices is imaged, then the three-dimensional network can be reconstructed, and this would provide a spatially correct representation of the image. However, with this method, there are uncertainties with the behaviour of the dye, and from the tendrils that were demonstrated in the images shown from CLSM it seems unlikely that the spatial integrity of the structure would be preserved. The PLM images with the broken networks of course are not useful, since the network is already broken. This leaves us with the *in-situ* PLM images, which bear additional scrutiny.

A thin sample of the fat network crystallized on the microscope slide provides an imperfect representation of the microstructural elements present in the entire three-dimensional sample, as has been discussed above. Those elements in the focal plane of the microscope appear sharp, larger, and well defined, whilst those in the depth of the sample appear diffuse and smaller. Therefore, such an image is essentially representing all of the microstructural elements in the sample (excepting those in direct geometrical shadow, assumed negligible) projected onto the two-dimensional focal plane of the microscope. Certainly, the exact spatial integrity of the image is not preserved, and therefore none of the traditional methods for the calculation of fractal dimensions are suitable for analysing this type of image.

If however, the images from the *in-situ* PLM method are rendered black and white by a thresholding method, one can ensure that each of the microstructural elements present in the original greyscale image are represented in the thresholded image. In this process, one may have to let those microstructural elements in focus appear larger, whilst those out of focus may only be represented by small points of white. However, *each* of the microstructural elements can be made to be represented in a thresholded

image by a white spot. A greyscale image essentially is composed of 255 levels of grey – a thresholding process assigns a threshold grey level, so that any pixels which have a grey value above the threshold value is assigned the colour black, and any image below the threshold values is assigned the colour white. Figure 30(A) shows a schematic of microstructural elements in a thin sample of fat, projected onto the focal plane of the microscope, and Figure 30(B) shows a schematic of this image thresholded to represent all of the microstructural elements within the sample.

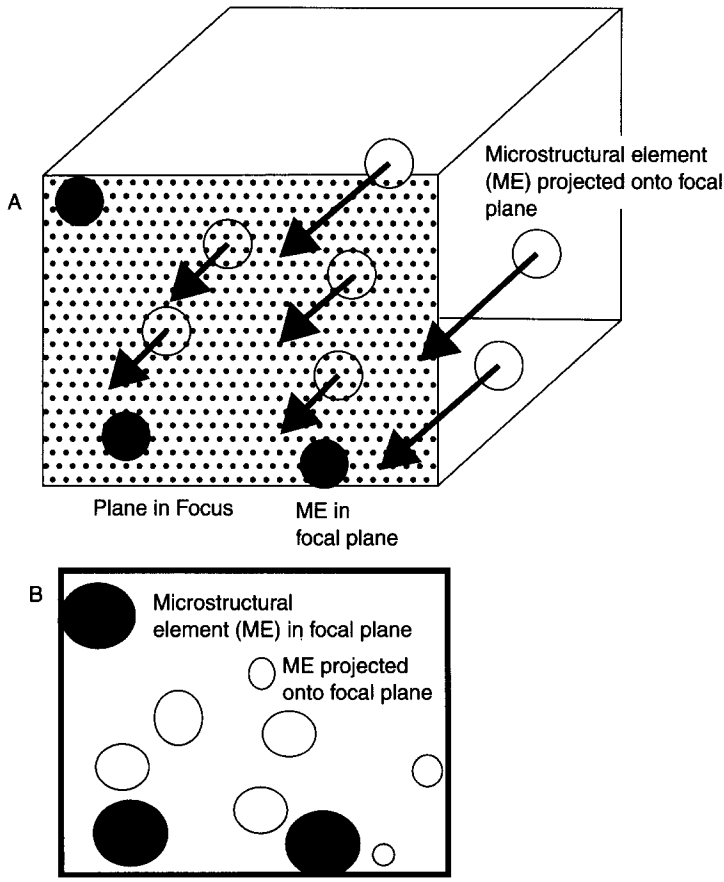

FIG. 30 (A) Schematic of microstructural elements in a thin sample of fat, as seen under a polarized light microscope. (B) Example of how an image taken of the situation in (A) would appear when thresholded.

How can the actual numbers of microstructural elements present aid in the calculation of the fractal dimension of the structure? The thresholded images are not suitable to be analyzed by the traditional methods of fractal dimension determination. The reason is because these images are subsets of two-dimensional space, but are representing a subset of a three-dimensional network. Furthermore, because of the need to utilize thresholding methods to ensure the representation of all the microstructural elements within the two-dimensional image, the sizes of the microstructural elements already in focus are increased, whilst those out of focus appears smaller than the magnification warranted. Therefore, the size of the individual microstructural elements are not representative of the size of the fractal, at whatever magnification the picture was taken. If we assume that the constituent particles (microstructural elements) of a particular fat network are of the same average diameter (not a bad assumption, from examining the microscopy images presented before), then for calculation of the mass fractal dimension, it is sufficient to just count the particles, regardless if some appeared larger when the image is thresholded. The number of particles present in a three-dimensional portion of the sample is counted by first representing all of the particles present in that portion of the sample in the plane of the image. Of course, those particles that did not appear in the picture due to geometrical shadowing are not counted, but the number of these can be rendered negligible by making the thickness of the sample very small. Use can then be made of a form of Eqn (2). This equation stems from one of the principal characteristics of a particle-aggregation fractal system, where the fractal dimension D relates the number of particles N_p to the linear size of the fractal R and the linear size of one particle (microstructural element) σ:

$$N \sim \left(\frac{R}{\sigma}\right)^D, N>>1 \tag{33}$$

Here, the fractal object is a mass fractal (a microstructure), and σ refers to the radius of the particles constituting the fractal (microstructural elements), whilst R corresponds to the radius of the entire fractal object. One can approximate R to be the length of a side of the square base of a constant-height volume that covers the fractal object if the fractal is in a $d = 3$ system, the length of an area for a $d = 2$ system and length of a line for a $d = 1$ system. Assuming a statistically constant particle size, or in our case, a statistically constant microstructural element size:

$$N \propto R^D \tag{34}$$

Taking logarithms:

$$\log_{10} N(R) = \log_{10} c + D \log_{10} R \tag{35}$$

where c is a constant, $N(R)$ is the number of particles in the fractal of length R, and R is the length of the line segment, length of a side of an area, or length of the square base of a constant-height volume which envelopes the fractal. The lower limit of this relationship then becomes the size of one microstructural element, i.e. $R = a$, $N(R) = 1$ is the lower limit. Therefore, proceeding in like manner to the traditional form of box-counting, $N(R)$ for various values of $R >> a$ is counted, and $\log_{10}(N(R))$ plotted vs. $\log_{10}(R)$, the resulting slope of the line being equal to D. D therefore represents the fractal dimension of the packing of the microstructural elements within a microstructure of the fat crystal network.

Images of the *in-situ* fat systems captured under the PLM were scanned into a Pentium 200 MHz IBM-compatible computer using a Hewlett Packard 6100C scanner. In order to analyze the photographs of the polarized micrographs taken of the fat systems, the images were thresholded. In order to do this, a particular threshold value has to be utilized, which allows all of the microstructural elements to be seen as white, and all of the background to be reduced to black. This is an especially difficult and crucial task, since one has to take care to ensure that all of the solid particles are represented in the resulting thresholded image. Algorithms exist to calculate threshold values; one such method that was used in this study is the statistical correlation method (Parker, 1994).

The statistical correlation method was used to calculate threshold values for some of the images scanned into the computer, but since each time it was possible to better judge the threshold value visually, human judgement of the threshold value was used in all of the analysis. In some cases, this involved causing microstructural elements in focus to appear slightly larger than they were under the magnification used, in order to ensure that the microstructural elements out of focus were counted as particles. It was important to ensure that all the microstructural elements were represented, for once again, it is necessary to project all of the microstructural elements onto the plane of focus of the image, so that the resulting fractal dimension calculated would have been in a system with a Euclidean dimension of three.

In order to calculate the value of D (with Euclidean dimension, $d = 3$), the number of microstructural elements $N(R)$ projected onto a square area of side of length R, drawn in the focal plane of the image, was counted. This count represents the number of particles present in a volume of constant depth and of width R through the fractal. Values of $\log_{10}(N(R))$

were plotted against $\log_{10}(R)$ for varying values of R. The resulting slope of the line was taken as being equal to D. Figure 31 shows the greyscale and thresholded images of milkfat (A and B), tallow (C and D), palm oil

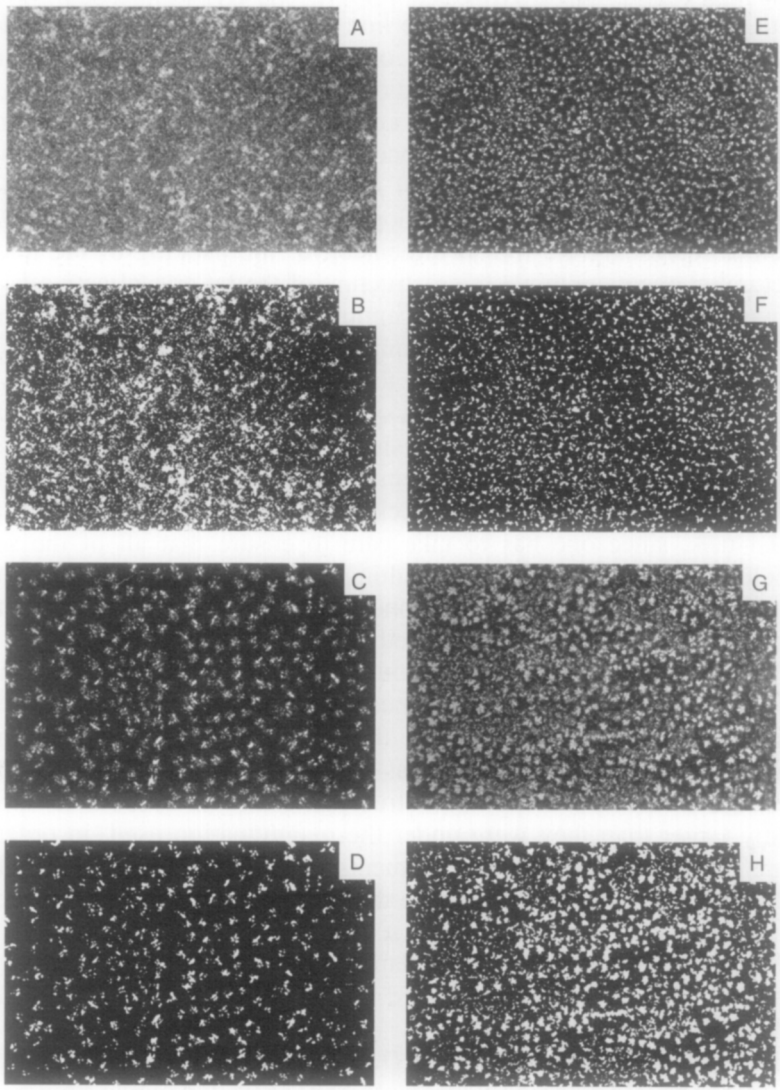

FIG. 31 Greyscale *in-situ* polarized light microscopy images and corresponding thresholded images of milkfat (A and B), tallow (C and D), palm oil (E and F), and lard (G and H).

(E and F) and lard (G and H). Figure 32 shows the plots of $\log_{10}(N(R))$ vs. $\log_{10}(R)$ for these fats (milkfat (A), tallow(B), palm oil (C), and lard (D)).

The images scanned into the computer were first opened with Corel PHOTO-PAINT-6, and the images inverted (black pixels made white and white pixels made black); this was because the program used to do the actual particle-counting counts "black" particles. The image was then saved and two copies opened in SCION IMAGE Release Beta 3b (© 1998, Scion Corporation). One of the images was then thresholded, using the other image as a greyscale reference, to ensure that all of the microstructural elements in the image were being represented by a black dot. Much effort is taken with ensuring that all microstructural elements are represented – this is often an impossible task with the entire image, especially if the image represents a non-constant depth of sample. It is of maximum importance to ensure that the depth/thickness of the samples is kept constant. In such cases, sometimes the entire image must be discarded and new samples prepared, or sometimes it is obvious that only part of the image is at a constant depth – then the analysis is confined to that part of the image only. Additionally, the microstructural elements in

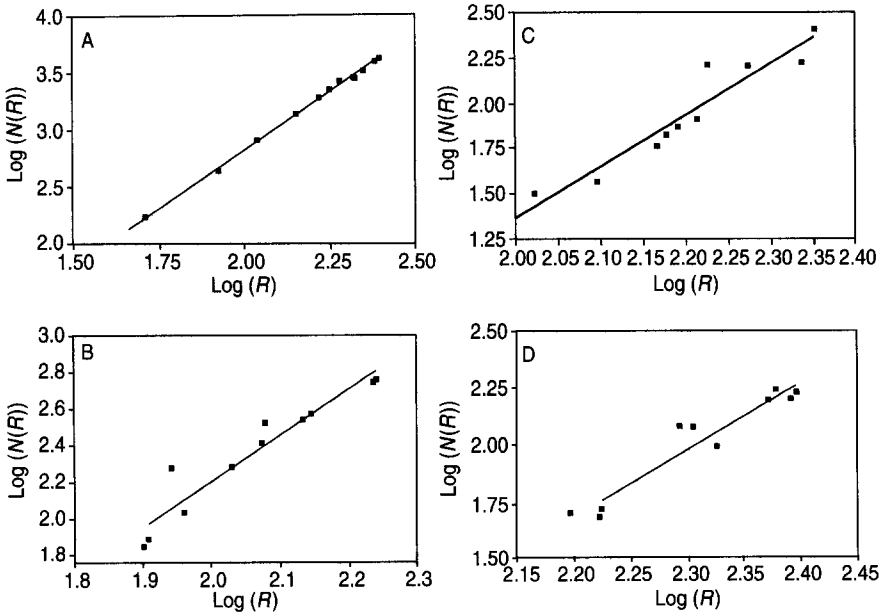

FIG. 32 Plots of $\log_{10}(N(R))$ vs. $\log_{10}(R)$ for: (A) milkfat, (B) tallow, (C) palm oil, and (D) lard.

some fats are just too densely packed to allow proper thresholding to represent individual microstructural elements with any degree of accuracy – in such cases, the fat cannot be analyzed by this method. The important aspect of this analysis to bear in mind is that the person taking the image must be aware of what the image represents – only someone that has taken the picture can be relied upon to decide at the thresholding stage which entities are microstructural elements. When the correct threshold has been achieved, SCION IMAGE allows one to select "boxes" of various sizes, drawn over the thresholded image, and to compute the area in pixels of each box, as well as the number of "particles" or thresholded microstructural elements, within each box. This facilitates the accumulation of values of $N(R)$ and R.

To investigate the effect of changing threshold value on the fractal dimension calculated, two fats – tallow (crystallized at 5°C for 24 h) and milkfat (crystallized at 20°C for 48 h) were analysed. The "correct" threshold value was chosen visually, and the fractal dimension calculated. Then, threshold values greater and less than the "correct" value was chosen and the fractal dimension calculated. Values of fractal dimension were then plotted against values of threshold. Figure 33 shows these plots for the two fats – tallow (A) and milkfat (B).

F. THE FRACTAL NATURE OF FAT CRYSTAL NETWORKS

As is evidenced by Figure 32, all of the fats analyzed (cocoa butter and milkfat at 20°C were also analyzed, but these plots are not shown) produced straight-line plots of $\log_{10}(N(R))$ vs. $\log_{10}(R)$. Additionally, all of the fractal dimensions calculated are between 2 and 3, as would be expected for fractal samples whose Euclidean dimension, d, is 3. Therefore, the level of structure bounded by the size of the microstructural elements and the size of the microstructures is fractal in nature. Furthermore, one can analyze PLM micrographs of this level of structure using the particle counting method, to yield a fractal dimension. This is not surprising, since the apparent self-similarity of this level of structure hinted at this level of structure adhering to a fractal packing geometry. Now, it must also be pointed out here that the phrase fractal geometry as applied to natural objects has met with a lot of controversy. Over the past decades, the idea that fractal geometry is an appropriate geometry to describe nature has been proposed by many researchers. To a mathematician, for an object to be characterized as being fractal, it must demonstrate a quantitative power-law scaling of the parameters of the system at infinitely many orders of magnitude. Physicists and other scientists, however, have maintained that an object which demonstrate a power-law scaling of parameters

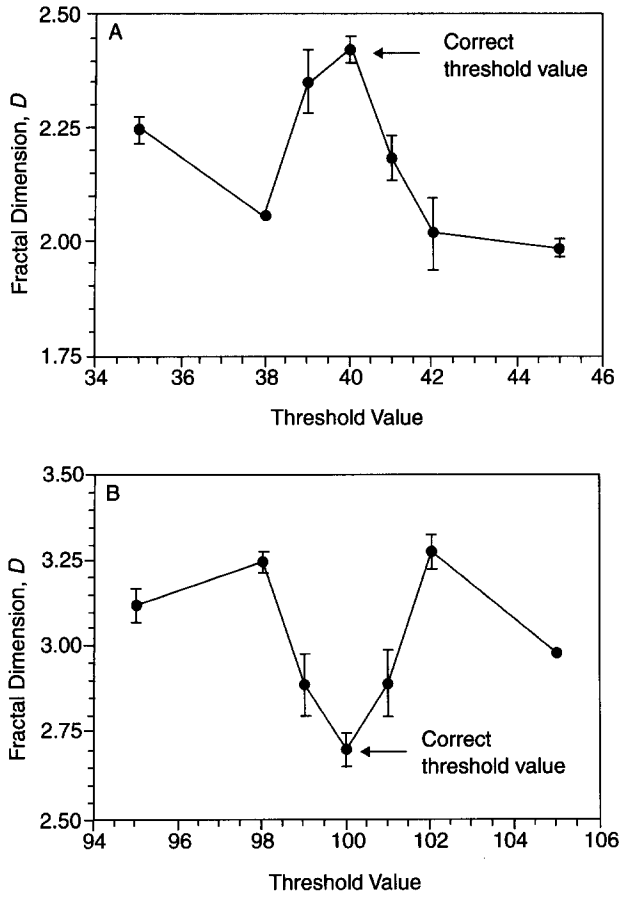

FIG. 33 Plots of fractal dimension vs. threshold value for (A) tallow at 5°C and (B) milkfat at 20°C. A linear log-log plot was obtained for each data point shown. Error bars represent statistical uncertainty in the slope.

between limited length ranges is no less a fractal. For example, the scaling of the number of microstructural elements as a power law function of the characteristic length of the system only spans a length scale between 1–8 μm and at most 100–120 μm. At any rate, the fractal-like scaling of natural objects, even within such narrow length ranges, can impart important scaling behavior to physical parameters of the system dependent upon structure. Indeed, because of this, whether the word "fractal" is justifiably used or not becomes dependent on ones definition of the word – whether as a mathematician or as a physicist. For more on

this debate, the reader is referred to an exchange of letters concerning this topic by Mandelbrot, Avnir and others (Avnir *et al.*, 1998; Mandelbrot, 1998; Pfeifer, 1998; Biham *et al.*, 1998). Whatever camp one belongs to, there is some amount of heuristic value in calling such natural objects fractal. In this thesis, it will be taken as understood that when the word fractal is used, it is used to describe the power-law scaling of the number of microstructural elements with length over a well-defined limited length scale: the length of the microstructural elements at the lower limit, and the length of the microstructures at the upper limit. Perhaps use of the phrase "spatial distribution of mass" is better suited than "fractal dimension," but realistically, when one calculates the fractal dimension as explained above, one is calculating a dimensionality of packing of the microstructural elements within the microstructures. This dimensionality is indicative of the spatial distribution of mass, of course, but the debate then becomes one on semantics. As long as the parameters that we refer to are properly defined, it is my opinion that one can continue to refer to the dimension calculated as the fractal dimension. Therefore, in this article, the parameter referred to as fractal dimension may perhaps more correctly be called a *scaling parameter* or an *apparent fractal dimension.*

The issue of thresholding is a contentious one with this analysis. As is evident from Figure 31, however, the thresholded images hold true to the task of representing *all* of the microstructural elements within the image as white dots (obviously, these images do not show the inverted greyscale and thresholded images, but represents the greyscale images as they appear under the microscope, with the thresholded images making microstructural elements appear as white). In some of the images, for instance the milkfat image shown in Figure 31(A) and (B), the upper right-hand side of the image is obviously not at the same depth as the rest of the image (i.e. the sample was thicker at this end of the image); in this image, only the left half of the image was used for the analysis. In some images, where the packing of the microstructural elements is very dense, it will be impossible to threshold the image to represent the individual microstructural images in the sample – such samples cannot be analyzed using this method. Ultimately, the method is a subjective method – it depends on the ability of the person doing the analysis to recognize which entities are microstructural elements, and to threshold the image to represent those microstructural elements in the thresholded image so they can be counted. As mentioned before, it is helpful for the person analyzing the images to also be the person who took the picture in the first instance. Additionally, details must be paid to such important things as making sure the sample is of uniform thickness, and that the image acquired is of the highest quality. However, even if the threshold value is not the "correct" value –

i.e. if the threshold value for a particular image was off by one or two threshold values (from 0 to 255), therefore leading to some microstructural elements being missed, or some being counted as more than one, the fact remains that this method has shown that the fat networks at this level is fractal in nature – i.e. even with a small amount of error, there is a scaling relationship between the number of microstructural elements and the length of the sample, bounded by the length of one microstructural element and the length of one microstructure. In fact, if the plots in Figure 32 are examined, it will be seen that there is some amount of scatter in the points, which is probably indicative of an imperfect thresholding method. In fact using this method of microscopy, it is virtually impossible to have the "correct" thresholding value – there will always be an element of error, due to the nature of the microscopy itself.

Figure 33 is interesting in that it suggests some amount of objectivity to the thresholding method for a particular image; it shows plots of fractal dimension vs. threshold value for two different fat systems – tallow (A) and milkfat (B). The plots shown in Figure 33 demonstrate a minima and a maxima at the visually "correct" threshold value (these are most probably local minimas and local maximas, if one is to plot fractal dimension against the entire range of possible threshold values). Now, these figures were generated by choosing threshold values which were greater than and less than the chosen "correct" threshold value, selected visually. As is demonstrated, deviations from the "correct" threshold value lead in most cases to steep deviations from the fractal dimension at this threshold value. The error bars in this figure represent the standard deviation derived from the fit of the log–log plot.

If a threshold value is not the correct value, then the thresholded image either over-represents the number of microstructural elements present, or under-represents the number of microstructural elements present. For the purposes of this discussion, the images of the network will be regarded as having the microstructural elements represented as black objects (inverted images), so therefore on a scale of 255, 0 represents black and 255 represents white. Increasing the threshold value in such an image implies that more of the pixels in the image is being relegated to the white background, and decreasing the threshold value means that more of the pixels in the image are being made black. There are two reasons that can cause the number of microstructural elements in the image to be over-represented:

(a) A threshold lower than the correct value may cause additional black spots that are not actual microstructural elements, but are background represented by a greyscale value, which because of the low threshold is rendered into a black object.

(b) A threshold higher than the correct value may cause black spots originally representing individual microstructural elements to be represented by more than one black spot in the thresholded image. This of course happens when the threshold is made so high that a microstructural element represented by uneven levels of greyscale values can be split into two or more black spots in the thresholded image.

There are also two reasons that may cause the number of microstructural elements in the image to be under-represented.

(c) A threshold lower than the correct value may cause two or more neighbouring microstructural elements to be represented as one black particle in the thresholded image. This occurs of course because the threshold is low enough to cause the greyscale value of the background separating the microstructural elements to be rendered black in the thresholded image.
(d) A threshold higher than the correct value may result in many of the microstructural elements not being represented in the thresholded image, since their greyscale values would be such that they are rendered as white in the thresholded image.

Eqn (34) states that the number of microstructural elements are proportional to the characteristic length of the system raised to a power equal to the fractal dimension. An over-representation of the number of microstructural elements therefore, results in an over-representation of the fractal dimension value. Similarly, an under-representation of the number of microstructural elements in the sample results in an under-representation of the fractal dimension value. In other words, over-representation results in too-high values of D, and under-representation results in too-low values of D.

Now, suppose an image of a fat is thresholded to a value which is visually judged to be in the vicinity of the "correct" threshold value. Let us assume for the moment that this value is actually lower than the theoretical "correct" value. Now, this means that the number of microstructural elements will either be over-represented or under-represented. If the number of microstructural elements are over-represented (due to reason (a), from the foregoing discussion), then as one increases the threshold value, the number of microstructural elements will become less over-represented until one increases the threshold value to the correct value. Therefore, from the initial threshold value chosen, the fractal dimension will decrease to the correct value. Increasing the threshold value beyond the correct value will result in either an over- or under-representation of the number of

microstructural elements. If there is an over-representation (which would be due to reason (b) from the foregoing discussion), then the correct value will lie at a minima of the fractal dimension vs. threshold value plot. If there is an under-representation (which would be due to reason (d) from the foregoing discussion), then the correct threshold value would be at a point of inflexion in the plot of fractal dimension vs. threshold value. Similar arguments as above, starting with a threshold value which is lower than the correct value and which causes an under-representation makes it obvious that the correct value would lie either at a maxima or at a point of inflexion. Therefore, the correct threshold value should always correspond to a local minima, maxima, or point of inflexion in the fractal dimension vs. threshold value plot.

Therefore, the results shown in Figure 33 are explained theoretically. What is surprising, however, is the fact that the "correct" value is only one value – one would expect there to be at least a few "correct" threshold values. However, this is a function of the images – images with microstructural elements packed in a low density conformation may have a few "correct" threshold values in a cluster, but those images which have been used in this thesis are quite dense, thereby perhaps explaining the steepness of the D vs. threshold value curves. With the dense images, it becomes obvious from examining the images that changing the threshold value by even one point may lead to the appearance/disappearance/merging of microstructural elements. The fact that the correct value of the threshold will lie in a local minimum or maximum point or point of inflexion in the plot of D vs. threshold value, however, helps to make the thresholding process more objective – now, one can choose a reasonable threshold value (one which seems to be causing the representation of *all* the microstructural elements), and then do a series of analyses for fractal dimension with this threshold value and threshold values above and below this value. The resulting plot will yield either a local minima, local maxima or inflexion point and any of these should correspond to the correct threshold value. It must be expected, although it has not been my experience, that one may encounter images where the local minima, maxima, or inflexion point is actually due to two or three adjacent threshold values. This said, it is quite possible that a plot of fractal dimension vs. threshold value will continually yield local minima and maxima throughout the range of threshold values possible (0–255). One still would have to visually examine the image to ensure that the local minima, maxima or inflexion point chosen to be the correct value of the threshold was indeed adhering to the principles of the particle-counting method, and a valid representation of the greyscale image. In fact, because of this reason, thresholding still does remain a very subjective process. Therefore, whilst the foregoing discussion on threshold values is useful in explaining the

results demonstrated in Figure 31, it must not be misconstrued that this discussion somehow absolves the process of its subjective nature. It is quite possible to have two or more local turning points quite close to each other in a plot of fractal dimension vs. threshold value (as is demonstrated by Figure 33). In these cases, it is absolutely essential for the operator to be able to discern the "correct" threshold. Additionally, it is of course required that a good first "guess" be made of the threshold, before even attempting the laborious analysis that is required to produce a plot of fractal dimension vs. threshold value, which as discussed, is not entirely reliable unless one can visually verify the legitimacy of the "correct" threshold value.

It is important to mention that fractal dimensions calculated on samples of a particular fat diluted with varying amounts of canola oil (up to and including 80% w/w) were statistically the same. This seems to suggest that the fractal dimension of the network as a measure of the packing, is a fundamental physical constant, influenced by the nature of the forces involved at the microstructural level. The canola oil in each case was seen to act solely as a diluent (with cocoa butter, lard, milkfat, and tallow). The same effect was observed for palm oil diluted with soya bean oil.

Using the particle-counting method, a value for the chemical length exponent, or the tortuosity of the network may also be calculated, but since this value is not required for the application of the weak link theory, the details of this calculation are not presented here. For the interested reader, this method has been published by Narine and Marangoni (1999b).

G. THE WEAK LINK REVISITED

Now that the general structural arrangement of the microstructure of fat crystal networks has been established, it is relevant to examine how this structural organization relates to the weak link theory. The model of the structure of fat crystal networks developed above identifies the microstructures as the largest structural building block of the network. It seems reasonable that any stress that is put upon the network will first be felt by the microstructures. The question is, how do the microstructures behave under this stress? Heertje and co-workers (Heertje *et al.* 1987; Juriaanse and Heertje, 1988; Heertje, 1993) have demonstrated that the microstructures are separated when the network is stressed, whilst remaining intact (maintaining their shape and size). It therefore seems reasonable to expect that when the network is stressed, the first level of structure that is stressed are the links between microstructures. Figure 34 shows a theoretical schematic of the network under stress. It seems

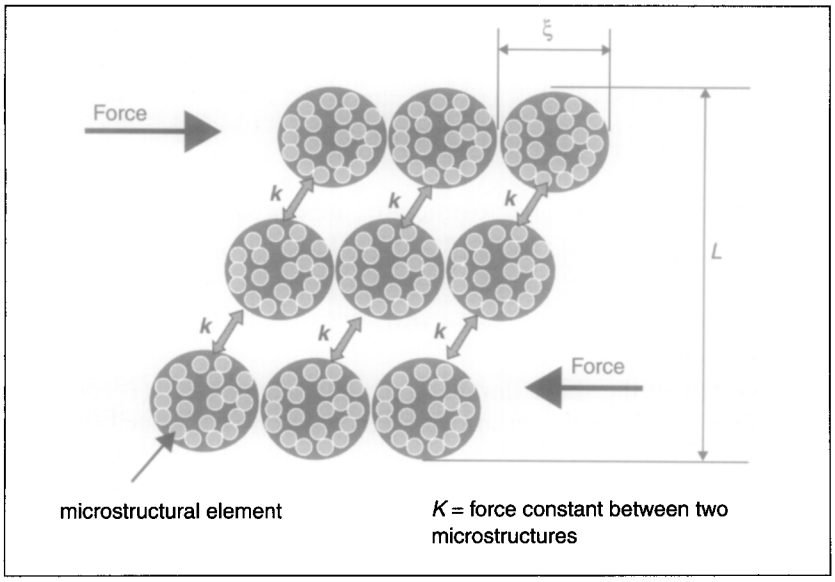

FIG. 34 Theoretical schematic of the fat crystal network under a small stress which is insufficient to exceed the elastic limit of the network.

reasonable to expect that the stressing of the network within the elastic limit results in a stressing of the links between microstructures, which are a repeating, regularly packed structural unit. Referring to Figure 34, if one were to express the force-constant of the links between microstructures as k, then the macroscopic elastic constant, K, (in one dimension) of the network could be written as:

$$K = \left[\frac{L}{\xi}\right]^{d-2} k \tag{36}$$

where ξ is the diameter of one microstructure, L is the macroscopic size of the system, and d is the Euclidean dimension of the sample (=3). However, as have been shown above, the structure within the microstructures is fractal in nature. We can therefore relate the diameter of the microstructure (or aggregate) to the particle volume fraction of the entire network, according to the development made in Section II. Therefore, using Eqn (8):

$$\xi \sim (\Phi_t)^{\frac{1}{D-3}} \tag{8}$$

and substituting this expression in Eqn (36):

$$K \sim \left[\frac{L}{(\Phi)^{\frac{1}{D-3}}} \right] k \tag{37}$$

Now, if the links between microstructures are constant, and the size of the system is a constant, we can write Eqn (37) as:

$$K \sim (\Phi)^{\frac{1}{3-D}} \tag{38}$$

Recognizing that the shear storage modulus of the network is related in a proportional manner to the tensile elastic constant, we can write Eqn (38) as:

$$G' \sim \Phi^{\frac{1}{3-D}} \tag{39}$$

The theory espoused by Eqn (39) relates the shear storage modulus to the particle volume fraction via the fractal dimension of the network. The particle volume fraction of the network is not easily measured (in fact, the author knows of no experimental method that yields this value). It must be stated clearly here that particle volume fraction is used to mean microstructural element volume fraction – it is obvious from the development above that the "particles" refers to the microstructural elements. It will be shown below that the solid fat content, Φ_{SFC}, is proportional to the particle volume fraction, Φ. Therefore, one may use Φ_{SFC} in the stead of Φ in Eqn (39), bearing in mind that the nature of the proportionality constant is now changed. One can now replace the proportionality sign by the constant γ, bearing in mind that this constant would be dependent on the links between microstructures, and the relationship between ξ, Φ, and D, as well as the nature of the proportionality between and Φ_{SFC} and Φ, given the origin of the proportionality constant, as developed above:

$$G' = \gamma \Phi_{SFC}^{\frac{1}{3-D}} \tag{40}$$

Eqn (40) is of course equivalent to the expression arrived at by Shih *et al.* (1990) for the weak link theory for colloidal gels. Therefore, from a structural perspective, it seems that use of this formulation for fat crystal networks is warranted. Not surprisingly, therefore, the work by Rousseau and Marangoni detailed in Section II showed that the weak link theory when applied to fats yielded plausible results. Additionally, these authors were not incorrect in assuming that the fractal dimensions that they

calculated from this rheological treatment were related to the microstructure – as have been shown above, such a fractal dimension is related to the way in which the microstructural elements are distributed in the microstructures of the fat network. The obvious challenge is therefore to compare the fractal dimensions calculated by rheological methods to those calculated by image analysis methods. The most important issue here of course is the need to emulate the same processing conditions for the rheologically prepared samples and the samples prepared for microscopy on a glass slide.

H. RELATING THE PARTICLE VOLUME FRACTION TO THE SOLID FAT CONTENT

The solid fat content, Φ_{SFC}, of a fat network may be defined as:

$$\Phi_{SFC} = \frac{n_{ME} V_{ME} \rho_{ME}}{M_T} \tag{41}$$

where n_{ME} is the number of microstructural elements, V_{ME} is the volume of one microstructural element, ρ_{ME} is the solids density of a microstructural element, and M_T is the total mass of the network (solid mass + liquid mass). Eqn (41) can be rewritten as:

$$n_{ME} = \frac{\Phi_{SFC} M_T}{V_{ME} \rho_{ME}} \tag{42}$$

Now, the total particle volume concentration, Φ_t of the network is given by:

$$\Phi_t = \frac{n_{ME} V_{ME}}{V_T} \tag{43}$$

where V_T is the total volume of the network. Substituting for n_{ME} in Eqn (42):

$$\Phi_t = \frac{\frac{\Phi_{SFC} M_T}{V_{ME} \rho_{ME}} V_{ME}}{V_T} \tag{44}$$

This yields:

$$\Phi_t = \frac{\rho_t}{\rho_{ME}} \Phi_{SFC} \tag{45}$$

where $\rho_t = M_T/V_T$, and is the density of the network itself. The solids density of the microstructural elements, ρ_{ME}, is higher than the density of the network, ρ_t, since the microstructural elements are very densely packed (recall the AFM image shown in Figure 22(A), which showed that the microstructural elements are made up of intertwined crystallites), whilst the network itself contains a lot of liquid oil and dispersed microstructural elements. However, as established by Eqn (24), the particle volume fraction of the network is proportional to the solid fat content of the network. Therefore, although it is difficult to measure the particle volume fraction of the network, the solid fat content may be used in its stead, bearing in mind that these two entities are not equal, but are proportional.

I. RHEOLOGY

Samples of the fat systems studied microscopically were studied rheologically as well. Different solid fat contents of a particular fat was achieved by using small dilutions with canola oil – the resulting samples were then analysed for G' and Φ_{SFC} and plots made of G' vs. Φ_{SFC} (Figure 33) and $\log_{10} G'$ vs. $\log_{10} \Phi_{SFC}$ (Figure 35). The samples studied rheologically were tempered in an identical manner to those studied microscopically. However, it was uncertain that the temperature history of the rheologically prepared samples mirrored those of the microscopic samples, due to the large difference in thickness of these samples. Additionally, the rheological samples were tempered in plastic moulds, whilst the microscopic samples were tempered between a glass slide and a glass coverslip. In an effort to compare the structure of the microscopic and rheological samples, atomic force microscope images discussed above were taken from rheological samples and spin-coated samples (similar to samples prepared on a microscopic slide) which were tempered identically. Beyond the similarity of these images, no further proof of the equivalence of these structures are available, other than the comparison of the fractal dimension values calculated from rheological measurements, and those calculated from the particle-counting method, shown in Table I.

The plots of G' vs. Φ_{SFC} shown in Figure 35 support the power-law dependence of G' on Φ_{SFC} suggested by Eqn (39). Figure 35(A) shows data for milkfat at 5°C. This is in the form of a straight line, which implies from Eqn (39) that the fractal dimension must be equal to 2. The microscopically-calculated fractal dimension for milkfat at 5°C is 2.02 (as shown in Figure 32 and Table I). Figure 35(B) shows data for tallow at 5°C, Figure 35(C) shows data for palm oil at 5°C, and Figure 35(D) shows

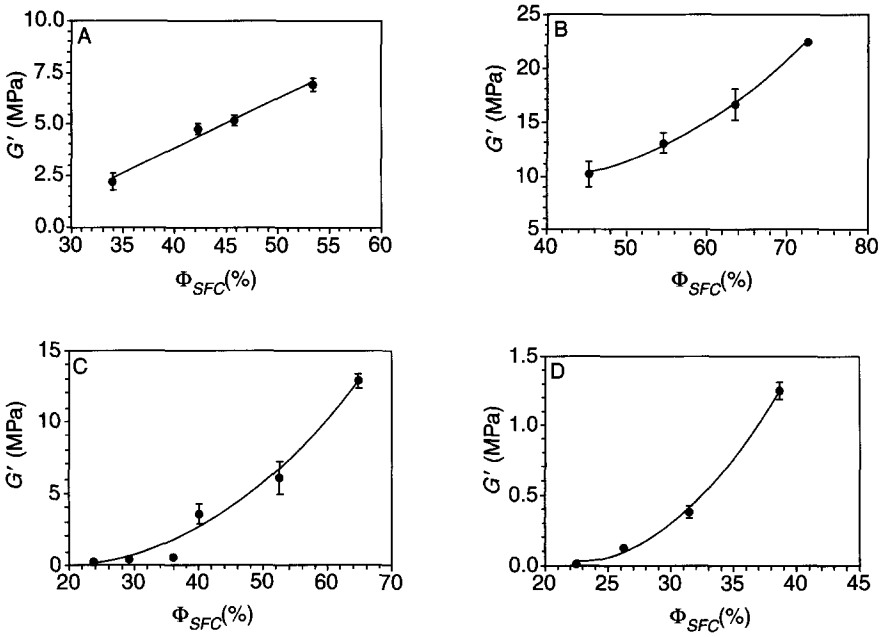

FIG. 35 Plots of G' vs. Φ_{SFC} for: (A) milkfat, (B) tallow, (C) palm oil, and (D) lard.

TABLE I

FRACTAL DIMENSION CALCULATED VIA IMAGE ANALYSIS COMPARED TO FRACTAL DIMENSION CALCULATED VIA RHEOLOGY USING THE WEAK LINK THEORY. ERRORS IN D ARE STANDARD ERRORS OF 3 REPLICATES

Fat system	Fractal dimension from image analysis	Fractal dimension from rheology (weak link regime)	Percentage deviation	Fractal backbone dimension, x
Cocoa butter (20°C) #1	2.31 ± 1.7%	2.37 ± 4.0%	2.5	1.10
NIE milkfat #4 (5°C) (Analyzed using DMA)	2.02 ± 1.2%	2.01 ± 15.7%	1.5	1.00
Palm oil (5°C)	2.82 ± 0.6%	2.82 ± 0.6%	0.0	1.10
Lard (5°C)	2.86 ± 0.6%	2.88 ± 0.5%	1.0	1.15
Tallow (5°C)	2.42 ± 1.2%	2.41 ± 6.4%	0.4	1.10

data for lard at 5°C. The strain levels used in the rheological analysis are 0.2%. All of Figure 35(B), (C), and (D) show a non-linear, power-law dependence of on G' on Φ_{SFC}. As has been explained, a plot of $\log_{10} G'$ vs. $\log_{10} \Phi_{SFC}$ yields a straight line with slope equal to $1/3 - D$; such plots are shown in Figure 36 for milkfat (A), tallow (B), palm oil (C) and lard (D). The fractal dimensions calculated in this manner are reported in Table I, where they are compared to the fractal dimensions calculated microscopically for the same fats systems, crystallized in a similar fashion.

The values of fractal dimensions calculated from image analysis of polarized light microscopy images and those calculated from the rheological measurements agree very well, as is shown in Table I. This agreement has a few implications. Firstly, it suggests that the structure of the samples created for microscopy and those created for rheology was similar. Additionally, it suggests that the weak link approach is applicable to the study of fat crystal networks, and that fat crystal networks are indeed fractal at certain length ranges. Furthermore, it demonstrates that with careful thresholding efforts, image analysis can provide very accurate numbers for the fractal dimension of the network.

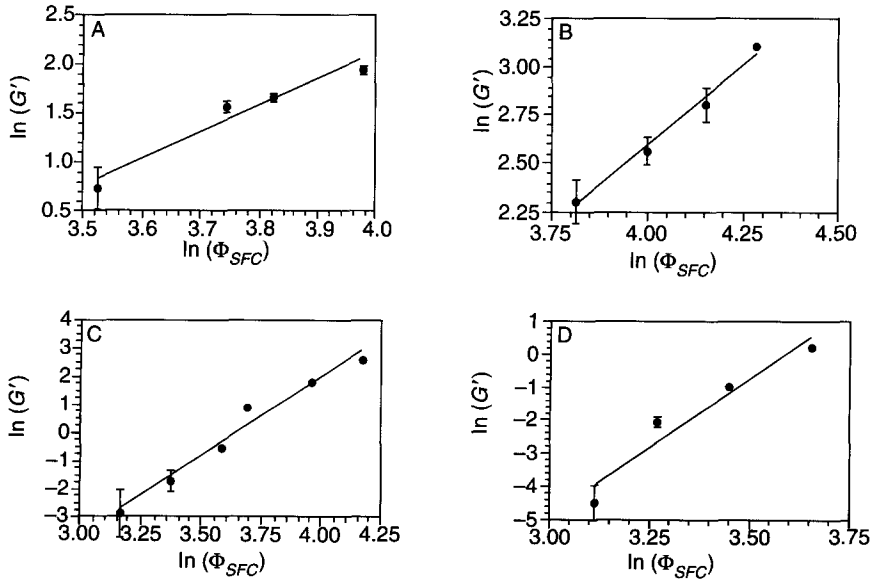

FIG. 36 Plots of $\log_{10} G'$ vs. $\log_{10} \Phi_{SFC}$ for: (A) milkfat, (B) tallow, (C) palm oil, and (D) lard.

J. PHYSICAL SIGNIFICANCE OF FRACTAL DIMENSION

The above discussion of experimental data shows that fat crystal networks are fractal within certain length ranges, and that the structural arrangement of the microstructure of fat crystal networks makes it possible to apply the weak link theory to analyze the mechanical properties of the networks. Central to this finding is the calculation of a fractal dimension. It is therefore relevant that we attach some physical significance to this quantity, if it is to be a useful parameter.

K. ELASTIC CONSTANT AND FRACTAL DIMENSION

Now that the weak link has been shown to be applicable to fat crystal networks, we can use Eqn (40) to predict the effect changes in fractal dimension will have on the shear storage modulus of the network. Now, the quantitative origins of the constant γ have not yet been addressed, and therefore any investigation of the effect of fractal dimension on the storage modulus must be made with the effects of γ removed. Therefore, if the elastic moduli of a series of fat systems are normalized with respect to the constant γ, one would have a situation described by:

$$(G'/\gamma) + \Phi_{SFC}^{\frac{1}{3-D}} \tag{46}$$

Table II shows the values of fractal dimension and γ for some 14 different fat systems, from rheological analysis. Using Eqn (46), a theoretical curve for G'/γ vs. D was created, for a constant Φ_{SFC} of 0.7; the solid line in Figure 37 represents this theoretical curve. The points on the curve represent data from the fat systems represented in Table II. All of the normalized elastic constants for the various fats were calculated for a 70% solid fat content value (i.e. $\Phi_{SFC} = 0.7$). As is evidenced by Figure 37, the theoretical curve of Eqn (46) predicts that the normalized elastic constant should decrease with increasing fractal dimension. The standard error bars represent the extent to which the fat systems studied rheologically deviate from this trend. As is evidenced by the figure, taking the error bars into consideration, the general trend of the theoretical curve is closely followed. A one way analysis of variance performed on this plot using GRAPHPAD (San Diego, Ca.) suggests that the normalized elastic constant strongly depend on the fractal dimension ($P < 0.0001$). The ramifications of this plot are important. It suggests that if one can influence the fractal dimension of a particular fat by altering processing conditions, one can manufacture model fats. In other words, alter processing conditions to

TABLE II

SUMMARY OF FAT NETWORKS STUDIED RHEOLOGICALLY WITH CORRESPONDING FRACTAL DIMENSIONS AND VALUES OF γ

Fat system	Fractal dimension, D	Pre-exponential factor, γ (MPa)
NIE butterfat #1	2.45	1.0×10^{-3}
CIE butterfat #1	2.16	9.5×10^{-3}
NIE butterfat #2	2.59	4.6×10^{-4}
EIE butterfat #2	2.50	9.9×10^{-4}
NIE butterfat #3 (DMA analysis)	1.96	2.6×10^{-1}
NIE butterfat #4 (DMA analysis)	2.01	2.2×10^{-1}
NIE palm oil	2.82	1.2×10^{-9}
CIE palm oil	2.82	2.0×10^{-9}
NIE lard	2.88	9.2×10^{-14}
CIE lard	2.84	6.7×10^{-10}
Cocoa butter #1	2.37	5.3×10^{-2}
Cocoa butter #2 (DMA analysis)	2.40	2.1×10^{-2}
Tallow	2.41	1.5×10^{-2}

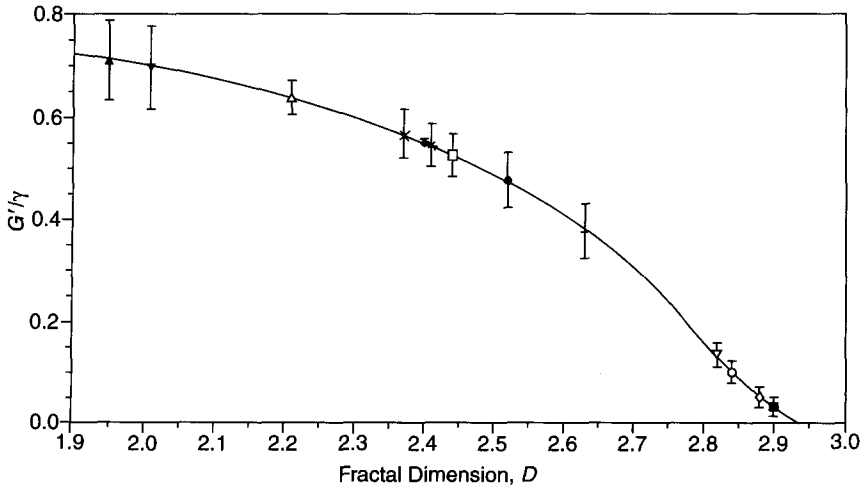

FIG. 37 G'/γ as a function of D. The solid line represents Eqn (46), symbols with error bars represent average values of rheological measurements (shown in Table II) and their standard errors.

make fats with smaller or larger elastic constants (which we have seen are related to hardness, although not in a direct manner), using fractal dimension as an indicator. One must realize here that this presupposes that the pre-exponential term γ remains constant when the processing conditions are changed, which as will be shown in Section IV, is not a good assumption. However, this development does tell us how fractal dimension in isolation affects the elastic constant of the network: it is now of course necessary to investigate those structural parameters which are indicators of the constant γ– the subject of Section IV.

L. ORDER, DENSITY, AND FRACTAL DIMENSION

The two methods presented to calculate fractal dimension are rather involved, and in the case of the rheological method, require specialized skill. Both methods take a fair amount of time, although the microscopic method is by far the easier and quicker method. However, it is useful to attempt to attach a visual index to the value of the fractal dimension.

Note that for a higher fractal dimension, the density of the packing of the microstructural elements must be higher – since the number of microstructural elements is proportional to the characteristic length raised to a power equal to the fractal dimension, according to Eqn (34). Density of packing of the microstructural elements does not refer to the traditional definition of density of the network (total mass/total volume), nor does it refer to the density *within* a typical microstructural element (which has been used in Eqn (45) as the symbol ρ_{ME}). The density of packing of the microstructural elements refers to the density of the microstructural elements *within* one microstructure. Therefore, if one is observing a particular fat after it has been processed differently, then the increase or decrease of the amount of microstructural elements within a certain characteristic length will signal the increase or decrease of the fractal dimension. However, given the nature of the PLM images, this is not a parameter that is easily ascertained without image analysis. Additionally, as is discussed below, the fractal dimension is not only dependent on the density of the packing of the microstructural elements, it is also dependent on the *order* in which they pack. Certainly, these two parameters are interrelated, since the order in which the elements pack also influences the density of the packing, and is itself influenced both by the nature of the inter-microstructural element forces and the mass and heat transfer limitations during the formation of the network.

Figure 38 shows a composite of four of the fat networks shown earlier – milkfat (A), tallow (B), palm oil (C) and lard (D). These images are of the fats crystallized at 5°C for 24 h, except for lard, which was crystallized

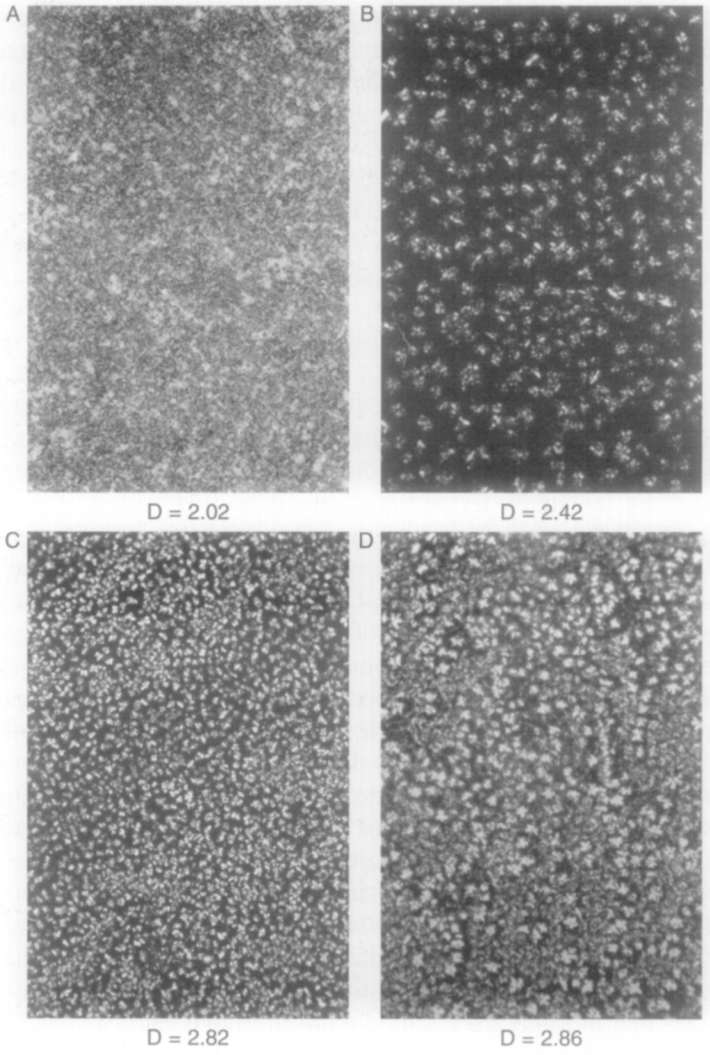

FIG. 38 Increasing fractal dimension implies increasing order of packing: (A) milkfat, (B) tallow, (C) palm oil, (D) lard.

for 72 h. As is evident from the figure, the order of packing of the microstructural elements increases from (A) through to (D). Additionally, the fractal dimension increases in the same way. It therefore seems that a higher fractal dimension implies a higher order of packing of the microstructural elements.

This result is not surprising. The fractal dimension is an index that is related to the order of the embedding space of the microstructural elements. If one can image that a plane is filled with close-packed microstructural elements taking up all the space, then that object is a two-dimensional object. If one can imagine a cube filled with close-packed microstructural elements taking up all space, then that object is a three-dimensional object. If one now takes the plane and starts putting kinks in it, the dimensionality of that space is raised to value between 2 and 3, as described before. The microstructural elements that were embedded in the fabric of the plane, now starts to look disordered – if the new positions of the microstructural elements are projected onto a plane, these positions will represent a disordered array. However, as the plane is kinked enough to start to approximate a cube (i.e. with higher fractal dimensions), then when the positions of the microstructural elements embedded in the fabric of the kinked plane are projected onto a plane, these positions start to look more ordered. This is exactly the situation we have when we look at a PLM image of the *in-situ* fat network. This picture is difficult to represent in a schematic, but a schematic of this process built on the basis of a one-dimensional space being raised to a two-dimensional space is useful in elucidating this concept.

If one considers a line, with microstructural elements placed at some equilibrium nearest-neighbour distance apart, then one has a picture represented by Figure 39(A). The projection of the positions of the microstructural elements onto a line represents an ordered array. Now, the line containing the microstructural elements represents a one-dimensional object. If one starts to put kinks in this line, one starts to raise the dimension of the line to a value just above 1, and less than 2. This scenario is represented in Figure 39(B). Now, the microstructural elements must still be placed at a nearest-neighbour equilibrium distance from each other on this new "space", so therefore, the projection of the positions of the microstructural elements onto a line begins to look disordered, as shown in the figure. It is useful to have a working quantitative definition of order in this analogy. When one looks at the projection of positions, one may define high order as the positions all being a common average distance apart from each other. Therefore, the standard deviation of the various distances apart of nearest-neighbour projection positions is a good representation of the deviation from order (lower standard deviation implies higher order). Figure 39(C) to (E) demonstrates situations in which more and more kinks are placed in the line containing the microstructural elements – therefore, the fractal dimension is increasing from (A) to (E). Table III shows the distance apart of nearest-neighbour projections of each situation (and lists an additional two situations following the same trend of kinks, not shown

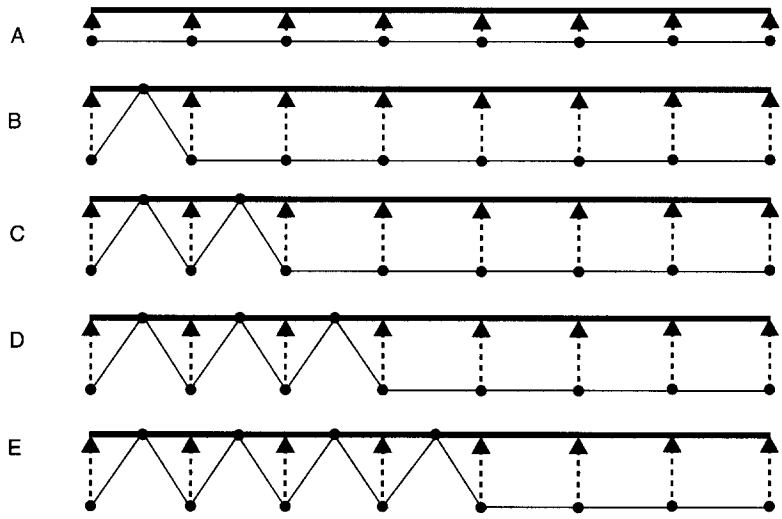

FIG. 39 Schematic of microstructural elements placed on a line at equal distances apart. The dimensionality of the line increases from (A) to (E). Microstructural elements on the thin line are projected onto the thick line.

TABLE III

SHOWING THE DECREASE IN STANDARD DEVIATION (AFTER AN INITIAL INCREASE) FROM AN AVERAGE DISTANCE BETWEEN PROJECTED POSITION OF BALLS ON A LINE, WITH INCREASING AMOUNTS OF KINKS IN THE LINE (FRACTAL DIMENSION IS PROPORTIONAL TO THE NUMBER OF KINKS – LESS KINKS, FRACTAL DIMENSION IS CLOSER TO 1, MORE KINKS, FRACTAL DIMENSION IS CLOSER TO 2).

Projected position	Distance between successive projected positions						
	1 kink	2 kinks	3 kinks	4 kinks	5 kinks	6 kinks	7 kinks
1	20	10	10	10	10	10	10
2	20	10	10	10	10	10	10
3	20	20	10	10	10	10	10
4	20	20	10	10	10	10	10
5	20	20	20	10	10	10	10
6	20	20	20	10	10	10	10
7	20	20	20	20	10	10	10
8		20	20	20	10	10	10
9			20	20	20	10	10
10				20	20	10	10
11					20	20	10
12						20	10
13							20
Standard deviation	0	4.63	5.27	5.16	4.67	3.89	2.77

in Figure 39), and the standard deviation in these values for each situation. As can be seen, as the fractal dimension increases, the order initially (for a small amount of kinks in the line) decreases, and then order begins to increase as the fractal dimension gets larger and larger (i.e. closer and closer to 2). Of course, the fractal dimension referred to here is qualitatively getting larger (the actual dimension has not been computed), but it is generally accepted that more and more kinks in a line represents higher and higher fractal dimensions, since the line is closer approximating a plane. This situation is exactly what happens in the case where dimension is between 2 and 3. An interesting effect to note is also that as the fractal dimension and order increases, so does the density of packing of microstructural elements in the observed region. This is of course, in agreement with the foregoing discussion on density and order.

M. ORDER AND HEAT LIMITATIONS

Increasing density and order of packing of the microstructural elements are accompanied by increases in fractal dimension. Increasing fractal dimension suggests that the shear storage modulus of the fat will decrease, although this does not take into consideration changes of the constant γ concomitant with changes in fractal dimension.

It is interesting to study the effect of crystallization characteristics on the fractal dimension, since changing the environmental conditions under which the fat network is formed will change the crystallization characteristics, and therefore one may be able to relate changes in environmental conditions to changes in fractal dimension. It is expected that the crystallization characteristics of the fat would be instrumental in determining the order of packing of the microstructural elements, due to the fact that the aggregation of the microstructural elements during formation of the network is through a process which is heat limited, at least at some stage during the aggregation. This process is heat limited, since, as we saw in Figure 27, there is growth of crystalline material (serving to increase the size of existing microstructural elements as well as the formation of new microstructural elements) during the aggregation process. This ongoing crystallization will result in the release of the latent heat of fusion, and the network must be able to absorb and dissipate this heat, if the crystalline material is not to re-melt or cause melting of neighbouring crystalline entities. It must be noted that the ordering effects of heat may be muted due to increased viscosity, leading to reduced mass transfer parameters in the crystallizing fat. Consequently, the nature of packing of the microstructural elements will be dependent on the way the heat of crystallization is released, which of course is also a function of the degree of supercooling

of the material, as well as the rate of heat transfer from the material during formation of the network. For instance, if the nature of the crystallization is such that all of the heat of crystallization is released in a short length of time (of course, this is dependent on the environmental conditions), then the network will be forced to absorb and/or dissipate this large amount of heat in a very small amount of time. As the schematic in Figure 40(A) shows, the most efficient way to achieve this dissipation of heat is to have the microstructural elements growing in ordered arrays, thereby allowing a maximum area of liquid oil (a good heat sink) around each centre of growth. However, if the heat of crystallization is released over a long period of time (as in Figure 40(B)), then the heat limitation is removed and the network is allowed to aggregate in a fashion which allows it to resort to its thermodynamically preferred packing, or a state which is close to its thermodynamically preferred packing (most fat crystal networks will stay in thermodynamically unstable states for long periods). Of course, the manipulation of the environmental conditions to affect these changes is not trivial – such varied parameters as degree of supercooling, rate of heat transfer, presence of different melting fractions in the fat, etc. are dependent

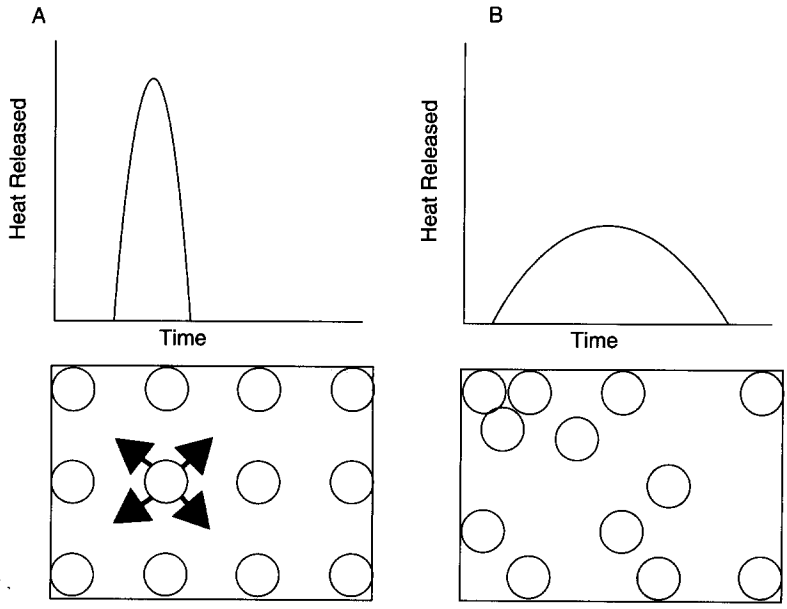

FIG. 40 Schematics showing the ordering effect of heat limitations on the network. (A) Heat is released in a short time, the network is forced to be ordered to dissipate heat. (B) Heat is released over a longer period, and the network assumes its preferred packing (represented here as disordered).

on how different environmental conditions will affect the crystallization heat profile of the formation of a fat crystal network. However, one can monitor the crystallization heat profile of a crystallizing network using a differential scanning calorimeter (DSC), under different environmental conditions, and from this profile, one may be able to predict increases or decreases in order, and therefore, fractal dimension. If there are initial releases of heat which are in a short period of time, then one would expect these narrow "peaks" in the heat-released vs. time graphs to be order-setting steps, since subsequent crystallization will occur as growth on the already established microstructural elements. It must however be stated here also that heat profiles demonstrating a broad "peak" in the heat-released vs. time graph may also demonstrate an ordered packing, since this may be the thermodynamically preferred packing of that fat crystallized under those conditions. However, if one can succeed in changing the heat profile of a particular fat by changing the crystallization conditions, any broadening or narrowing of initial peaks in the heat-released vs. time graphs should contribute to less order or more order, respectively. Some points to note here are that the crystallization heat profile of a sample of the fat crystallizing in a DSC pan will not necessarily represent the heat profile of a fat crystallized in bulk, and almost certainly will not represent the heat profile of a fat crystallized in a scraped-surface heat exchanger. It is also uncertain that one can approximate the same environmental conditions on a microscope slide as in a DSC pan, or for a sample prepared for rheology. However if, for instance, increasing the rate of the cooling in the DSC for a particular fat results in a heat profile demonstrating a sharper or broader initial peak in the heat-released vs. time graph, then one should expect the packing of the microstructural elements for that fat to be more or less ordered when the rate of cooling is increased in any statically crystallized fat sample. However, the extent to which the peak in question was sharpened or broadened would not necessarily be matched for the fat crystallized statically in a bulk sample, due to the difference in heat transfer characteristics between the sample in a DSC pan and the sample which is prepared for rheology, for example. However, there would be some amount of sharpening or broadening of the peak for the bulk sample as well.

1. Experimental

In an effort to illustrate the ordering effect of sharp peaks in a heat-released vs. time graph of the crystallization of fat networks, the DSC profiles of the four fats shown in Figure 38 were monitored. Samples of milkfat, tallow, palm oil, and lard were melted to 80°C and immediately placed within aluminum pans that were then hermetically sealed. A

Dupont Model 2090 differential scanning calorimeter was then used to monitor changes in heat flow of these samples during the crystallization of the samples. Similar empty pans were used as standards. The machine was operated at a rate of 5°C per minute. The samples were cooled at this rate down to at least –20°C. Figure 41 shows heat-released vs. temperature plots for the four fats – milkfat (A), tallow (B), palm oil (C) and lard (D). Since the samples were all cooled at an identical rate, the broadness or narrowness of peaks represents the relative time in which the heat was released.

Figure 42(A) shows heat-released vs. temperature DSC plots for samples of milkfat cooled at different rates – 20°C/min (A), 12°C/min (B), 5°C/min (C) and 1°C/min (D). The samples were prepared in a manner identical to that is described above, and the measurements were performed on the same calorimeter listed above. This was done in order to demonstrate the effectiveness of using changes in processing conditions to affect changes in order of packing of microstructural elements and therefore changes in fractal dimension for a particular fat.

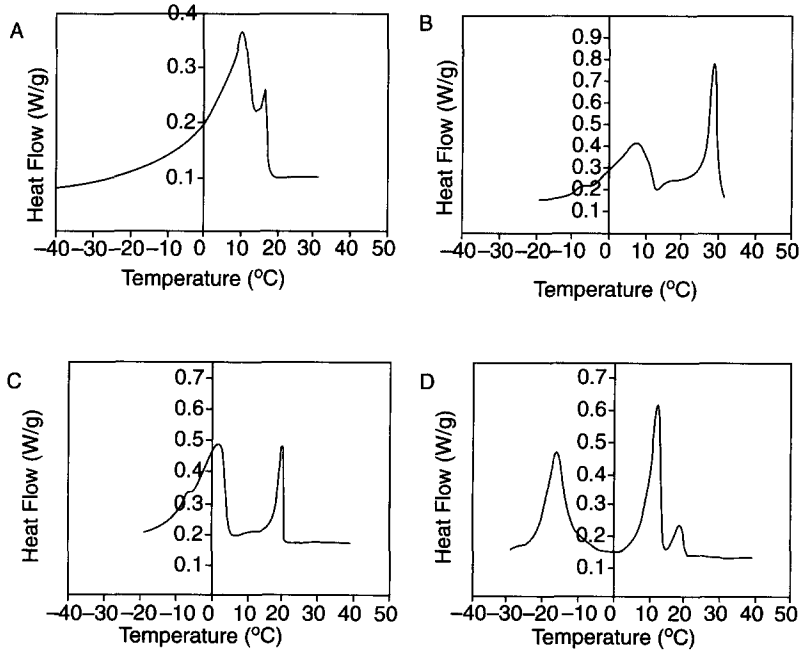

FIG. 41 DSC profiles of fat samples cooled at 5°C per min. (A) milkfat, (B) tallow, (C) palm oil, (D) lard.

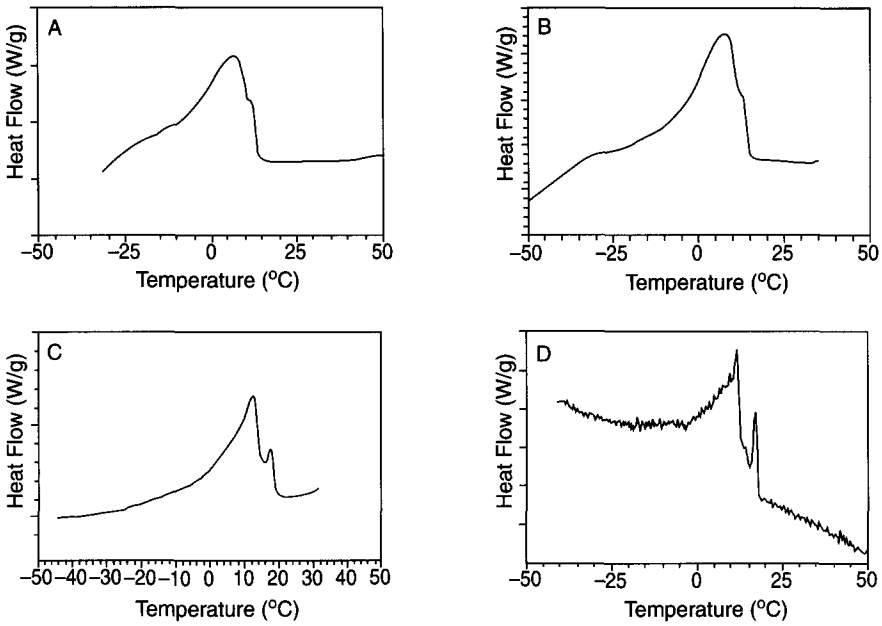

FIG. 42 Showing DSC profiles of milkfat, with different rates of cooling. (A) 20°C/min, (B) 12°C/min, (C) 5°C/min, and (D) 1°C/min.

Microscopy slides for *in-situ* polarized light microscopy were prepared as described before, with milkfat samples being prepared according to two tempering methods. In one method (slow cooling method), the sample was melted at 80°C for 30 min, then kept at 40°C for 30 min, then at 25°C for 60 min, then at 20°C for 60 min, then at 15°C for 60 min, then at 10°C for 60 min, then refrigerated at 5°C. The tempering steps listed above were performed using SANYO MIR1530 Cooled Incubator. In the other method (fast cooling method), samples were melted at 80°C for 30 min, then kept at 40°C for 30 min, and then refrigerated at 5°C. Figure 43(A) shows a PLM micrograph of the milkfat sample cooled using the fast cooling method, and Figure 43(B) shows a micrograph of the sample cooled using the slow cooling method, after 10 days of both sets of samples being incubated at 5°C.

Rheological samples of 100% milkfat and various dilutions with canola oil (95% w/w, 90% w/w, 85% w/w, and 80% w/w milkfat-canola oil) were prepared for the Perkin Elmer DMA 7 rheometer. The rheometer had a 1 cm diameter parallel-plate geometry. The milkfat and milkfat-canola oil samples were melted to 80°C and poured into moulds constructed of

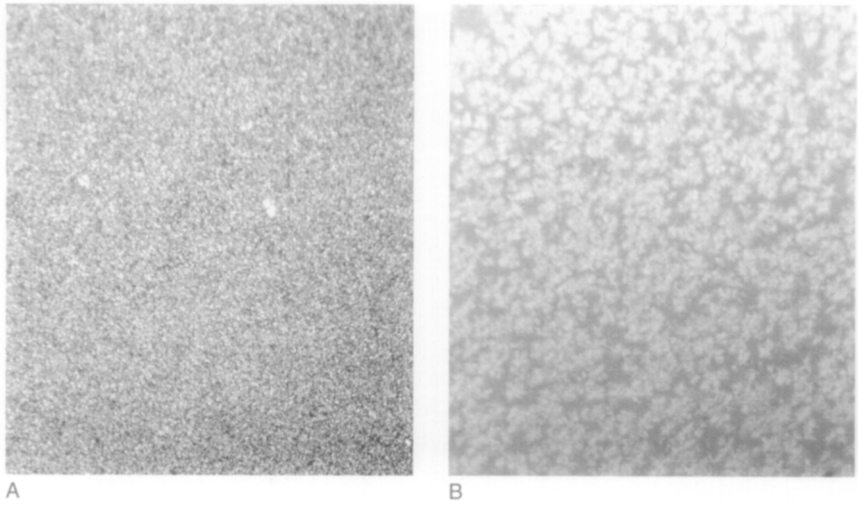

FIG. 43 (A) Sample of milkfat cooled quickly. (B) Sample of milkfat cooled slowly. Both samples are at 5°C, and the magnification is the same (10× objective lens used to image both samples on the same microscope).

plastic material, each mould being cylindrical with a height of 0.5 cm and a diameter of 1 cm. Samples of the 100% milkfat and dilutions were also put into tubes suitable for measurement of solid fat content in a Bruker Minispec 120 pulsed-NMR machine. Two sets of samples for rheological and solid fat content measurements were prepared – one set were tempered according to the fast cooling method and one set according to the slow cooling method, described above. Each dilution analysed rheologically and for solid fat content was prepared in triplicate.

After incubation at 5°C for 10 days, the samples were transferred to the temperature-controlled DMA cell, set to 5°C. The upper plate was lowered manually until contact with the sample was established. All compression measurements were performed under a static force of 5 kPa to ensure proper mechanical contact. On top of the static stress, a dynamic stress wave was applied at a frequency of 1 Hz, increasing from 2.5 to 5 kPa at 1 kPa/ min^{-1}. A clear elastic region was observed in this stress range, and compressive storage, or Young's modulus (E) was recorded in triplicate. Strains were of the order of 0.01%. Values of Φ_{SFC} were then measured in triplicate. Plots of log E vs. log Φ_{SFC} were made. Since $E/3$, = G' then a plot of log E vs. log Φ_{SFC} should yield as its slope $1/(3 - D)$. Values of fractal dimension were therefore calculated for the two sets of samples. For the samples cooled slowly, the fractal dimension was 2.65 and for the samples cooled quickly, the fractal dimension was 2.27.

2. *Discussion*

Figure 41 is somewhat limited in what it can suggest about the effects of processing conditions on crystallization conditions, which may lead to order or disorder in the packing of microstructural elements. This is because the fats shown are all different, and therefore the appearance of a broad or narrow peak in one fat cannot strictly be compared to the appearance of a narrow or broad peak in another fat. The appearance of increased order or disorder due to the broadness of the peaks can only strictly be compared with samples of the same fat processed differently. This is because some fats will be inherently (thermodynamically) disordered, whilst others will be inherently ordered. Given this, if we compare Figure 41 to the micrographs shown in Figure 38, some useful conclusions can be drawn. The micrographs shown in Figure 38 shows the same fats whose DSC profiles are represented in Figure 41. However, the micrographs in Figure 38 were all taken at 5°C. Therefore, any comparisons made must necessarily exclude those features in the DSC profiles which are below 5°C. As is evident from Figure 41, all of the fats with a sharp initial peak above 5°C (tallow (B), palm oil (C), and lard (D)) demonstrate very ordered packing in the microstructural elements in Figure 38. Milkfat (Figure 41(A)) demonstrate a relatively broad peak, and its microstructural elements are packed in a relatively disordered fashion. The fats were all processed identically, so therefore it appears that the presence of the initial sharp peaks in the heat released vs. temperature DSC plots have an ordering effect on the packing of the microstructural elements.

Figure 42 demonstrates that if one decreases the rate of cooling of milkfat, a sharp initial peak appears – this peak is represented as a shoulder in the DSC profiles of the samples which are cooled at 20°C per min (Figure 42(A)) and 12°C per min (Figure 42(B)). However, in the DSC profiles of the samples cooled at 5°C per min (Figure 42(C)) and 1°C per min (Figure 42(D)), this peak appears more defined, and represents a greater amount of heat released over a narrow temperature range. Therefore this suggests that if milkfat is cooled slowly, the fat will demonstrate a relatively ordered packing of the microstructural elements compared to a situation where it is cooled quickly. It is uncertain what is causing the peak to appear – but it is most probably due to the composition of the milkfat (it is well-known that milkfat is composed of a number of different melting fractions, e.g. Marangoni and Lencki, 1998). The sharp peak could be due to the highest melting fraction in milkfat crystallizing out before any of the other fractions. If the fat is cooled quickly, this event would not be an initial effect, since practically all of the fractions will crystallize out at once. However, if the fat is cooled slowly enough, the

highest melting fraction (or the highest melting fraction compounded with an amount of the middle melting fraction) would have the time to crystallize before the crystallizing temperature of the other fractions is reached. Additionally, if the highest melting fraction has a narrow melting range (which it does – see Marangoni and Lencki, 1998), then the burst of heat released as it crystallizes will be in a narrow temperature range. Almost certainly, this sharp crystallization peak is due to the high melting fraction of milkfat crystallizing out in isolation or with a small amount of compounded middle melting fraction. Given this sharp burst of crystallization, the appearance of microstructural elements of the high melting fraction of milkfat will establish an ordered template upon which the rest of the fractions will grow. This is indeed the case when one examines Figure 43 – the micrograph of the sample cooled slowly (Figure 43(B)) demonstrate a relatively ordered packing of the microstructural elements compared to the sample cooled quickly (Figure 43(A)). Additionally, in agreement with the discussion of order and fractal dimension above, the fractal dimension calculated for the samples cooled slowly was 2.65 compared to 2.27 for the samples cooled quickly. As is evidenced by the micrographs shown in Figure 43, the sizes of the microstructural elements are different in the two differently prepared samples. This is a good indication that the constant γ for these samples are also different, since it has been suggested that this constant depends in part on the nature of the microstructural elements. In fact, the rheological analysis yielded γ values of 2.0×10^{-4} MPa and 7.0×10^{-2} MPa, for the slow and fast cooled samples, respectively. This issue will be revisited in Section IV, but it is important to note here that the changes effected in the fractal dimension by changing the processing conditions are not isolated, but in fact are followed as well by changes in the constant γ. The point here is that it is myopic to assume that the elastic constant of the network will change only according to the changes in D due to different processing conditions – chances are that γ will also change.

N. CONCLUSIONS

It has been shown in this section, from a structural basis established by a multitude of microscopy techniques, that fat crystal networks crystallized statically are fractal within certain length ranges. Furthermore, it was shown that the weak link theory is applicable to fat crystal networks. The microscopical method developed to calculate fractal dimensions produced values which were in good agreement with those calculated from application of the weak link theory. However, it must also be mentioned that the microscopical method requires the use of a subjective method of thresholding, which brings into question the value of its use in an industrial

setting. Additionally, it was discussed above that many fat systems with densely-packed microstructural elements may not be suitable to be analysed by this method. Through the choice of fat systems suitable to be analysed by this method, however, it has been shown that the rheological method of analysis employed by Rousseau and Marangoni (detailed in Section II) is valid for fat networks.

It has been established that a higher degree of order in the packing of the microstructural elements represents a higher fractal dimension. Additionally, it has been shown that processing conditions may be changed in ways that can result in changes in the fractal dimension. It is important to realize that changes in crystallization behaviour seen with a sample of a particular fat under different processing conditions are not necessarily reproducible with samples of greater bulk. If the temperature trajectory of the crystallization process can be determined, the relative broadening or narrowing of initial peaks in the temperature–time curve due to changes in processing conditions will produce dis-ordering or ordering effects. The origin of these effects is however not straightforward – factors such as supercooling, rate of transfer of heat from the containing vessel, ease of nucleation events, formation of different polymorphs, existence of separate fractions, etc., will all play a role.

The structure of the network developed in this chapter has been for fats that were crystallized under static conditions, without any shearing of the fat (as is usually done in industry) and without any heat-removal techniques such as those employing scraped-surface heat exchangers. Additionally, the fats were not crystallized under conditions of severe supercooling. Therefore, the structure that is presented here is not necessarily representative of fat crystal networks crystallized under industrial-like conditions. Some controversy presently exists about whether fats that were crystallized in scraped-surface heat exchangers at high levels of supercooling are indeed fractal. This work can make no claims about the validity of any side of this argument, since none of the fats studied here were crystallized under such conditions. Suffice to say that from brief discussions with other researchers (personal communication with Dr Pieter Walstra and Dr William Kloek), it seems unlikely that fats crystallized under such industrial-like conditions are fractal in nature.

IV. MECHANICAL MODEL AT LOW DEFORMATIONS: INVESTIGATING γ

The quantification of the spatial distribution of microstructural elements within the microstructures in fat crystal networks has been studied in Section III. The weak link theory was applied to the structure of fat crystal

networks, producing a relationship of the shear storage modulus (G') to the solid fat content (Φ_{SFC}) via the mass fractal dimension (D) of the network and a constant γ. All of these parameters are well-defined, except for the constant γ, which has been proposed to be dependent on the nature of the microstructural elements, the links between microstructures, the relationships between ξ (size of microstructures), Φ (microstructural element volume fraction), and D, and the proportionality between Φ_{SFC} and Φ. The exact dependence of the constant γ on network properties has not been formulated: it is the motivation of the model outlined in this section to formulate a relationship of γ to fundamental chracteristics of the fat network in a manner that would relate γ to structural characteristics of the network. As will be demonstrated, it is not possible to formulate an *exact* relationship for γ, but it is worthwhile to identify some of the parameters that affect its value.

Network models aimed at relating the shear storage modulus to the particle volume fraction for fat crystal networks are summarized in Section II. One of the reasons previous models of fat crystal networks have failed was that they predicted a linear relationship between the storage modulus and the solid fat content of the network. As suggested by the weak link theory and shown by Figure 35 (Section III), the storage modulus of the network actually depends on the solid fat content in a power law fashion. This relationship has also been documented by a variety of other researchers in the field (e.g. Nederveen, 1963; Payne, 1964; Papenhuijzen, 1971, 1972; van den Tempel, 1979; Vreeker *et al.*, 1992b; Narine and Marangoni, 1999a, 1999b, 1999c).

The implications for altering the mechanical properties of fat crystal networks (by following changes in structure, which implies changes in γ and/or D) by varying processing conditions will also briefly be discussed in this section.

A. THEORY

The storage modulus of fat crystal networks are virtually independent of frequency (in LVR) and in the linear viscoelastic region demonstrate a very low value of damping (Nederveen, 1963; Rousseau *et al.*, 1996c). An example of the lack of variation of the storage modulus with frequency is shown in Figure 44. This suggests that the viscosity of the liquid (oil) portion of the network plays no essential part in the transmittance of forces; if this was the case, one would expect increases of the loss modulus (at frequencies corresponding to the relaxation time of the network) with increases in frequency (Nederveen, 1963). The fact that fat crystal networks do demonstrate a measurable storage modulus as well as a yield value suggests that the solid fat particles are the entities responsible for the

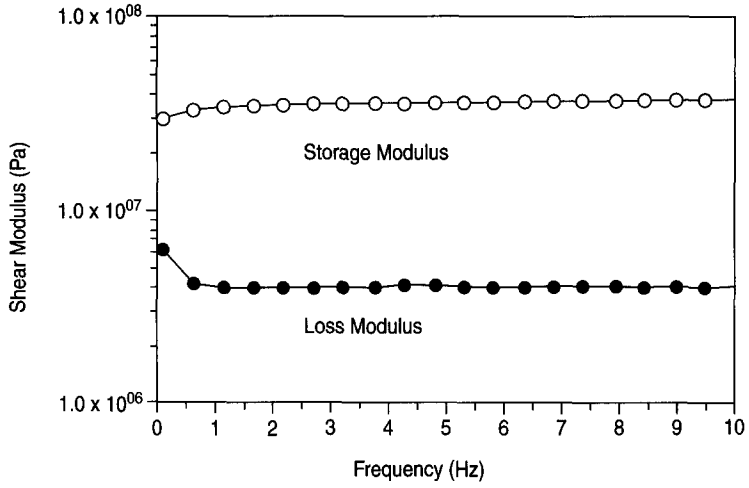

FIG. 44 Shear elastic modulus, G', and loss modulus, G'' plotted against frequency for cocoa butter (solid fat content of sample is 75% and strain level is 0.5%).

storage modulus and therefore these particles must have strong mutual interactions.

B. STRUCTURAL MODEL

As presented in Section III, at the microstructural level, the solid network is an orthodox amorphous solid, whilst the intra-microstructural level is fractal in nature. The arrangement of the microstructures can be imagined as an assembly of chains, each chain consisting of a linear array of microstructures with an average small distance apart. The chains are branched and interlinked to form a three-dimensional network with oil present in the void volume, both within and outside the microstructures. In this way the network is similar to the network as described by van den Tempel (1961). However, van den Tempel did not consider that the particles forming the chains were clusters of smaller particles arranged in a fractal manner; the way the microstructures are clusters with microstructural elements arranged within them in a fractal manner. In a later publication, van den Tempel (1979) did consider that the netwok is formed via interaction of clusters rather than primary particles, but did not consider the fractal arrangement of the "primary particles" within the clusters. Evidence of the existence of ordered microstructures were presented in Section III, and is also given by Heertje and co-workers (Heertje *et al.*,

1987; Juriaanse and Heertje, 1988; Heertje, 1993). The fractal nature of the microstructures was demonstrated in Section III.

The relationship given by the weak link theory was formulated by assuming the elastic constant of the network is dependent on the nature of the links between microstructures, as opposed to the strength of the microstructures themselves. This theory is applicable to fat crystal networks at relatively high percentages of solid content. The weak link theory suggests that when a deforming force is placed on the fat crystal network such that the resulting deformation is within the linear viscoelastic region of the network, the links between the microstructures are stressed, rather than the microstructures themselves.

C. FRACTAL NETWORK MODEL

In a 1 cm^3 sample containing N_ξ microstructures, with N_σ microstructural elements in each microstructure, the particle volume fraction (microstructural element volume fraction) of the network is given by:

$$\Phi = \frac{4}{3}\pi\left(\frac{\sigma}{2}\right)^3 N_\sigma N_\xi \tag{47}$$

where σ is the diameter of a microstructural element assumed to be spherical. This assumption is not a bad assumption for most natural fat systems at high solid fat contents as have been discussed in Section III. However, this is an important assumption of the model being developed, and should be taken into consideration when large deviations from sphericity are observed. The number of microstructural elements within a microstructure is given by the following equation:

$$N_\sigma \sim \left(\frac{\xi}{\sigma}\right)^D \tag{48}$$

$$\Rightarrow \quad N_\sigma = c(\xi)^D \tag{49a}$$

where ξ is the diameter of a microstructure and c is a proportionality constant. As explained in Section III, the fractal dimension of a fat crystal network may be calculated by utilizing Eqn (49a) in the following form:

$$N_\sigma = c(R)^D \tag{49b}$$

where $\sigma \leq R \leq \xi$. Taking logarithms:

$$\log(N_\sigma) = D\log(R) + \log(c) \tag{50}$$

Therefore, a plot of $\log(N_\sigma)$ vs. $\log(R)$ yields $\log(c)$ as the intercept and D as the slope. Therefore, form Eqn (47):

$$\Phi = \frac{4}{3}\pi\left(\frac{\sigma}{2}\right)^3 c(\xi)^D N_\xi \tag{51}$$

The number of microstructures in a sample of volume 1 cm^3 may therefore be written as:

$$N_\xi = \frac{6\Phi}{c\pi\sigma^3\xi^D} \tag{52}$$

If the distance between neighboring microstructures in a chain is small compared to ξ, the total length of all the chains present in the 1 cm^3 sample is:

$$N_\xi\xi = \frac{6\Phi\xi}{c\pi\sigma^3\xi^D} \tag{53}$$

It can be safely assumed that the total chain length is made up of straight chains oriented in three mutually perpendicular directions in a cubic sample, given the regular manner in which the microstructures have been observed to pack. Therefore, when the network is stressed in a given direction only one third of the total chain length represents the number of chains supporting stress in that direction. In a cube of volume 1 cm^3, a cross-section of area 1 cm × 1 cm cuts through the following number of 1 cm chains:

$$\frac{N_\xi\xi}{3} = \frac{2\Phi\xi^{1-D}}{c\pi\sigma^3} \tag{54}$$

These are therefore the total length of chains that transmit stress from one part of the sample to the other.

D. FORCES ACTING WITHIN THE NETWORK

It is assumed that the attractive forces between microstructures consist of van der Waals interactions between microstructural elements that form nearest-neighbors at the interface between two microstructures. Again, this is an important assumption of the model being developed. At this point, the author cannot account for any other forces acting in the network at this level of structure. As explained below, polar forces at this level of structure are relatively negligible. Furthermore, the fat particles are non-polar and the oil is a non-polar medium. However, this assumption

must be taken into account when considering "real" systems with significant amounts of water present or significant amounts of polar components present. One can imagine that if the microstructures all are of the same size and shape, there will be some m interactions due to nearest-neighbor interactions between microstructural elements at the edge of two neighboring microstructures. Therefore, as far as the storage modulus of the network constitutes a measures of the mechanical strength of the network at small deformations, all of the microstructural elements present do not contribute to the mechanical strength. The relatively few microstructural elements that link the microstructures together are moved with respect to their nearest neighbors in a neighboring microstructure when the network is stressed, whilst the microstructures themselves behave as rigid units. This view of the behavior of the network under a deforming stress is shared by Papenhuijzen (1972). The assumption that van der Waals interactions are the interactions of importance with fat particles is not new (van den Tempel, 1961, Nederveen, 1963; Payne, 1964) and as Nederveen (1963) has stated, it may be calculated that dipolar forces are about a factor of 10^{10} smaller than van der Waals forces, making these negligible enough to ignore.

It is difficult to take into consideration non-spherical shapes in a calculation of van der Waals forces, although this has been attempted before (Vold, 1951). Therefore, in the following development, the microstructural elements are assumed to be spherical, as explained above, a reasonable assumption. Below, we summarize a development of the calculation of van der Waals interaction between two microstructural elements, developed by Nederveen (1963). The Lennard-Jones potential between two non-polar atoms is formulated as:

$$U = -\lambda r^{-6} + \mu r^{-12} \tag{55a}$$

$$\lambda = 2 | U_o | r_o^6 \tag{55b}$$

$$\mu = \frac{\lambda}{2} r_o^6 \tag{55c}$$

where U is the potential energy of two molecules at a distance r. When the two molecules are at their equilibrium distance r_o apart, the potential energy is U_o. In order to calculate the attractive energy between two spheres consisting of a large number of molecules (say, q/m^3), Eqn (55a) must be integrated over the volumes of both spheres:

$$U = q^2 \int_{v_1} \mathrm{d}v_1 \int_{v_2} \mathrm{d}v_2 \, (-\lambda r^{-6} + \mu r^{-12}) \tag{56}$$

where dv_1, dv_2, V_1 and V_2 are volume elements and volumes of the two spheres 1 and 2 and r is the distance between dv_1 and dv_2. Hamaker (1937) had before Nederveen carried out the integration of the attractive term. By carrying out the integration for the repulsive term as well, it is possible to calculate the stiffness of a van der Waals bond for small deviations from equilibrium, such as is the case when the network is deformed during measurement of the storage modulus. Nederveen performed the integration for two spheres with equal radii R separated by a distance d (making the distance between the centres of the two spheres $C = 2R + d$). The steps of the integration are cumbersome and unnecessary to re-state at this point. It is sufficient to say that for $d << R$, Nederveen's integration agreed with an independent check by the authors and yielded:

$$U = \frac{-AR}{12d}\left[1 - \frac{1}{420}\left(\frac{r_o}{d}\right)^6\right] \tag{57}$$

where $A = \pi^2 q^2 \lambda$ is the Hamaker's constant. The attractive force between the two spheres is given by differentiation of Eqn (57) with respect to d:

$$F = \frac{\partial U}{\partial d} = \frac{2AR}{12d^2}\left[1 - \frac{1}{60}\left(\frac{r_o}{d}\right)^6\right] \tag{58}$$

Eqns (57) and (58) suggests that there is an equilibrium distance where the potential energy between the two spheres is a minimum and the force between them becomes zero:

$$d_o = \frac{r_o}{\sqrt[6]{60}} \tag{59}$$

If the deformation ε of all volume elements in the two spheres is homogeneous, then d may be written as a function of the radius of the spheres:

$$d = d_o + 2R\varepsilon \tag{60}$$

When Eqns (59) and (60) are substituted into Eqn (58):

$$F = \frac{AR^2\varepsilon}{d_o^3}\left(1 - \frac{11R\varepsilon}{d_o}\right) \tag{61}$$

This equation is valid only when $11R\varepsilon/d_o$ is small compared to unity. Therefore, for very small deformations, the force between the two spheres varies linearly with the deformation (ε).

It is expected that as two microstructural elements move apart due to a stress on the network, the resulting gap is filled with the liquid oil present in these networks. Papenhuijzen (1972) has shown that by considering the microstructural elements as spheres and using a corrected Stokes equation:

$$f_h = 3\pi\eta_L R u \alpha \tag{62}$$

where f_h is the force necessary to move a sphere with diameter R at speed u to a flat plate, η_L is the viscosity of the oil and α is a correction factor which depends on the distance between the sphere and the plate, the corresponding hydrodynamic force can be expressed as:

$$f_h = \frac{3\pi\eta_L R^2 u}{8d} \tag{63}$$

As reported by Kamphuis and Jongschaap (1985), the elongation rate between the two spheres is assumed to be very small:

$$u << \frac{A}{\eta_L R d} \tag{64}$$

and therefore only the Lennard-Jones potential as described above needs to be taken into account. These authors also suggested that the inertial forces are negligible with respect to the interactive forces (Kamphuis *et al.*, 1984). This is assumed as well in our treatment. Again, it is important to note these assumptions, which simplifies the model considerably. There seems to be plausible reasons why these can be made, as explained above.

Figure 45 shows a schematic of two neighboring microstructures. The force between two neighboring microstructural elements is given by Eqn (61). If the microstructural elements are assumed identical, the interaction between neighboring microstructural elements can be represented by a spring. Therefore, the forces between microstructures can be represented as m identical springs of spring constant k in parallel. If one assumes that the pairs of microstructural elements are *all moved the same distance apart*, then the total force can be approximated by:

$$F = \sum_1^m k_n \Delta x = \sum_1^m f_n = mf \tag{65}$$

where f is the restoring force of one spring of force constant k extended by a distance of Δx. Therefore, if there are m identical pairs of microstructural elements at the interface between two microstructures, the force between the microstructures is given by:

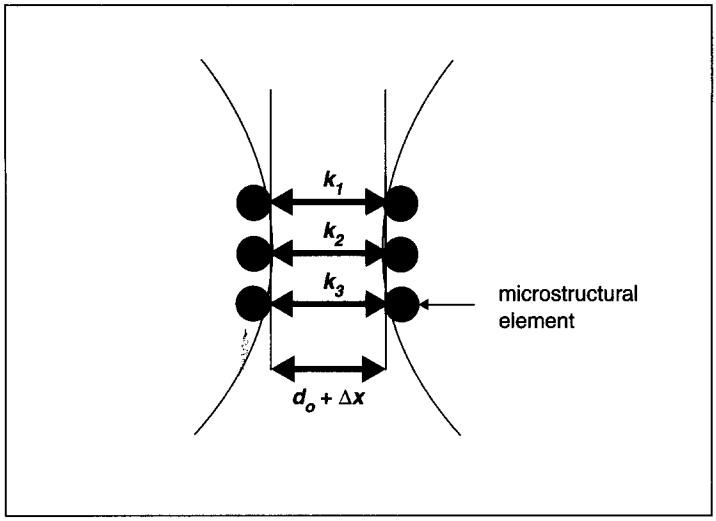

FIG. 45 Schematic showing forces between two microstructures.

$$F = m\frac{A\sigma^2\varepsilon}{4d_o^3}\left(1 - \frac{11\sigma\varepsilon}{2d_o}\right) \tag{66}$$

where R in Eqn (61) has been replaced by $\sigma/2$ to represent the radius of the microstructural elements.

E. STORAGE MODULUS

In a sample that is a cube of volume 1 cm^3 which is stressed in one direction, the number of chains carrying the stress is given by Eqn (54). Therefore, the stress s transmitted through a 1 cm × 1 cm cross-section is given by (van den Tempel, 1961; Nederveen, 1963; Kamphuis and Jongschaap, 1985):

$$s = m\frac{A\sigma^2\varepsilon}{4d_o^3}\frac{2\Phi\xi^{1-D}}{c\pi\sigma^3}\left(1 - \frac{11\sigma\varepsilon}{2d_o}\right) = m\varepsilon\frac{A\Phi\xi^{1-D}}{2c\pi\sigma d_o^3}\left(1 - \frac{11\sigma\varepsilon}{2d_o}\right) \tag{67}$$

The tensile modulus of the network is then given by:

$$E = \frac{s}{\varepsilon} = m\frac{A\Phi\xi^{1-D}}{2c\pi\sigma d_o^3}\left(1 - \frac{11\sigma\varepsilon}{2d_o}\right) \tag{68a}$$

When the deformation is small enough that one is in the linear elastic region and the following relationship holds:

$$\frac{11}{2}\frac{\sigma\varepsilon}{d_o} < 0.1 \tag{68b}$$

Eqn (68a) reduces to:

$$E = \frac{s}{\varepsilon} = m\frac{A\Phi\xi^{1-D}}{2c\pi\sigma d_o^3} \tag{69}$$

The storage shear modulus is given by:

$$G' = \frac{E}{3} = m\frac{A\Phi\xi^{1-D}}{6c\pi\sigma d_o^3} = m\frac{A\Phi\xi^{2-D}}{6c\pi\sigma\xi d_o^3} \tag{70}$$

If the fractal dimension within microstructures is D, i.e. the spatial distribution of the microstructural elements within the microstructures is characterized by D, the scaling relationship between the average microstructural size ξ and the solid volume fraction Φ can be found by approximating the solid volume fraction inside the microstructures as the overall solid volume fraction (as was demonstrated in Section II):

$$\xi \sim \Phi^{\frac{1}{D-d}} \tag{71}$$

From Eqn (71):

$$\xi^{2-D} \sim \left[\Phi^{\frac{1}{D-d}}\right]^{2-D} = \Phi^{\frac{2-D}{D-d}} \tag{72}$$

Therefore:

$$\Phi\xi^{2-D} \sim \Phi\Phi^{\frac{2-D}{D-d}} = \Phi^{\frac{d-2}{d-D}} \tag{73}$$

From the above:

$$G' \sim m\frac{A}{6c\pi\sigma\xi d_o^3}\Phi^{\frac{d-2}{d-D}} = m\frac{A}{6c\pi\sigma\xi d_o^3}\Phi^{\frac{1}{d-D}} \tag{74}$$

Recalling from Section III that Φ and Φ_{SFC} are related:

$$\Phi = \frac{\rho_t}{\rho_{ME}}\Phi_{SFC}$$

(where ρ_t is the density of the entire network, and ρ_{ME} is the density *within* the microstructural elements) then Eqn (74) becomes:

$$G' \sim m\left(\frac{\rho_t}{\rho_{ME}}\right)^{\frac{1}{3-D}} \frac{A}{6c\pi\sigma\xi d_o^3}\Phi_{SFC}^{\frac{1}{3-D}} \tag{75}$$

Equation (75) therefore reduces to a form equivalent to weak link relationship. Comparing the weak link relationship developed in Section III and Eqn (75):

$$\gamma \sim \frac{mA}{6c\pi\sigma\xi d_o^3}\left(\frac{\rho_t}{\rho_{ME}}\right)^{\frac{1}{3-D}} \tag{76}$$

F. DIMENSIONAL ANALYSIS

The relationships represented by Eqns (75) and (76) do not have an equal sign, but instead, both represent a scaling relationship. Therefore, the model does not provide an absolute formulation, but instead helps to demystify the origins of γ– i.e. identify some of the structural parameters which affect the value of γ.

The scaling nature of the relationship stems from the following relationship:

$$\xi \sim \Phi^{\frac{1}{D-d}} \tag{71}$$

now, if we write this equation as:

$$\xi = k\Phi^{\frac{1}{D-d}} \tag{77}$$

then k has dimensions of L.

Therefore, if one re-visits Eqns (73) and (74):

$$\Phi\xi^{2-d} = k^{2-D}\Phi^{\frac{2-D}{D-d}}\Phi = k^{2-D}\Phi^{\frac{d-2}{d-D}} \tag{78}$$

which implies that:

$$G' = \frac{k^2k^{-D}mA}{6c\pi\sigma\xi d_o^3}\Phi^{\frac{1}{d-D}} \tag{79}$$

Taking into consideration the relationship of Φ to Φ_{SFC}, Eqn (79) becomes:

$$G' = \frac{k^2 k^{-D} mA}{6c\pi\sigma\xi d_o^3}\left(\frac{\rho_t}{\rho_{ME}}\right)^{\frac{1}{d-D}} {\Phi_{SFC}}^{\frac{1}{d-D}} \tag{80}$$

which implies that:

$$\gamma = \frac{k^2 k^{-D} mA}{6c\pi\sigma\xi d_o^3}\left(\frac{\rho_t}{\rho_{ME}}\right)^{\frac{1}{d-D}} \tag{81}$$

One can express the dimensionalities of the parameters in the system as: $[c] = L^{-D}$, $[k] = L$, $[\sigma] = L$, $[\xi] = L$, $[d_o] = L$, $[A] = NL$ (N = newton), m, π and $(\rho_t/\rho_{ME})^{1/(d-D)}$ are dimensionless quantities. Therefore, the right-hand side of Eqn (81) is dimensionally equal to:

$$\frac{L^2 L^{-D} NL}{L^{-D} LLL^3} = \frac{N}{L^2} = Pa \tag{82}$$

The dimension of the constant γ is of course Pa – this shows that Eqn (76) is dimensionally correct. Therefore, could a scaling constant be defined, the subsequent equality would be dimensionally correct. If one has an "approximately proportional to" relationship (like there is in a scaling relationship), dimensional analysis must take into consideration the dimensions of the constant of proportionality.

G. DISCUSSION

It is important to note that the power law relationship between G' and Φ_{SFC} of the weak link theory and Eqn (75) is only valid for deformations of the fat network small enough such that Eqn (68) holds. Additionally, Eqn (75) has been manipulated to represent the same functional form as the weak link theory. As a result, the average diameter of the microstructures in the network ξ appears in the denominator of Eqn (76). However, according to Eqn (71), ξ is related to the solid volume fraction. It is important to realize that Eqns (75) and (76) are only valid at high solid fat contents. It has been experimentally proven that at high solid fat contents, the constant γ is independent of the solid fat content; plots of $\log_{10} G'$ vs. $\log_{10} \Phi_{SFC}$ of some 14 different fat systems were statistically good straight lines with a measurable intercept corresponding to $\log_{10}\gamma$ (Table II, Section III). This therefore would suggest that ξ as it appears in

the denominator of Eqns (75) and (76) does not change significantly over the applicable range of solid fat content. Furthermore, the authors have observed no measurable change in the diameter of microstructures of cocoa butter observed in its natural state at 20°C and at dilutions of 5, 10, 15, 20, 25, and 30% w/w with canola oil. The canola oil in this case was used purely as a diluent to vary the solid fat content.

The dependence of the hardness of fats on the solid fat content has been studied by a variety of researchers (e.g. Bailey, 1950; Nederveen, 1963; Vreeker *et al.*, 1992b; Narine and Marangoni, 1999a, 1999b, 1999c; Haighton, 1976). In all cases hardness depended on the solid fat content in a power law fashion. Given that storage modulus has been shown to be proportional to hardness in fat crystal networks (Narine, 2000), this power law relationship is supported by Eqn (75). Furthermore, as is demonstrated by Figure 36 (Section III), a plot of ln G' vs. ln Φ_{SFC} yields a straight line, verifying the power law dependence of G' on Φ_{SFC}. Additionally, as have already been shown in Section III, rheologically calculated values of fractal dimension agree well with fractal dimensions calculated from image analysis. This suggests that Eqn (75) is correct in its description of fat crystal networks, as far as variation of G' with Φ_{SFC} and D is described by the model.

Practicle size has been shown experimentally to be an important parameter in the hardness of fat crystal networks (e.g. Bailey, 1950; Nederveen, 1963; Shama and Sherman, 1970; Haighton, 1976; de Man, 1961; de Man, 1964; Mulder and Walstra, 1974; Foley and Brady, 1984; Kawanari, 1996) but previous network models except for those by van den Tempel (1961, 1979) failed to show a dependence on particle size in the final expression for the shear storage modulus (e.g. Nederveen, 1963; Payne, 1964; Papenhuijzen, 1971, 1972; Kamphuis *et al.*, 1984; Kamphuis and Jongschaap, 1985). Overwhelming experimental evidence has been submitted by other researchers (de Man, 1961; de Man, 1964; Mulder and Walstra, 1974; Foley and Brady, 1984; Kawanari, 1996) which demonstrate that the hardness of fat crystal networks are inversely proportional to the particle size (microstructural element size). This is also supported by Eqn (75). Equation (75) demonstrates a dependence on both the size of the microstructures and the size of the microstructural elements.

As a visual example of the effect a decrease in microstructural element size has on the shear storage modulus, Figure 46 shows a marked decrease in particle size from the sample of non-interesterified lard/canola oil to the sample of chemically interesterified lard/canola oil. There is a corresponding decrease in the shear storage modulus as well; the shear storage modulus increases from 1.25×10^4 Pa to 3.34×10^5 Pa, as would

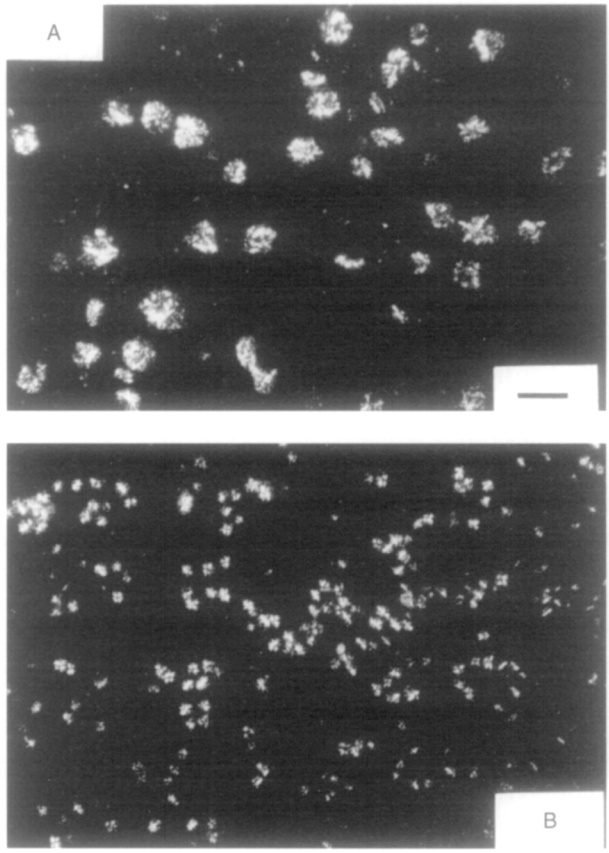

FIG. 46 Polarised light microscopy images of (A) 70% w/w samples of non-interesterified lard/canola oil and (B) chemically interesterified lard/canola oil. These samples were first broken and dispersed in paraffin oil. The horizontal bar represents 6 μm.

be expected from the decrease in the diameter of the microstructural elements shown dispersed in the images.

As is demonstrated by Figure 47(A), a plot of G' vs. $1/\sigma$ yields a proportional relationship, as is predicted by Eqns (75) and (76), and as has been shown before by other researchers (de Man, 1961; de Man, 1964; Mulder and Walstra, 1974; Foley and Brady, 1984; Kawanari, 1996). The fit to a straight line yields an r^2 value of 0.68. The fit is significantly improved when G' is plotted versus $1/c\sigma\xi$ as is seen in Figure 47(B), the r^2 value here being 0.98. This relationship is again predicted by Eqns (75) and (76). The fact that the straight line fit to the plot of G' versus $1/c\sigma\xi$ is

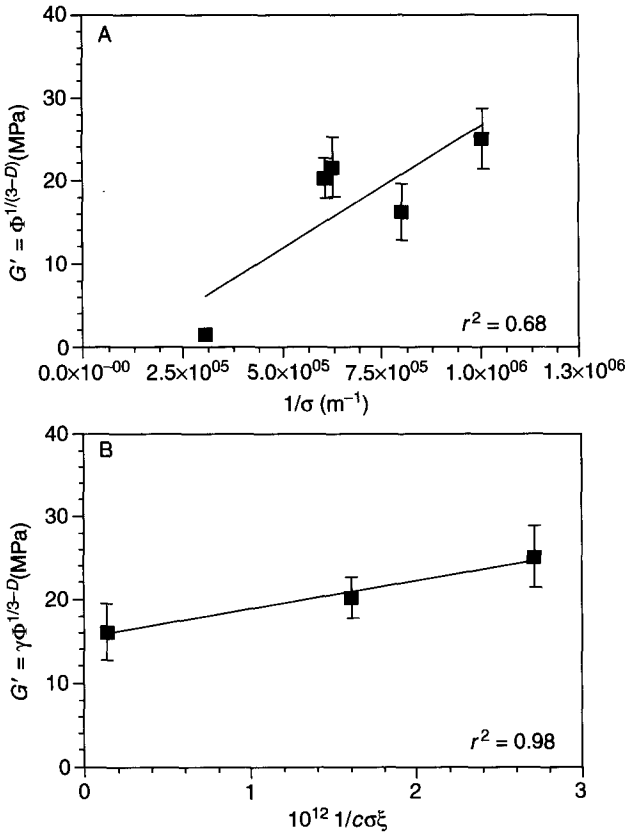

FIG. 47 (A) Plot of G' vs. $1/\sigma$ for five different fat systems. (B) Plot of values of G' vs. $1/c\sigma\xi$ for three different fat systems. For both (A) and (B), symbols with errors bars represent average values of rheological measurements and their standard deviations.

better than the plot of G' vs. $1/\sigma$ is important to note, since it seems that changes in σ are followed by changes in both c and ξ. It is not surprising that these parameters are co-variants, since from Eqns (48) and (49a), the parameter c is a measure of how many microstructural elements of a particular diameter σ are contained in a microstructure of a particular diameter ξ for that particular fat with a particular value for the fractal dimension D. Obviously, changes in ξ and σ also affects the value of c. Consequently, a better analysis of the agreement of the model with such parameters as c, σ and ξ is provided by evaluating the effect of these parameter on G' collectively rather than individually. Measurements of m,

d_o and A are difficult to perform. The authors know of no method to measure A, and the methods of microscopy discussed in Section III do not allow for an accurate measurement of m or d_o.

The morphology of the microstructural elements also affects the mechanical strength of the network (e.g. Cornily and leMeste, 1985; Hoerr and Waugh, 1955; Hoerr, 1960). Since the interactions between the microstructural elements in this model were developed for spherical microstructural elements, obviously morphological changes of these elements would vary the form of Eqn (75). Additionally, changes in morphology would probably cause changes in the Hamaker's constant as well. Morphology and size of crystals are affected by the particular polymorphism of the fat crystals formed (Chapman, 1962; Hoerr, 1960). Therefore, it is to be expected that changes in polymorphism may affect the network in a manner not predicted by Eqn (75), even though to a certain extent the Hamaker's constant will be affected by polymorphic changes. However, the Hamaker's constant as is represented in this model is little more than a fudge-factor – there is no known method of calculating these for fat crystal networks. The triglyceride composition also influences the size and rigidity of the crystals (Bailey, 1950). Therefore, it is important to establish a relationship between Hamaker's constant and triglyceride composition and polymorphism. Certainly, the model would be significantly improved if the crystalline packing and the molecular nature of the fat were represented in an explicit manner, rather than through the rather opaque relationship with the Hamaker's constant. However, at this time, the authors can think of no method to begin this process, other than by molecular modelling of the triglyceride molecules into crystalline structures. This is a non-trivial task beyond the scope of this thesis and the capabilities of the authors. However, it is important to identify the areas where the model may be improved.

In an effort to examine the potential of utilizing changes in processing conditions to affect structure, and therefore γ and D, samples of milkfat were cooled rapidly and slowly, and then the structure investigated. The methods of cooling are given in subsection M in Section III. Figure 48(B) demonstrates that the milkfat samples that were cooled slowly and those that were cooled rapidly had very different solid fat contents. After some initial changes, the solid fat contents of both samples seem to indicate that both samples have achieved some kind of equilibrium solid fat content. As is to be expected, the solid fat content of the rapidly-cooled (solid circles) sample of milkfat is higher. From Eqn (75), this implies that the sample cooled rapidly would have a higher storage modulus.

Figure 49 demonstrates the DSC melting profiles of the differently-cooled samples of milkfat. As is evident from the figure, the rapidly

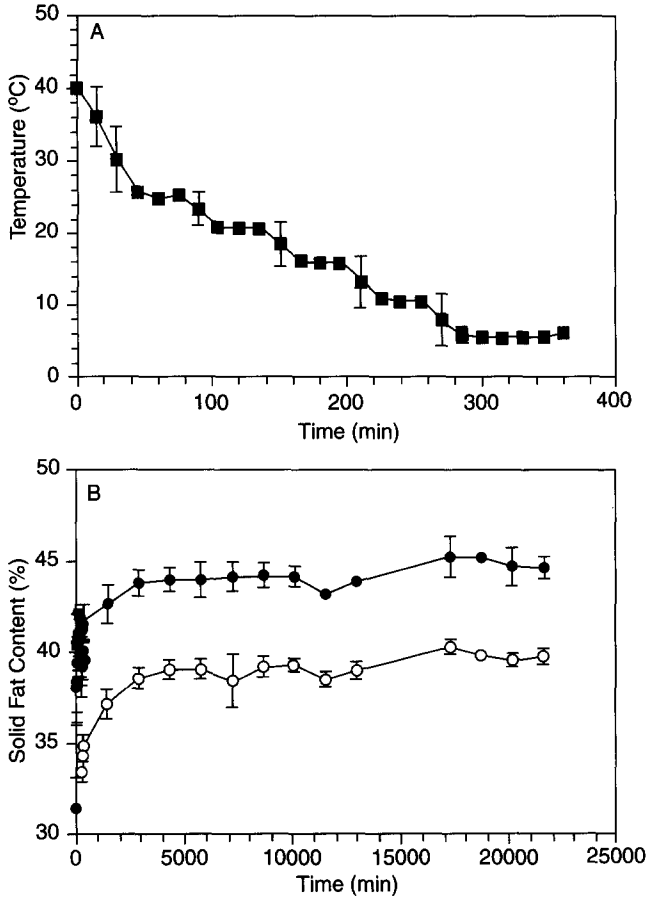

FIG. 48 (A) Cooling profile of milkfat cooled according to the slow-cooling method. (B) Solid fat content vs. time for the differently-cooled milkfat samples (solid circles – rapidly cooled, open circles – slowly cooled).

cooled samples (Figure 49(A)) had a very similar melt profile compared to the slowly-cooled samples (Figure 49(B)). This suggests that the crystalline nature of both samples were the same – i.e. both samples demonstrated the same polymorphic form of milkfat.

Figure 43 (Section III) demonstrates that the size of the microstructural elements of the slowly-cooled milkfat samples are much larger than those in the rapidly-cooled samples. From Eqn (76), this result suggests that the value of γ for the slowly-cooled samples should be much lower than those of the rapidly-cooled samples. As was reported in III, subsection M.2,

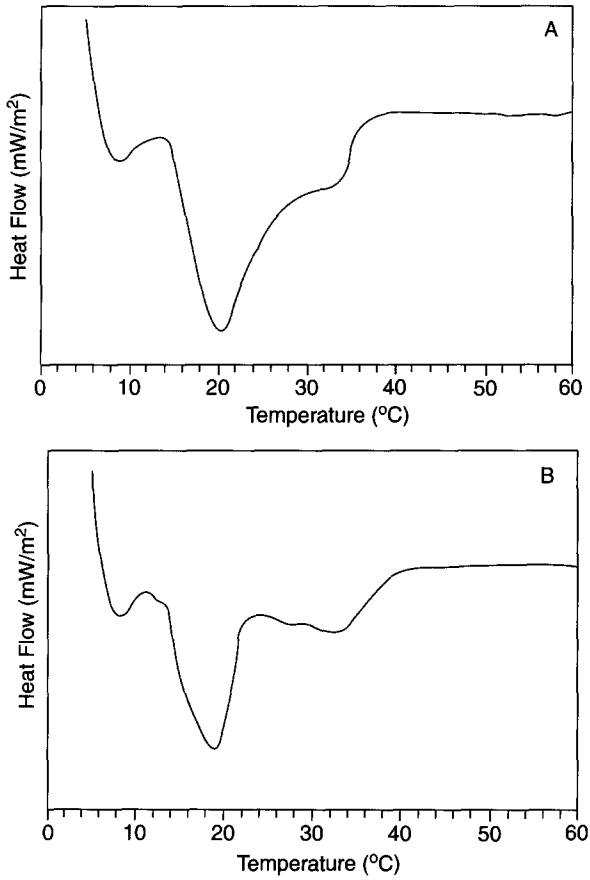

FIG. 49 Differential scanning calorimeter (DSC) measurements showing the melt profiles of milkfat (a) rapidly cooled, (b) slowly cooled.

rheological analysis yielded γ values of 2.0×10^{-4} MPa and 7.0×10^{-2} MPa for the slow cooled and rapidly cooled samples, respectively. Therefore, the γ values of the slow cooled samples are two orders of magnitude lower than those of the rapidly-cooled samples. From Eqn (75), this implies that the sample cooled rapidly would have a higher storage modulus.

From Section III, subsection M.2, rheological analyses of the differently cooled samples yielded different fractal dimensions – the slow cooled samples yielded a fractal dimension value of 2.65, whilst the rapidly cooled samples yielded a D of 2.27. From the discussion in Section III and

from Eqn (75), one would expect from this result that the storage modulus of the rapidly-cooled samples would be higher.

Therefore, from the foregoing discussion, parameters such as microstructural element size, solid fat content, fractal dimension, and γ all suggest that the storage modulus of the rapidly cooled samples will be higher than that of the slowly cooled samples. Figure 50(A) demonstrates that these predictions were correct, according to Eqns (75) and (76), since at all values of solid fat content, the elastic moduli of the rapidly cooled samples (solid circles) are higher than those of the corresponding slowly cooled samples.

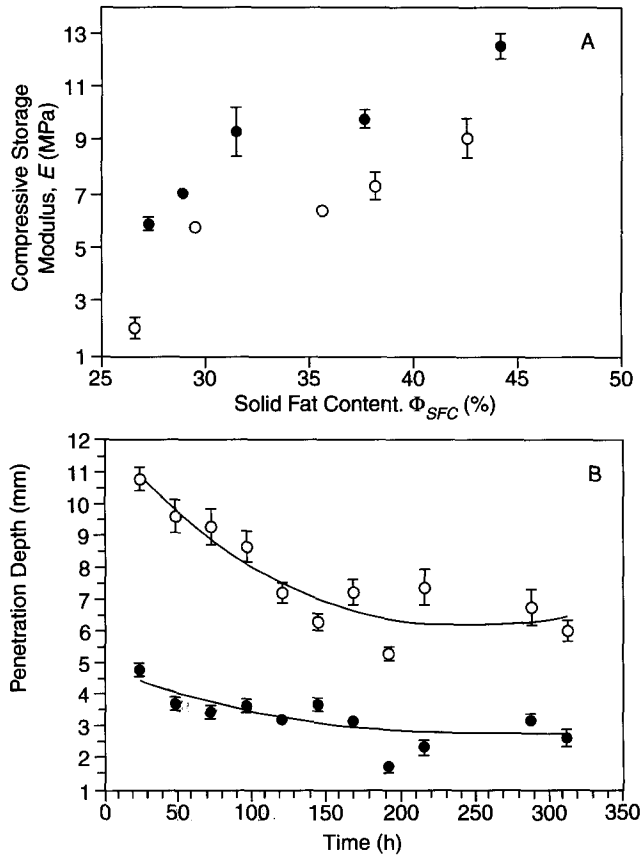

FIG. 50 (A) Compressive storage modulus vs. solid fat content, for milkfat samples cooled rapidly (solid circles) and slowly (open circles). (B) Penetration depth vs. time (measured from the point at which both set of samples reached 5°C) for rapidly cooled (solid circles) and slowly cooled (open circles) samples of milkfat.

The hardness of fats as measured by cone penetrometry are proportional to the elastic moduli, however, the nature of the constant of proportionality of this relationship is not easily defined (Narine, 2000; Narine and Marangoni, 2000a). However, Figure 50(B) demonstrates that the hardness of the rapidly-cooled samples (solid circles demonstrating lower penetration depths) were consistently higher than the hardness of the slowly cooled samples (open circles demonstrating higher penetration values). Of interest is also that after approximately 8 days, the hardness of each set of samples had equilibrated to constant values. This suggests that by changing only the processing conditions of the fat, it was possible to produce two sets of fats with a large difference in hardness (60% from Figure 50(B)). Furthermore, up until a period of approximately two weeks, this difference in hardness was constant.

Therefore, a good case is made by this experiment for the possibilities that exist for producing fats with tailored mechanical properties by varying the way the fat is processed, without changing the chemical composition of the fat. Unfortunately, the way the fats were processed in this experiment is very different from the way fats are crystallized in industry, and therefore it is uncertain what industrial implications are motivated by this study. Additionally, it is important to realize that in this study, *all* of the measurable structural parameters as well as the solid fat content suggested (based on the model espoused by Eqn (75) that the storage modulus (and therefore hardness) should be higher for the milkfat cooled rapidly. It is quite conceivable that in some cases, these parameters will be changed through processing in directions which may cause them to promote changes in storage modulus that are in different directions. Furthermore, although all of the structural parameters examined in this study support the model espoused by Eqns (75) and (76), it should be realized that *all* parameters implicated in the model were not measured (because of the difficulty in measuring these) simultaneously. However, in the absence of such measurements, it is reasonable to conclude that all experimental evidence presented in this thesis support the model.

H. CONCLUSIONS

Whilst Eqn (75) does not provide an absolute formulation for γ in the weak link theory, it does identify key network parameters that are important in determining the shear storage modulus of fat crystal networks. Futhermore, it agrees well with experimental observations and with the weak link theory, which has been shown in Section III to be valid for fat crystal networks. The equation provides impetus for the development of phenomenological investigations of relationships between triglyceride composition

and polymorphism and values of Hamaker's constants and size of microstructural elements. Insight on the changes in mechanical strength of fat networks whose characteristics such as size of microstructural elements, size of microstructures and distances between microstructures have been altered through processing conditions was also provided.

To certain extents, the model presented in this section represents an idealization of the structure of fat crystal networks. It is therefore important that the assumptions highlighted during the development of the model be taken into consideration whenever the model is used. At best, the model provides an indication of the structural influences on the parameter γ, but levels of structure such as the crystalline and molecular structures are not adequately represented.

REFERENCES

Aubert, C. and Cannell, D. S. 1986. Restructuring of colloidal silica aggregates. *Phys. Rev. Lett.* **56**, 738.

Avnir, D., Biham, O. *et al.* 1998. Is the geometry of nature fractal? *Nature* **279**, 39–40.

Bailey, A. E. 1950. "Melting and Solidification of Fats". New York, Interscience Publishers.

Ball, R. C. 1989. Fractal colloidal aggregates: consolidation and elasticity. *Physica D* **38**, 13–15.

Biham, O., Malcai, O. *et al.* 1998. Is nature fractal? *Nature* **279**, 784–786.

Bolle, C., Cameti, C. *et al.* 1987. Kinetics of salt-induced aggregation in polystyrene lattices studied by quasielastic light scattering. *Phys. Rev. A* **35**, 837.

Bremer, L. G. B., Bijsterbosch, B. H. *et al.* 1990. On the fractal nature of the structure of acid casien gels. *Colloid Surf.* **51**, 159–170.

Bremer, L. G. B., Bijsterbosch, B. H. *et al.* 1993. Formation, properties and fractal structure of particle gels. *Advances in Colloid and Interface Sci.* **46**, 117–128.

Bremer, L. G. B., van Vliet, T. *et al.* 1989. Theoretical and experimental study of the fractal nature of the structure of casien gels. *J. Chem. Soc., Faraday Trans.* **85**, 3359–3372.

Brooker, B. E. 1990. Low temperature microscopy and X-ray analysis of food systems. *Trends in Food Sci. and Techn.* **1**, 100–103.

Brown, W. D. 1987. "The Structure and Physical Properties of Flocculating Colloids". University of Cambridge.

Brown, W. D. and Ball R. C. 1985. Computer simulation of chemically limited aggregation. *J. Phys. A* **18**, L517.

Buchheim, W. 1982. Aspects of samples preparation for freeze-fracture/freeze-etch studies of proteins and lipids in food systems. A review. *Food Microstruct.* **1**, 189–208.

Buscall, R., Mills, P. D. A. *et al.* 1988. Scaling behaviour of the rheology of aggregate networks formed from colloidal particles. *J. Chem. Soc., Faraday Trans.* **84**, 4249–4260.

Chapman, D. 1962. The polymorphism of glycerides. *Chem. Rev.* **62**, 433–456.

Chen, M. and Russel B. 1991. Characteristics of flocculated silica dispersions. *J. Colloid and Interface Sci.* **141**(2), 565–577.

Cornily, G. and leMeste M. 1985. Flow behavior of lard and its fraction at 15 C. *J. Texture Stud.* **16**, 383–402.

Cotton, F. A. 1971. "Chemical Applications of Group Theory." New York, Wiley Interscience.

Courtens, E., Pelous, J. *et al.* 1987. Brillouin-scattering measurements of phonon-fracton crossover in silica aerogels. *Phys. Rev. Lett.* **58**(2), 128–131.

Crownover, R. M. 1995. "Introduction to Fractals and Chaos." Boston, Jones and Bartlett.

de Gennes, P. G. 1979. "Scaling Concepts in Polymer Physics." Ithaca, NY, Cornell University Press.

de Man, J. M. 1961. Physical properties of milkfat II. Some factors influencing crystallization. *J. Dairy Res.* **28**, 117–122.

de Man, J. M. 1964. Effect of cooling procedures on consistency, crystal structure and solid fat content of milkfat. *Dairy Industries* **29**, 244–246.

de Man, J. M. 1982. Microscopy in the study of fats and emulsions. *Food Microstruct.* **1**, 209–222.

de Man, J. M. and Beers, A. M. 1987. Fat crystal networks: structure and rheological properties. *J. Text. Stud.* **18**, 303–318.

Dietler, G., Aubert, C. *et al.* 1986. Gelation of colloidal silica. *Phys. Rev. Lett.* **57**, 3117.

Dimon, P., Sinha, S. K. *et al.* 1986. Structure of aggregated gold colloids. *Phys. Rev. Lett.* **57**, 595.

Edwards, S. F. and Oakeshoot R. B. S. 1989. The transmission of stress in an aggregate. *Physical D* **38**, 88–92.

Falconer, K. 1990. "Fractal Geometry." Chichester, Wiley.

Feng, S. and Sen P. 1984a. Percolation on elastic network: new exponent and threshold. *Phys. Rev. Lett.* **52**, 216.

Feng, S., Sen, P. *et al.* 1984b. Percolation on two-dimensional elastic networks with rotationally invariant bond bending forces. *Phys. Rev. B* **30**, 5386.

Flint, O. 1984. Applications of light microscopy in food analysis. *Microscope* **32**, 133–140.

Flint, O. 1991. Microscopy in the development of new food products. *European Microsc. Anal.* **10**, 21–23.

Foley, J. and Brady, J. P. 1984. Temperature-induced effects on crystallization behaviour, solid fat content and the firmness of milk fat. *Journal of Dairy Research* **51**, 579–589.

Forrest, S. R. and Witten, J. T. A. 1979. Long range correlations in smoke-particle aggregates. *J. Phys. A.* **12**, L109.

Friedlander, S. K. 1977. "Smoke, Dust and Haze." New York, Wiley.

Hagiwara, T., Kumagai, H. *et al.* 1997. Analysis of aggregate structure in food protein gels with the concept of fractal. *Biosci. Biotech. Biochem.* **61**, 1663–1667.

Hagiwara, T., Kumagai, H. *et al.* 1998. Fractal analysis of aggregates in heat-induced BSA gels. *Food Hydrocolloids* **12**, 29–36.

Haighton, A. J. 1976. Blending, chilling and tempering of margarines and shortenings. *J. Am. Oil Chem. Soc.* **53**, 397–399.

Hamaker, H. C. 1937. The London-van der Waals attraction between spherical particles. *Physica [IV]* **10**, 1058.

Hausdorf, F. 1991. Dimension und Ausseres Mass. *Mathematische Annalen* **79**, 157–179.

Heertje, I. 1993. Microstructural studies in fat research. *Food Structure* **12**, 77–94.

Heertje, I., Leunis, M. *et al.* 1987a. Product microscopy of fatty products. *Food Microstruct.* **6**, 1–8.

Heertje, I., van der Vlist, P. *et al.* 1987b. Confocal laser scanning microscopy in food research: some observations. *Food Microstruct.* **6**, 115–120.

Heertje, I., van Eendenburg, J. *et al.* 1988. The effect of processing on some microstructural characteristics of fat spreads. *Food Microstruct.* **7**, 189–193.

Hoerr, C. W. 1960. Morphology of fats, oils and shortenings. *J. Am. Oil Chem. Soc.* **37**, 539–546.

Hoerr, C. W. and Waugh, D. F. 1955. Some physical characteristics of rearranged lard. *J. Am. Oil Chem. Soc.* **32**, 37–41.

Ione, S. 1987. "Video Microscopy." New York, Plenum Press.

Jullien, R. and Botet, R. 1987. "Aggregation and Fractal Aggregates." Singapore, World Scientific Publishing Co. Pte Ltd.

Juriaanse, A. C. and Heertje, I. 1988. Microstructure of shortenings, margarine and butter – a review. *Food Microstruct.* **7**, 181–188.

Kalab, M. 1983. Electron microscopy of foods. In "Physical Properties of Foods" (M. Peleg and E. B. Bagley, eds). Westport, CT, AVI Publishing Co., 43–104.

Kamphuis, H. and Jongschaap R. J. J. 1985. The rheological behaviour of suspensions of fat particles in oil interpreted in terms of a transient-network model. *Colloid Polym. Sci.* **263**, 1008–1024.

Kamphuis, H., Jongschaap R. J. J. *et al.* 1984. A transient-network model describing the rheological behaviour of concentrated dispersions. *Rheol. Acta* **23**, 329–344.

Kantor, Y. and Webman, I. 1984. Elastic properties of random percolating systems. *Phys. Rev. Lett.* **52**(21), 1891–1894.

Kawanari, M. 1996. Butter's characteristics: effect of processing. *Inform.* **7**(10), 1104–1110.

Kolb, M., Botet, R. *et al.* 1983. Scaling of kinetically growing clusters. *Phys. Rev. Lett.* **51**, 1123.

Leibniz, G. W. 1721. "Principia Philosophiae, More Geometrico Demonstrata."

Lin, M. Y., Lindsay, H. M. *et al.* 1989. Universality in colloid aggregation. *Nature* **339**, 360–362.

Mandelbrot, B. B. 1982. "The Fractal Geometry of Nature." New York, Freeman.

Mandelbrot, B. B. 1998. Is nature fractal? *Nature* **279**, 783–784.

Marangoni, A. G., Barbut, S. *et al.* 2000. On the structure of particulate gels – the case of salt-induced cold gelation of heat-denatured whey protein isolate. *Food Hydrocolloids* **14**, 61–74.

Marangoni, A. G. and Hartel, R. W. 1998. Visualization and structural analysis of fat crystal networks. *Food Technol.* **52**(9), 46–52.

Marangoni, A. G. and Lencki R. W. 1998. Ternary phase behavior of milk fat fractions. *J. Agric. Food Chem.* **46**, 3879–3884.

Marangoni, A. G. and Rousseau D. 1996. Is plastic fat rheology governed by the fractal nature of the fat crystal network? *J. Amer. Oil Chem. Soc.* **73**, 991–993.

Marangoni, A. G. and Rousseau D. 1998a. The influence of chemical interesterification on physicochemical properties of complex fat systems 1. Melting and crystallization. *J. Am. Oil Chem. Soc.* **75**, 1265–1271.

Marangoni, A. G. and Rousseau D. 1998b. The influence of chemical interesterification on the physicochemical properties of complex fat systems. 3. Rheology and fractality of the crystal network. *J. Am. Oil Chem. Soc.* **75**, 1633–1636.

Meakin, P 1983. Formation of fractal clusters and networks by irreversible diffusion-limited aggregation. *Phys. Rev. Lett.* **1983**(51), 1119.

Meakin, P. 1988. Fractal aggregates. *Adv. Colloid Interface Sci.* **28**, 249–331.

Medalia, A. I. 1971. *Surf. Colloid Sci.* **4**, 1.

Mulder, H. and Walstra P. 1974. "The Milk Fat Globule – Emulsion Science as Applied to Milk Products and Comparable Foods." Wagningen, The Netherlands, Centre for Agricultural Publishing.

Mullins, W. W. and Sekerka R. F. 1963. Morphological stability of a particle growing by diffusion or heat flow. *J. Appl. Phys.* **34**, 323.

Narine, S. S. 2000. "Structure and Mechanical Properties of Fat Crystal Networks." Department of Food Science. Guelph, University of Guelph.

Narine, S. S. and Marangoni A. G. 1999a. Mechanical and structural model of fractal networks of fat crystals at low deformations. *Phys. Rev. E* **60**(6), 6991–7000.

Narine, S. S. and Marangoni A. G. 1999b. Fractal nature of fat crystal networks. *Physical Review E* **59**(2), 1908–1920.

Narine, S. S. and Marangoni A. G. 1999c. Factors influencing the texture of plastic fats. *Inform* **10**(6), 565–570.

Narine, S. S. and Marangoni A. G. 1999d. The difference between cocoa butter and salatrim lies in the microstructure of the fat crystal network. *J. Am. Oil Chem. Soc.* **76**, 7–13.

Narine, S. S. and Marangoni A. G. 1999e. Microscopic and rheological studies of fat crystal networks. *J. Cryst. Growth* **198/199**, 1315–1319.

Narine, S. S. and Marangoni A. G. 1999f. Relating structure of fat crystal networks to mechanical properties: a review. *Food Res. Int.* **32**, 227–248.

Narine, S. S. and Marangoni A. G. 2000a. Elastic modulus as an indicator of macroscopic hardness of fat crystal networks. *Lebensmittelwissenschaft und Technologie*, in press.

Narine, S. S. and Marangoni A. G. 2000b. Structure of fat crystal networks: quantification, interrelationships, and prediction of elastic properties. *Proceedings of the 3rd International Symposium on Confectionery Science*, Pennslyvania State University, Department of Food Science and the PMCA, University Park, PA, USA.

Nederveen, C. J. 1963. Dynamic mechanical behavior of suspensions of fat particles in oil. *J. Colloid and Interface Science* **18**, 276–291.

Papenhuijzen, J. M. P. 1971. Superimposed steady and oscillatory shear in dispersed systems. *Rheol. Acta* **10**, 493–502.

Papenhuijzen, J. M. P. 1972. The role of particle interactions in the rheology of dispersed systems. *Rheol. Acta* **11**, 73–88.

Parker, J. R. 1994. "Practical Computer Vision Using C." New York, Wiley.

Payne, A. R. 1964. The elasticity of carbon black networks. *J. Colloid Sci.* **19**, 744–754.

Pfeifer, P. 1998. Is nature fractal? *Nature* **279**, 784.

Rojanski, D., Huppert, D. *et al.* 1986. Integrated fractal analysis of silica: adsorption, electronic energy transfer, and small-angle X-ray scattering. *Phys. Rev. Lett.* **56**(23), 2505–2508.

Rousseau, D., Forrestiere, K. *et al.* 1996a. Restructuring butterfat through blending and chemical interesterification. 1. Melting behavior and triacylglycerol modifications. *J. Am. Oil. Chem. Soc.* **73**, 963–972.

Rousseau, D., Hill, A. R. *et al.* 1996b. Restructuring butterfat through blending and chemical interesterification. 2. Microstructure and polymoprhism. *J. Am. Oil Chem. Soc.* **73**, 973–981.

Rousseau, D., Hill, A. R. *et al.* 1996c. Restructuring butterfat through blending and chemical interesterification. 3. Rheology. *J. Am. Oil. Chem. Soc.* **73**, 983–989.

Rousseau, D. and Marangoni, A. G. 1998a. Tailoring the textural attributes of butterfat/canola oil blends via *Rhizopus arrhizus* lipase-catalyzed interesterification. 1. Compositional modifications. *J. Agric. Food Chem.* **46**, 2368–2374.

Rousseau, D. and Marangoni, A. G. 1998b. Tailoring the textural attributes of butterfat/canola oil blends via *Rhizopus arrhizus* lipase-catalyzed interesterification. 2. Modifications of physical properties. *J. Agric. Food Chem.* **46**, 2375–2381.

Rousseau, D., Marangoni, A. G. *et al.* 1998. The influence of chemical interesterification on the physicochemical properties of complex fat systems. 2. Morphology and polymorphism. *J. Am. Oil Chem. Soc.* **75**, 1833–1839.

Sargeant, J. A. 1988. The application of cold stage scanning electron microscopy to food research. *Food Microstruct.* **7**, 123–135.

Schaefer, D. A., Martin, J. E. *et al.* 1984. Fractal geometry of colloidal aggregates. *Phys. Rev. Lett.* **52**, 2371.

Schaefer, D. W. and Keefer K. D. 1986. Structure of random porous materials: Silica Aerogel. *Phys. Rev. Lett.* **56**(20), 2199–2202.

Schroeder, M. 1991. "Fractals, Chaos, Power Laws." New York, W. H. Freeman and Company.

Shama, F. and Sherman P. 1970. The influence of worksoftening on the viscoelastic properties of butter and margarine. *J. Texture Stud.* **1**, 196–205.

Sherman, P. 1968. The influence of particle size on the viscoelastic properties of flocculated emulsions. 5th In. Congress on Rheology, Kyoto, Japan.

Shih, W. H., Shih, W. Y. *et al.* 1990. Scaling behavior of the elastic properties of colloidal gels. *Phys. Rev. A* **42**, 4772–4779.

Shukla, A. and Rizvi S. S. H. 1996. Relationship among chemical composition microstructure and rheological properties of butter. *Milchwissenschaft* **51**(3): 144–148.

Sonntag, R. C. and Russel W. B. 1987. Elastic properties of flocculated networks. *J. Colloid Interface Sci.* **116**, 485–489.

Stading, M., Langton, M. *et al.* 1993. Microstructure and rheological behaviour of particulate β-lactoglobulin gels. *Food Hydrocolloids* **7**, 195–212.

Stanley, H. E. 1984. Fractal concepts in aggregation and gelation: an introduction. In "Kinetics of Fractal Aggregation" (F. Family and D. P. Landau, eds.) Elsevier Science Publishers B. V.: 1–4.

Uriev, N. B. and Ladyzhinsky, I. Y. 1996. Fractal models in the rheology of colloidal gels. *Colloids and Surfaces A* **108**, 1–11.

Vacher, R., Woignier, T. *et al.* 1988. Structure and self-similarity of silica aerogels. *Phys. Rev. B* **37**(11), 6500–6503.

Van den Tempel, M. 1961. Mechanical properties of plastic-disperse systems at very small deformations. *J. Colloid and Interface Sci.* **16**, 284–296.

Van den Tempel, M. 1979. Rheology of concentrated suspensions. *J. Colloid and Interface Sci.* **71**(1), 18–20.

Vold, M. H. 1951. Van der Waals' attraction between anisotropic particles. *J. Colloid Sci.* **9**, 451.

Vreeker, R., Hoekstra, L. L. *et al.* 1992a. Fractal aggregation of whey proteins. *Food Hydrocolloids* **6**, 423–435.

Vreeker, R., Hoekstra, L. L. *et al.* 1992b. The fractal nature of fat crystal networks. *Colloids and Surfaces* **65**, 185–189.

Weitz, D. A., Huang, J. S. *et al.* 1985. Limits of the fractal dimension for irreversible kinetic aggregation of gold colloids. *Phys. Rev. Lett.* **54**, 1416.

Weitz, D. A. and Oliveria M. 1984. Fractral structures formed by kinetic aggregation of aqueous gold colloids. *Phys. Rev. Lett.* **52**, 1433.

Witten, T. A. and Sander L. M. 1981. Diffusion-limited aggregation, a kinetic critical phenomenon. *Phys. Rev. Lett.* **47**(19), 1400–1403.

Witten, T. A. and Sander L. M. 1983. Diffusion-limited aggregation. *Phys. Rev. B* **27**(9), 5686–5697.

Xu, C., Zipfel, W. *et al.* 1996. Multiphoton fluorescence excitation: New spectral windows for biological nonlinear microscopy. *Proc. Natl. Acad. Sci.*, USA.

Yiu, S. H. 1985. A fluorescence microscopic study of cheese. *Food Microstruct.* **4**, 99–106.